



UNIVERSITÀ DEGLI STUDI DI VERONA

*DEPARTMENT OF*

*Medicine*

*GRADUATE SCHOOL OF*

*Life and Health Sciences*

*DOCTORAL PROGRAM IN*

*Clinical and Experimental Biomedical Sciences*

29° Cycle - Year 2014

**Calcium Sensing Receptor,  
Calcium Binding Proteins and Astrocytic  
Changes in Alzheimer's Disease**

S.S.D. BIO/17

IN *CO-TUTELLE DE THÈSE* WITH

UNIVERSIDAD DEL PAÍS VASCO / EUSKAL HERRIKO UNIBERTSITATEA

*DEPARTMENT OF*

*Neuroscience*

*DOCTORAL PROGRAM IN*

*Neuroscience*

Coordinator doctoral program in the University of Verona:

**Prof. Paolo Moghetti**

Coordinator doctoral program in the UPV/EHU:

**Prof. Pedro Rolando Grandes Moreno**

Tutor in the University of Verona:

**Dr. Anna Maria Chiarini**




Tutor in the UPV/EHU:

**Prof. José Julio Rodríguez Arellano**

Doctoral Student: **Emanuela Gardenal**

This work is licensed under a Creative Commons Attribution-NonCommercial-NoDerivs 3.0 Unported License, Italy. To read a copy of the licence, visit the web page:

<http://creativecommons.org/licenses/by-nc-nd/3.0/>

-  **Attribution** — You must give appropriate credit, provide a link to the license, and indicate if changes were made. You may do so in any reasonable manner, but not in any way that suggests the licensor endorses you or your use.
-  **NonCommercial** — You may not use the material for commercial purposes.
-  **NoDerivatives** — If you remix, transform, or build upon the material, you may not distribute the modified material.

*Calcium Sensing Receptor, Calcium Binding Proteins  
and Astrocytic Changes in Alzheimer's Disease*  
Emanuela Gardenal  
PhD thesis  
Verona, 14 May 2017

## ABSTRACT

Alzheimer's disease (AD) is a neurodegenerative disorder characterized by memory loss and cognitive dysfunctions including language problems, disorientation, loss of organization and planning skills and other neuropsychiatric symptoms that drive towards a final stage of total incapability of managing self-care. The main pathological features are brain atrophy, neuronal and synaptic loss,  $\beta$ -amyloid accumulation, plaques deposition and neurofibrillary tangles formation. Nowadays there is no treatment able to cure this disease, but several drugs are administered to patients to ease the symptoms and slow the disease progression. Since  $\beta$ -amyloid plaques are one of the main hallmarks of AD, multiple efforts have been addressed in order to test new therapies targeting and decreasing this burden. However, it is still not clear if this is the origin or just a consequence of AD. Thus, many classical and new pathological mechanisms are under study to decipher the real mechanism and progression of the disease.

So far, several transgenic animal models have been developed to study the pathogenesis of AD (see Table 1.1). Among these, the 3xTg-AD mouse is the unique animal model which develops both  $A\beta$  plaques and neurofibrillary tangles with a spatio-temporal pattern that closely mimics human AD. Indeed, 3xTg-AD mice start to intracellularly accumulate  $\beta$ -amyloid around 3-6 months of age with a subsequent increased extracellular secretion from 9 months and deposition of neuritic plaques from 12 months of age, at this time these mice start to show also a clear increase in tau hyperphosphorylation with formation of neurofibrillary tangles.

The research work conducted for this PhD thesis has had the aim to study distinct aspects of AD pathology within the hippocampus and entorhinal cortex, key areas affected by the AD pathology and responsible of the memory loss and behavioural impairments, in the 3xTg-AD mouse model by using a detailed and distinct immunohistochemical approach.

Therefore, in the Results section, starting by, **chapter 3**, the immunoreactivity changes of the Calcium sensing receptor (CaSR) were analysed in the hippocampus of the 3xTg-AD mice. CaSR role in AD has recently started to be a main centre of attention, since  $A\beta$  peptides were shown to bind and activate CaSR which through this interaction is able to induce the hyperproduction and secretion of  $A\beta$  itself. In addition, following the activation of this pathological mechanism, CaSR is hyperexpressed. Experiments performed on human cortical astrocytic cultures treated with toxic exogenous  $A\beta$  have demonstrated that the inhibition of the CaSR through an allosteric antagonist, such as NPS 2143, result in the total block of this detrimental pathological mechanism. CaSR immunoreactivity measurement in the hippocampus of the 3xTg-AD mice showed an increase of its expression in specific areas involved also by early  $A\beta$  accumulation and plaques depositions such as the Cornu Ammonis 1 (CA1) and the dentate gyrus with major expression in the projection neurons.

In **chapter 4**, following the Calcium changes hypothesis appearing in AD and its progression, the alteration of calcium binding proteins such as parvalbumin and calretinin has been studied in the hippocampus of 3xTg-AD mice 18 months old, when the presence of  $\beta$ -amyloid and tangles is evident. These proteins are an extremely relevant marker for different subpopulations of GABAergic inhibitory interneurons, which surprisingly are usually considered less vulnerable in AD pathology. In this study, a decrease in the numerical density (Nv) of parvalbumin and calretinin neurons was identified in the CA1 region of hippocampus, which is the hippocampal subfield showing the highest level of  $A\beta$  plaques burden in this model. This work is of major relevance since it characterizes and indicates a specific neuronal vulnerability underestimated in AD, which could be key to better elucidate the neuronal circuits that are affected during the pathology progression.

Finally, in **chapter 5** is reported the study of the alterations of a trophic factor that has shown to be of major importance not only in AD but also in physiological aging: S100 $\beta$ . In this project I have contributed to the characterisation of S100 $\beta$ -positive astrocytes in the 3xTg-AD mouse model to study another possible aspect of AD pathology that is considered to be the potential astrocytic dysfunction hypothesis. For this purpose, the Nv and a complete morphological analysis (including the surface and volume analysis of total cell, processes and somata) was performed in the S100 $\beta$ -positive cells within the entorhinal cortex of transgenic animals and their non-transgenic counterpart from 1 month until 18 months of age. Whilst the Nv was not altered, an increase in the S100 $\beta$ -positive profiles was identified at 18 months of age both in aged and 3xTg-AD mice compared to younger mice and a significant increase was found also between the 3xTg-AD and non-transgenic animals at 18 months of age (an increase in the 3xTg-AD mice of 69.74% and 76.73% in the surface area and volume, respectively, comparing to age-matched control animals).

Altogether these three, seemingly, independent and disconnected studies demonstrate how complicated and variable is the aetiology and progress of AD and highlight the need to deeply investigate more targets other than neuronal pathology to further understand the pathologic mechanisms of this disease and its progression. Furthermore, a deep characterization in animal models such as the 3xTg-AD mice (centre of this work) is necessary to have a strong background knowledge of the pathological features and alterations present in them in order to achieve a better understanding and interpretation of the potential and possible outcomes which could direct us for the always important and key aspects of drug testing. Hopefully, this could be later on reproduced in human material providing new insights to a combined therapy targeting all neuronal cells: neurons and glia. Thus implying a global nervous cell understanding and treatment strategy.

## RIASSUNTO

Il morbo di Alzheimer è una malattia neurodegenerativa caratterizzata da perdita di memoria e disfunzioni cognitive che includono problemi nel linguaggio, disorientamento, perdita delle capacità di organizzazione e pianificazione ed altri sintomi neuropsichiatrici fino al raggiungimento di uno stadio finale in cui il paziente necessita una assistenza totale. Le principali caratteristiche patologiche sono l'atrofia corticale, la perdita di neuroni e sinapsi, l'accumulo di proteina  $\beta$ -amiloide, la deposizione di placche neuritiche e la formazione di grovigli neurofibrillari composti dalla proteina tau iperfosforilata.

Al giorno d'oggi ancora non esiste una terapia in grado di curare questa malattia, sebbene diverse tipologie di farmaci siano somministrate ai pazienti per diminuire i sintomi e rallentare la progressione della malattia. Un approccio terapeutico molto studiato negli ultimi anni consiste nel cercare di eliminare le placche di  $\beta$ -amiloide che costituiscono uno degli elementi patologici più importanti nonostante non sia ancora ben chiaro se siano la causa o la conseguenza dello sviluppo di questa malattia. Lo studio dei meccanismi patologici che causano e fanno progredire la malattia di Alzheimer è ancora aperto e un'ampia attività di ricerca si sta effettuando per far luce il più possibile su questa patologia complessa.

Diversi modelli animali transgenici sono stati finora sviluppati per lo studio della malattia di Alzheimer (vedi Tabella 1.1). Fra questi, il topo triplo transgenico (3xTg-AD) è l'unico modello animale che sviluppa placche di  $\beta$ -amiloide e grovigli neurofibrillari con un andamento spazio-temporale più simile alla malattia di Alzheimer nell'uomo. Infatti i topi 3xTg-AD iniziano ad accumulare proteina  $\beta$ -amiloide a livello intracellulare intorno ai 3-6 mesi d'età con conseguente aumento della sua secrezione a 9 mesi, ed infine a partire dai 12 mesi d'età la deposizione di placche senili accompagnata da un'aumentata iperfosforilazione di tau con formazione di grovigli neurofibrillari.

Il lavoro di ricerca condotto durante il mio dottorato ha avuto lo scopo di studiare, mediante l'impiego di un dettagliato approccio immunohistologico, diversi tipi di alterazioni nell'ippocampo e nella corteccia entorinale nei topi 3xTg-AD, le quali risultano essere le aree della corteccia cerebrale maggiormente colpite sin dalla fase pre-sintomatica della malattia.

Nel **Capitolo 3** di questa tesi viene descritta una alterazione nell'espressione del "Calcium sensing receptor" (CaSR) nell'ippocampo dei topi 3xTg-AD. Il ruolo del CaSR nell'Alzheimer è recentemente diventato oggetto di attenzione grazie a degli studi che hanno dimostrato la capacità dei peptidi di  $\beta$ -amiloide di interagire ed attivare il CaSR, il quale in seguito a questa interazione induce l'iperproduzione e secrezione della stessa  $\beta$ -amiloide. Successivamente all'innesco di questo meccanismo patogenetico, il CaSR risulta anche iperespresso. Esperimenti condotti su colture primarie di astrociti umani hanno dimostrato che questo meccanismo è completamente inibito utilizzando un

antagonista allosterico del CaSR come il composto NPS2143. L'analisi dell'espressione del CaSR nell'ippocampo dei topi 3xTg-AD ha dimostrato un suo aumento in specifiche aree coinvolte nell'accumulo iniziale di  $\beta$ -amiloide e nella successiva deposizione di placche, quali il Cornu Ammonis 1 (CA1) e il giro dentato (DG).

Nel **capitolo 4**, le “calcium binding proteins” quali parvalbumina e calretinina sono state studiate nell'ippocampo dei topi 3xTg-AD a 18 mesi di età seguendo l'ipotesi riguardante la disomeostasi del calcio nella patogenesi e progressione del morbo di Alzheimer. Queste proteine sono oltretutto un marker molto utilizzato per differenti sottopopolazioni di interneuroni inibitori GABAergici. In questo studio è stata identificata una diminuzione nella densità numerica (Nv) dei neuroni positivi per parvalbumina e calretinina nella regione CA1 dell'ippocampo, la quale corrisponde all'area con maggior carico di placche di  $\beta$ -amiloide in questo modello animale. Questo lavoro ha permesso di caratterizzare una specifica vulnerabilità neuronale sottostimata nella malattia di Alzheimer, la quale rende maggior chiarezza sui circuiti neurali affetti nella progressione di questa patologia.

Infine, nel **capitolo 5** è riportato lo studio delle alterazioni del fattore trofico S100 $\beta$  la cui importanza è stata dimostrata non solo nell'Alzheimer, ma anche nell'invecchiamento fisiologico. In questo progetto ho contribuito alla caratterizzazione di astrociti positivi per S100 $\beta$  nei topi 3xTg-AD al fine di studiare un'ulteriore ipotesi per la malattia di Alzheimer che consiste nella “disfunzione astrocitaria”. A questo scopo, sono state analizzate la Nv e le caratteristiche morfologiche (superficie e volume dell'intera cellula, dei processi e del soma) delle cellule positive per S100 $\beta$  nella corteccia entorinale di topi da 1 a 18 mesi di età. Mentre la Nv è risultata inalterata, è stato rilevato un generale aumento dei profili positivi per S100 $\beta$  ai 18 mesi di età sia nei topi 3xTg-AD, sia in quelli non transgenici. Un aumento ancor più significativo è stato però misurato nei topi 3xTg-AD quando paragonati ai non transgenici (69,74% e 76,73% in area della superficie e volume rispettivamente).

In conclusione, questi tre apparentemente indipendenti e disconnessi studi dimostrano quanto complicata e variabile sia l'eziologia e la progressione della malattia di Alzheimer e mettono in luce la necessità di studiare più a fondo anche ulteriori meccanismi patogenetici che esulano dalla semplice patologia neuronale. Inoltre, la caratterizzazione dettagliata di modelli animali come i topi 3xTg-AD utilizzati in questo lavoro è necessaria per poter avere una profonda conoscenza di base delle caratteristiche patologiche presenti in essi, in modo tale da avere una miglior pianificazione e comprensione degli esiti che possono derivare dal loro utilizzo nel test di nuovi farmaci.

La riproduzione in futuro di questi studi su materiale umano potrebbe fornire un punto di partenza per un approccio terapeutico combinato che riguardi un corretto ripristino funzionale sia dei neuroni che della glia nonché una strategia differente e più mirata per il blocco della produzione anomala della proteina  $\beta$ -amiloide.

# LIST OF CONTENTS

<b>Chapter 1 – General Introduction</b>	p. 15
<b>1.1. Alzheimer’s Disease: clinical and histopathological features</b>	p. 15
<i>1.1.1. The discovery of Alzheimer’s Disease</i>	p. 15
<i>1.1.2. Clinical features</i>	p. 15
<i>1.1.3. Pathogenic hallmarks</i>	p. 18
<i>1.1.4. Braak stages</i>	p. 20
<i>1.1.5. APP function and processing</i>	p. 22
<i>1.1.5.1. <math>\beta</math>-secretase</i>	p. 25
<i>1.1.5.2. <math>\gamma</math>-secretase</i>	p. 25
<i>1.1.5.3. <math>\alpha</math>-secretase</i>	p. 26
<i>1.1.6. Tau structure and function</i>	p. 26
<i>1.1.7. Amyloid hypothesis and tau hypothesis</i>	p. 28
<b>1.2. The hippocampal formation: brain areas involved in memory formation</b>	p. 31
<i>1.2.1. Introduction on memory formation</i>	p. 31
<i>1.2.2. Histological description of the memory-related regions early affected in AD</i>	p. 32
<i>1.2.2.1. The Nucleus basalis of Meynert</i>	p. 32
<i>1.2.2.2. The Dentate Gyrus</i>	p. 33
<i>1.2.2.3. The Cornu Ammonis or proper hippocampus</i>	p. 34
<i>1.2.2.4. The Entorhinal Cortex</i>	p. 35
<i>1.2.3. Hippocampal connectivity</i>	p. 37
<b>1.3. Animal models</b>	p. 39
<i>1.3.1. Chemical induced animal models for AD</i>	p. 39
<i>1.3.2. Transgenic animal models for AD</i>	p. 40
<i>1.3.2.1. Single and double transgenic mouse models of AD</i>	p. 40
<i>1.3.2.2. The 3xTg-AD mouse model</i>	p. 42
<b>1.4. Calcium Sensing Receptor in AD</b>	p. 45
<i>1.4.1. Calcium Sensing Receptor structure and dimerization in the brain</i>	p. 45
<i>1.4.2. Regional and cellular distribution of the CaSR in the brain</i>	p. 47
<i>1.4.3. Functions of CaSR in the nervous system</i>	p. 47
<i>1.4.4. CaSR role in the pathogenesis of AD</i>	p. 50
<b>1.5. Calcium Binding Proteins in AD</b>	p. 52
<i>1.5.1. Hippocampal features and distribution of Parvalbumin neurons</i>	p. 53
<i>1.5.2. Hippocampal features and distribution of Calretinin neurons</i>	p. 53
<i>1.5.3. Parvalbumin alterations in AD</i>	p. 54

1.5.3.1. <i>PV alterations in the hippocampus</i>	p. 54
1.5.3.2. <i>PV alterations in the entorhinal cortex</i>	p. 56
1.5.3.3. <i>PV alterations in other cortical areas</i>	p. 56
<b>1.5.4. Calretinin alterations in AD</b>	p. 57
1.5.4.1. <i>CR alterations in the hippocampus</i>	p. 57
1.5.4.2. <i>CR alterations in the entorhinal cortex</i>	p. 57
1.5.4.3. <i>CR alterations in other cortical areas</i>	p. 58
<b>1.6. Astrocytes and their involvement in Alzheimer's disease</b>	p. 59
1.6.1. <i>Physiological functions of astrocytes</i>	p. 59
1.6.2. <i>Astrocytic physiological alterations in Alzheimer's disease animal models and cell cultures</i>	p. 60
1.6.3. <i>Astrocytic morphological and numerical alterations in ageing and Alzheimer's disease mouse models</i>	p. 62
<b>Aim of the thesis</b>	p. 67
<b>Chapter 2 – Material and Methods</b>	p. 69
2.1. <b>Animal model</b>	p. 69
2.2. <b>Animal perfusion</b>	p. 69
2.3. <b>Antibodies</b>	p. 70
2.4. <b>Immunohistochemistry</b>	p. 71
2.5. <b>Optical density measurement</b>	p. 74
2.6. <b>Cell counting</b>	p. 76
2.7. <b>Morphometric analysis</b>	p. 77
2.8. <b>Statistics</b>	p. 78
<b>Chapter 3 – Calcium-Sensing Receptor Immunoreactivity is increased in the Hippocampus of the 3xTg-AD mouse model</b>	p. 79
3.1. <b>CaSR expression is increased in 3xTg-AD animals</b>	p. 79
3.2. <b>The increase of CaSR expression in CA1 and DG is layer-specific</b>	p. 82
3.3. <b>CaSR increase in hippocampus occurs in the same areas affected by <math>\beta</math>-amyloid accumulation</b>	p. 84
3.4. <b>Discussion</b>	p. 86
<b>Chapter 4 – Parvalbumin and Calretinin regional changes in the hippocampus of the 3xTg-AD mouse model</b>	p. 88
4.1. <b>Parvalbumin optical density and cell numerical density in hippocampal CA1 and DG</b>	p. 88
4.2. <b>Calretinin optical density and cell numerical density in the hippocampus of the 3xTg-AD mice</b>	p. 91
4.3. <b>Discussion</b>	p. 93



<b>Chapter 5 – Changes of S100<math>\beta</math>-positive astrocytes in the entorhinal cortex during ageing and the progression of Alzheimer’s disease</b>	p. 97
<b>5.1. The numerical density of S100<math>\beta</math>-positive astrocytes does not change during ageing and AD pathology, but GFAP and GS astrocytic populations show slightly alterations</b>	p. 97
<b>5.2. Age-dependent increase in S100<math>\beta</math>-positive profiles</b>	p. 99
<b>5.3. S100<math>\beta</math>-positive astroglial profiles in 3xTg-AD</b>	p. 101
<b>5.4. Hypertrophy of S100<math>\beta</math>-positive astrocytes is associated with the presence of A<math>\beta</math> plaques</b>	p. 104
<b>5.5. Distinct astrocytic populations show different morphological alterations during AD progression</b>	p. 105
<b>5.6. Discussion</b>	p. 107
<b>Chapter 6 – Conclusions</b>	p. 110
<b>Funding</b>	p. 113
<b>References</b>	p. 114
<b>Appendix</b>	p. 129

## LIST OF FIGURES

Figures	Description	Page n.
<b>Chapter 1</b>		
Figure 1.1	The pathogenic hallmarks of AD	p. 19
Figure 1.2	The Braak staging of A $\beta$ and tau pathology in AD brains	p. 22
Figure 1.3	The pathways of APP processing	p. 24
Figure 1.4	Representation of hippocampal anatomic structure and entorhinal connections	p. 36
Figure 1.5	Representation of the CaSR domains and their ligands specificity	p. 46
Figure 1.6	Drawing representing the astrocytic hypothesis of AD	p. 66
<b>Chapter 2</b>		
Figure 2.1	Schematic representation of mouse dorsal hippocampus selection for OD analysis	p. 75
<b>Chapter 3</b>		
Figure 3.1	CaSR expression and localization in mouse hippocampus	p. 80
Figure 3.2	Changes of CaSR expression in hippocampal CA1	p. 81
Figure 3.3	Modification of CaSR expression in hippocampal DG	p. 84
Figure 3.4	CaSR and $\beta$ -amyloid relationship in hippocampus during AD progression	p. 85
<b>Chapter 4</b>		
Figure 4.1	Parvalbumin expression changes in mouse hippocampus with AD	p. 90
Figure 4.2	Calretinin expression changes in mouse hippocampus with AD	p. 92
<b>Chapter 5</b>		
Figure 5.1	Numerical density of S100 $\beta$ -positive astrocytes in the EC is not altered during ageing between the 2 genotypes	p. 98
Figure 5.2	GS and GFAP positive astrocytes are less numerous and show alterations in their Nv in the EC of 3xTg-AD mice compared to the non Tg	p. 99
Figure 5.3	Increase in the S100 $\beta$ -positive profiles of astrocytes at old age of non Tg and 3xTg-AD mice	p. 100
Figure 5.4	Increase of the s100 $\beta$ -positive astrocytes' surface area and volume in the EC of 3xTg-AD mice and the non Tg controls between the age of 1 and 18 months	p. 102
Figure 5.5	Increment in the surface and volume of s100 $\beta$ -positive astrocytes in close vicinity to senile plaques in EC of 3xTg-AD mice at age of 18 months	p. 105
Figure 5.6	S100 $\beta$ , GFAP and GS differently label astrocytes	p. 106

## LIST OF TABLES

Tables	Description	Page n.
<b>Chapter 1</b>		
Table 1.1	Summary of the most used transgenic mouse models of AD	p. 44
<b>Chapter 2</b>		
Table 2.1	Summary of the primary antibodies used in this research work and their details	p. 71
Table 2.2	Summary of the secondary antibodies used in this research work and their details	p. 71
<b>Chapter 3</b>		
Table 3.1	CaSR IOD values of the hippocampal CA1 and DG subfields in both non Tg and 3xTg-AD mice at 9, 12 and 18 months of age	p. 82
Table 3.2	CaSR IOD values of the hippocampal CA1 layers with statistical significance between non Tg and 3xTg-AD mice at 9, 12 and 18 months of age	p. 83
Table 3.3	CaSR IOD values of the hippocampal DG layers with statistical significance between non Tg and 3xTg-AD mice at 9, 12 and 18 months of age	p. 83
<b>Chapter 4</b>		
Table 4.1	Values of PV-positive cells Nv in the CA1 and the sublayers which show significant reduction in the 3xTg-AD mice respect to the non Tg mice	p. 89
Table 4.2	Values of PV IOD in the CA1 and the sublayers with significant reduction in the 3xTg-AD mice respect to the non Tg mice	p. 89
Table 4.3	Values of CR-positive cells Nv in the CA1 and the sublayers which show significant reduction in the 3xTg-AD mice respect to the non Tg mice.	p. 91
Table 4.4	Summary of published reports on PV- and CR-expressing neuronal subpopulations in AD	p. 96
<b>Chapter 5</b>		
Table 5.1	S100 $\beta$ morphometric values in the non Tg mice at 1, 9, 12 and 18 months of age	p. 101
Table 5.2	S100 $\beta$ morphometric values in the 3xTg-AD mice at 1, 9, 12 and 18 months of age	p. 103
Table 5.3	S100 $\beta$ morphometric values in the 3xTg-AD mice compared to the non Tg at 18 months of age	p. 103
Table 5.4	S100 $\beta$ morphometric values of astrocytes close and far from A $\beta$ plaques in the 3xTg-AD mice 18 months old	p. 104

## **Acknowledgements**

First of all, I would like to thank my family, my parents, my brothers and my sister for supporting me during the entire PhD with their patience and understanding and for having always believed in me.

This PhD work has been developed under a co-tutoring agreement between the University of Verona and the University of the Basque Country.

From the University of Verona, I would like to express my gratitude to my first supervisor, Dr. Anna Maria Chiarini, she guided me during these three years and gave me the possibility to do an international PhD Degree. My thanks go also to Prof. Ubaldo Armato and Dr. Ilaria Pierpaola Dal Prà for giving me the opportunity to work in the Histology Unit of the University of Verona and to all the colleagues who worked with me in this laboratory: Yao Chen, Raffaella Pacchiana, Daisong Liu and Michele Rossin.

From the University of the Basque Country, I would like to deeply thank my second supervisor, Prof. José Julio Rodríguez Arellano, for hosting me in his laboratory in Bilbao and helping me a lot in developing this PhD Thesis. A special thanks to Fátima Zallo, who helped me enormously in all the experimental part and for making my stay in Bilbao more sweet and comfortable. I would like to thank also Laura Escobar for her important support with the confocal microscopy and Maribel who helped me in the mouse facility.

I am grateful also to Prof. Alexei Verkhratsky of the University of Manchester for his challenging collaboration and help.

## Abbreviations

A $\beta$	Amyloid- $\beta$
AD	Alzheimer's disease
ADAM	a disintegrin and metalloprotease
ANOVA	One-way Analysis of Variance
ApoE4	Apolipoprotein E4
APP	Amyloid precursor protein
BACE1	$\beta$ -site APP cleaving enzyme-1
Ca <sup>2+</sup>	Calcium
CA1/2/3	Cornu Ammonis 1/2/3
CaBPs	Calcium binding proteins
CaSR	Calcium-Sensing Receptor
CB	Calbindin
CC	Corpus Callosum
CDR	Clinical Dementia Rating
CR	Calretinin
DG	Dentate Gyrus
EC	Entorhinal cortex
FAD	Familial Alzheimer's Disease
FC	Frontal cortex
GABA	$\gamma$ -aminobutyric acid
GCL	Granular Cell Layer
GFAP	Glial fibrillary acidic protein
GS	Glutamine synthetase
Hi	Hippocampus
HIF	hypoxia-inducible factor
HIPP cells	hilar perforant path-associated cells
IOD	Inverse Optical Density
LEC	Lateral Entorhinal Cortex
LTP	long-term potentiation
mGluR	metabotropic Glutamate Receptors
MCI	Mild cognitive impairment
MEC	Medial Entorhinal Cortex
Mol L	Molecular Layer
MMSE	Mini-mental state examination
nbM	nucleus basalis of Meynert
NFTs	Neurofibrillary tangles
NOS	Nitric Oxide Synthase
NSCC	Nonselective Cation Channels
NT	Neurofibrillary thread
NINCDS/ADRDA	National Institute on Neurological and Communicative Disorders and Stroke and the Alzheimer Disease and Related Disorder Association
Non Tg	Non-transgenic
NPY	Neuropeptide Y

Nv	Numerical density
OC	Occipital cortex
OD	Optical Density
Olf C	Olfactory cortex
IOD	Inverted Optical Density
ITC	Inferior temporal cortex
PB	Phosphate Buffer
PC	Parietal cortex
PCL	Pyramidal Cell Layer
PFC	Prefrontal cortex
PFA	paraformaldehyde
PS1/2	Presenilin 1/2
PV	Parvalbumin
ROI	Region of interest
SEM	Standard error of the mean
SOM	Somatostatin
St Lac	Stratum Lacunosum-Moleculare
St Luc	Stratum Lucidum
St Or	Stratum Oriens
St Rad	Stratum Radiatum
TC	Temporal cortex
TMB	Transmembrane domain
TS	Trizma-base Saline
VC	Visual cortex
VEGF	Vascular Endothelial Growth Factor
3xTg-AD	Triple transgenic mouse model of AD

# Chapter 1

## General Introduction

### 1.1. ALZHEIMER'S DISEASE: CLINICAL AND HISTOPATHOLOGICAL FEATURES

#### *1.1.1. The discovery of Alzheimer's Disease*

Alzheimer's Disease (AD) was described for the first time by the German psychiatric and neuropathologist Aloysius "Alois" Alzheimer who presented the case of his patient, Auguste D, at the 37th Assembly of the Southwest German Psychiatrists in Tübingen in 1906. When Professor Alois Alzheimer met and assessed Auguste D, she was only 51 years old and she was admitted for her weakness of memory, persecution mania, sleeplessness, and restlessness (Toodayan, 2016). She died 5 years later and Alzheimer obtained her brain for the corresponding neuropathological study and assessment in order to determine the anatomical alterations and relate them with the behavioral symptoms. Using the Bielschovsky silver method on sections of her cerebral cortex, Alzheimer observed advanced changes in the neurofibrils which formed tangled bundles of fibrils where neurons were disintegrated. Moreover, he also described the presence of senile plaques (as later named), as small miliary foci containing deposits of a peculiar material (Alzheimer, 1907). Few years later, his former boss, Emil Kraepelin, inaugurated the term Alzheimer's Disease in the new edition of her *Handbook of Psychiatry* (Kraepelin, 1910); changing the original description of Alois Alzheimer in his manuscript of 1907 where he named it as "dementia praecox" (Alzheimer, 1907; Stelzmann et al., 1995).

#### *1.1.2. Clinical features*

Alzheimer's Disease is the main cause of dementia in the elderly and represent a significant health burden. Dementia is generally described as an acquired syndrome of cognitive impairment determined by brain dysfunction.

A recent report estimated that there were 46.8 million people worldwide living with dementia in 2015 and this number is expected to increase to 74.7 million in 2030 and 131.5 million in 2050. Much of the increase will be in developing countries since in these countries the standard of living is becoming higher (Prince et al., 2015).

The clinical diagnosis of Alzheimer's disease is conducted following the National Institute on Neurological and Communicative Disorders and Stroke and the Alzheimer Disease and Related Disorder Association (NINCDS/ADRDA) criteria which was established in 1984 and recently reviewed (McKhann et al., 1984, 2011; Dubois et al., 2007). The NINCDS/ADRDA criteria define AD as a gradual and progressive decline in two or more cognitive domains confirmed by clinical neuropsychological testing and associated with impairment in social and occupational functions. These criteria allow the clinical classification of AD into "probable" and "possible", the diagnosis is confirmed as "definitive" by means of a histopathological exam of the brain after the death of the patient. The criteria established by the Diagnostic and Statistical Manual of Mental Disorders, whose Fifth Edition has become recently available (DSM-5) are equally applicable as the NINCDS/ADRDA criteria (Tarawneh and Holtzman, 2012; American Psychiatric Association, 2013).

Several tests are commonly used to evaluate patients suspected of dementia. Among the cognitive screening tests, the most used is the Mini-Mental Status Examination (MMSE) which consist of nineteen items measuring orientation, memory, concentration, language and praxis (Folstein et al., 1975). The most widely applied instrument of clinical staging which measures the severity of dementia is the Clinical Dementia Rating (CDR). The CDR is a 5-point scale obtained by the evaluation of the subject through a structured interview which covers six domains of cognitive and functional performance: memory, orientation, judgement and problem solving, community affairs, home and hobbies and personal care (Morris, 1997). Another frequently used scale for measuring cognition, especially in clinical trials, is the Alzheimer's Disease Assessment Scale-Cognitive (ADAS-Cog), which consist of 11 parts evaluating cognitive functions (Mohs et al., 1997).



The testing of biomarkers such as the level of A $\beta$ <sub>42</sub> in the CSF is used by far only for research purposes and permit to describe the individuals as “probable or possible AD dementia with evidence of the AD pathophysiological process” (McKhann et al., 2011; Tarawneh and Holtzman, 2012). The existing dichotomy between the neurobiology of AD and the clinical manifestations has stimulated a strong debate since the asymptomatic pathological manifestation of the disease and the early appearance of symptoms related to pathophysiological and/or topological markers might be considered for the more recent therapeutic approaches that could prevent or definitely block the disorder. New research criteria have been proposed by the International Working Group for New Research Criteria for the Diagnosis of AD permitting the diagnosis of AD with a high level of accuracy even at a prodromal stage. According to this new algorithm, the diagnosis of AD is made when concur both clinical evidence of the disease and *in vivo* presence of biological markers (Dubois et al., 2007, 2010).

Cognitive symptoms in AD appear over a decade after the beginning of the pathology and they progress very slowly in the early stages of mild AD. At the beginning, most individuals present short-term memory impairment with difficulty in learning and recalling new information, in addition, aphasia, disturbances of visuospatial skills may occasionally arise. Slight environmental disorientation and language impairment start to appear. Early AD affected people usually experience difficulties with executive functions, such as planning and organizational tasks, insight, judgement and problem solving. In this stage some cases exhibit also behavioral changes as apathy and reduced motivation and depressive symptoms. The patients are typically unaware of their illness (Tarawneh and Holtzman, 2012; Cummings, 2016). All these symptoms become more severe with the progression of pathology. Patients with moderate to severe AD show serious memory deficit in retaining new information, marked disorientation problems also in familiar environments, inability to recognize relatives and aggravated decline of executive functions. In addition, at advanced stages patients manifest neuropsychiatric symptoms, which include agitation, hallucinations, delusions, disruption of sleep-wake cycles, anxiety and depression. All cognitive functions are compromised at late stages of the disease, patients

totally depend on others and need a full time nursing care (Tarawneh and Holtzman, 2012; Cummings, 2016).

An intermediate stage between normal aging and dementia has been defined as “mild cognitive impairment” (MCI; Petersen et al., 2011). The main criteria to define MCI is the memory impairment confirmed by a cognitive test, but revisions introduced also the evaluation of executive functions in the diagnosis, generally daily living activities are preserved in MCI patients. The MCI criteria might be useful for the identification of cases at high risk of AD even if some individuals diagnosed of MCI never develop AD, but they later show to have other kinds of non-AD dementia, some patients remain stable and others regress probably because of a misdiagnosed depression (Tarawneh and Holtzman, 2012).

The most important risk factor for AD is age, since the clinical symptoms onset is usually after the age of 50. With regards to the age of appearance of the symptoms, there is a distinction between an *early-onset* (AD) that affects people younger than 60 years and a *late-onset* Alzheimer’s Disease which is characterized by the manifestation of the syndrome after the age of 60. Patients with early-onset AD frequently have a familial history that might be associated also with genetic mutations involving the genes encoding for amyloid precursor protein (APP), presenilin-1 (PS1) and presenilin 2 (PS2). Nevertheless, AD is mostly a sporadic, age-dependent, late-onset disease. Moreover, AD is more frequent among women than men and in individuals that bear the Apolipoprotein E4 allele form (Rebeck et al., 1993). Comorbidities that might contribute to AD development are hypothyroidism, vitamin B12 deficiency and depression (Tarawneh and Holtzman, 2012; Cummings, 2016).

### ***1.1.3. Pathogenic hallmarks***

Alzheimer’s Disease is neuropathologically characterized by the extracellular deposition of  $\beta$ -amyloid ( $A\beta$ ) proteins with the formation of neuritic plaques, and the intraneuronal presence of aggregated hyperphosphorylated tau proteins, which generate neurofibrillary tangles and neuropil threads. The distribution pattern of these typical hallmarks in the human AD brain was well described and classified in sequential stages by Braak and Braak in 1991 (Braak and Braak, 1991). This

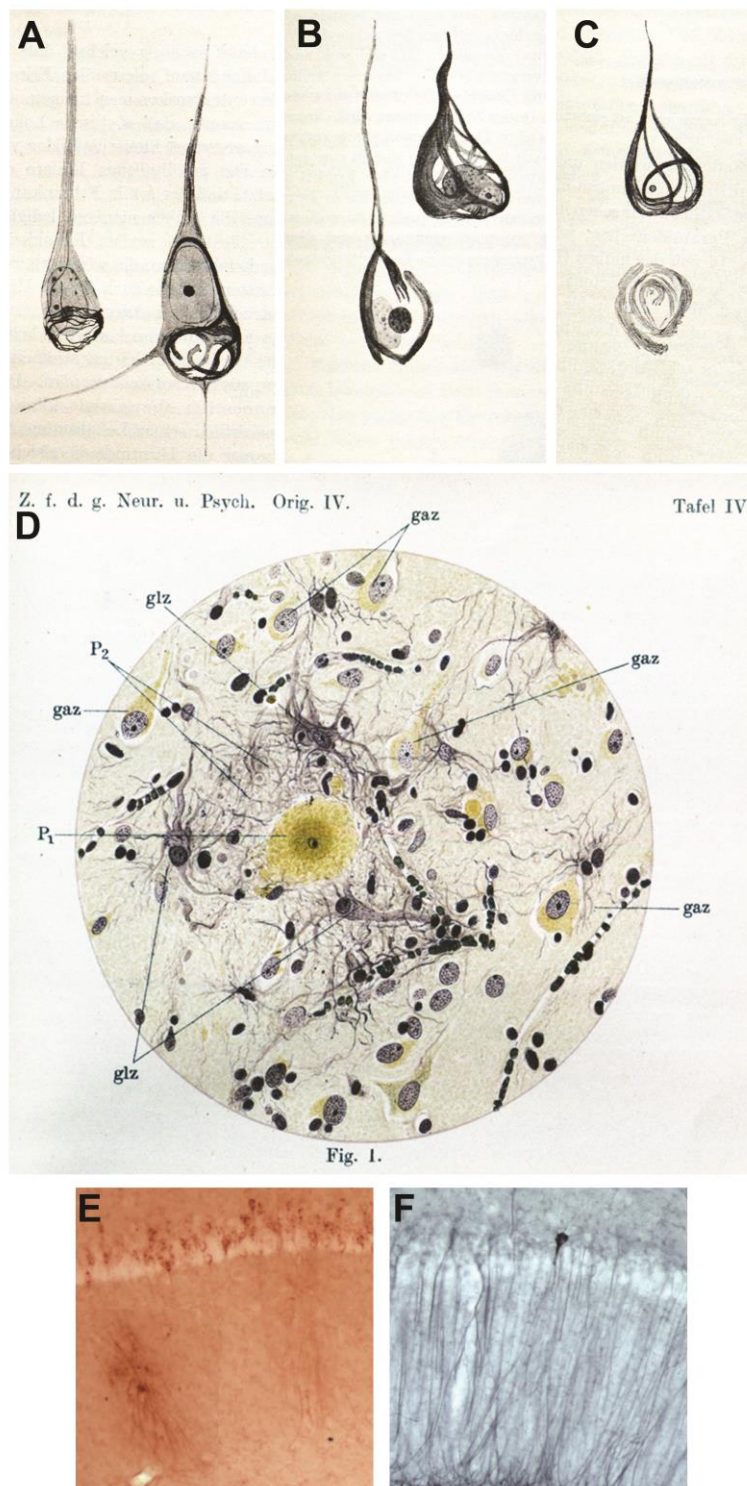


**Figure 1.1 The pathogenic hallmarks of AD.** (A-D) Drawings of A. Alzheimer: (A) Example of neurofibrillary changes at early stages of AD. (B) Fibrillary changes in neurons at a progressed stage of AD. (C) Neurofibrillary changes at terminal stages of AD. (D)  $\beta$ -amyloid plaque (P1) surrounded by reactive astrocytes (glz). Adapted from Alzheimer, 1910. (E) Intracellular and extracellular accumulation of  $A\beta$  in the pyramidal layer of hippocampal CA1. (F) Intracellular accumulation of hyperphosphorylated tau in the pyramidal layer of hippocampus of the 3xTg-AD mouse model (picture from personal unpublished material of Rodríguez J.J.).

histopathological classification is routinely used in the post-mortem biopsy examination to confirm the AD diagnosis. These features are followed by alterations of neuroglia such as astrogliosis and atrophy of astrocytes and microglial cell activation, neuronal and synapse loss and synaptic dysfunction, the latter usually parallel tangle formation (Olabarria et al., 2010, 2011, Rodríguez et al., 2010, 2013; Serrano-Pozo et al., 2011; Yeh et al., 2011; Fig. 1.1 A-D).

Macroscopically, a typical cortical atrophy can be observed by means of MRI scan. This atrophy affects symmetrically mainly the medial temporal lobes and with a lesser severity the primary motor, sensory and visual cortices and result in cortical thinning and lateral ventricles dilatation (Serrano-Pozo et al., 2011).

#### ***1.1.4. Braak stages***

The cerebral cortex, mainly the isocortex, is the main site of amyloid deposition. Cases with severe neurofibrillary (NF) changes consistently show high densities of amyloid deposits, while those rich in amyloid are not always affected by NF changes. Moreover, a few cases with moderate NF changes do not reveal the presence of amyloid (Braak and Braak, 1991). Braak and Braak described two different classifications: one on the basis of amyloid pathology (stages A, B and C) and another one on the basis of tau pathology progression (stages from I to VI). The distribution pattern of amyloid deposits permits to identify three stages (Fig. 1.2 A). In *stage A*, few amyloid deposits are found in the basal portion of frontal, temporal and occipital isocortex, the hippocampal formation is devoid of amyloid, while the presubiculum and the entorhinal cortex are weakly stained. In *stage B* almost all isocortical association areas present amyloid deposits, the basal portion of frontal, temporal and occipital isocortex show a typical laminar distribution of the deposits, the hippocampal formation is only mildly involved in subiculum and CA1; bands of amyloid may also be present in the entorhinal cortex (EC). The *stage C* is characterized by the presence of densely packed amyloid deposits in virtually all isocortical areas with a laminar distribution. Also primary isocortical areas (sensory and motor core fields) show depositions. The hippocampal formation shows the same pattern for *stage B* (Braak and Braak, 1991).

Two kinds of neurofibrillary changes can be distinguished in AD brains: neurofibrillary tangles (NFTs) and neuropil threads (NTs). NFTs develop within the nerve cell soma from where they may extend into the dendrites; when the parent cell deteriorates, the NFT converts into an extracellular structure (“ghost tangle”). NTs consist of argyrophilic processes of nerve cells loosely scattered throughout the neuropil. NFT and NT show a regular distribution pattern, hence their observation made possible the distinction of six stages grouped in the *transentorhinal*, *limbic* and *isocortical stages* (Fig. 1.2 B; Braak and Braak, 1991). In the first two stages (I and II), the *transentorhinal stages*, the neurofibrillary changes are confined to the transentorhinal region, a transition zone between the proper entorhinal cortex and the temporal isocortex. In the *limbic stages*, the stages III and IV, both transentorhinal and entorhinal cortex are severely affected, but in stage III “ghost tangles” can be observed only in the transentorhinal region, while in stage IV they are extended also to the entorhinal region. The hippocampal formation in stage III is mildly involved in the CA1 region and subiculum. Some changes are exhibited in the basal portion of frontal, temporal and occipital association areas. Most cases display mild changes of magnocellular forebrain nuclei, anterodorsal nucleus of the thalamus, and amygdala. These latter changes are all more severe in stage IV. In the *isocortical stages* V and VI all the previous changes are more aggravated and extended virtually all components of the hippocampal formation are involved as well as all isocortical association areas are affected. In stage VI there is a consistent loss of neuronal cells, accompanied by numerous ghost tangles in the EC and hippocampal CA1. NTs are present also in the primary sensory areas, alterations are now extended to the reticular nucleus of the thalamus and the lateral tuberal nucleus of the hypothalamus. Besides, the extrapyramidal system and substantia nigra are also involved in this stage (Braak and Braak, 1991).

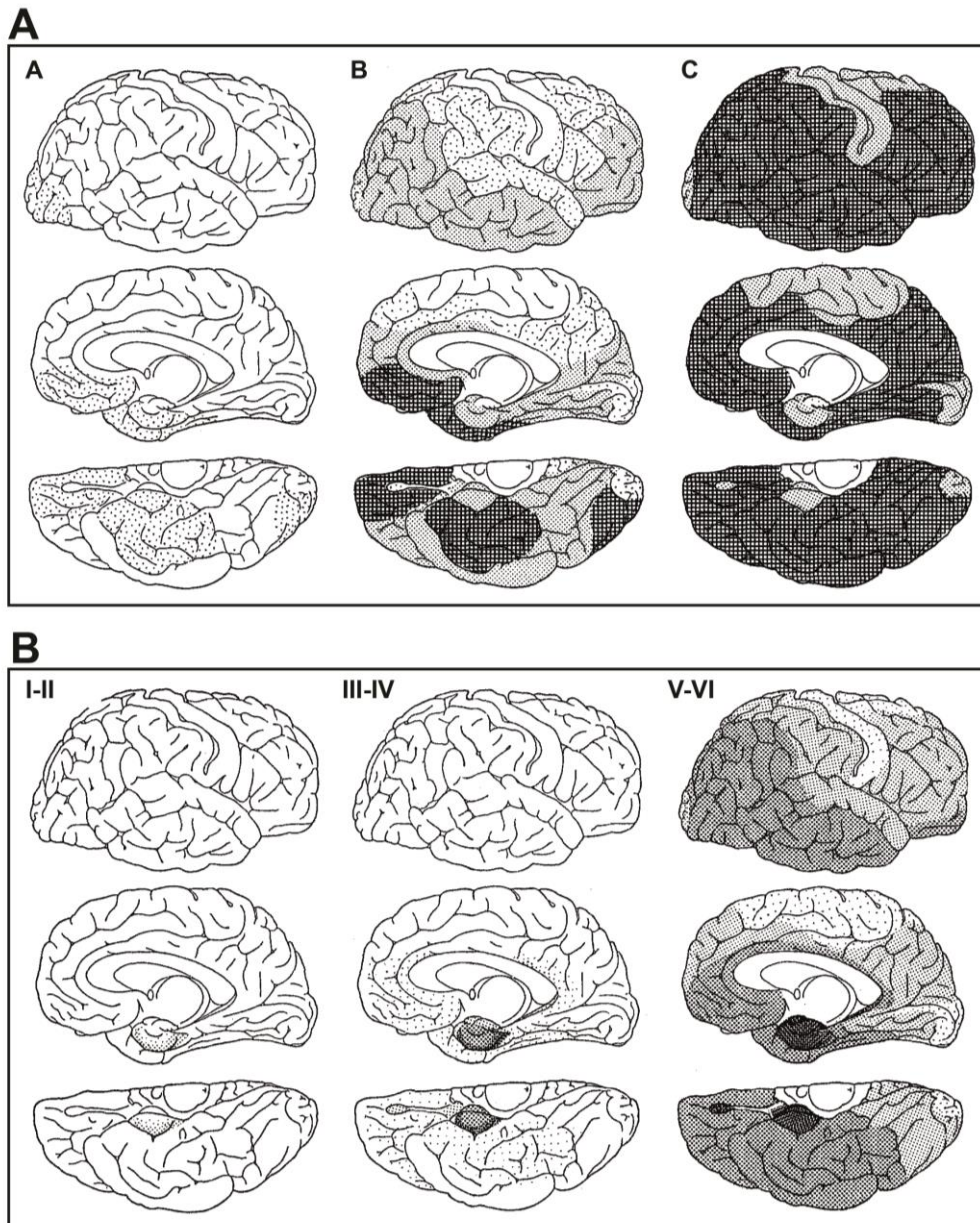


**Figure 1.2 The Braak staging of A $\beta$  and tau pathology in AD brains.** (A) The three stages of amyloid pathology in AD brains (stages A, B, C from left to right). (B) A simulation that summarize the distribution of the six stages of diffusion of the NFTs in the AD brains (trans-entorhinal stages, I and II; limbic stages, III and IV; isocortical stages, V and VI). Adapted from Braak and Braak, 1991.

### ***1.1.5. APP function and processing***

Normal brains physiologically produce A $\beta_{40}$ /A $\beta_{42}$  peptides from the amyloid precursor protein (APP) cleavage and among these two variants, A $\beta_{40}$  is the most abundant, while A $\beta_{42}$  is the most prone to aggregate (Masters and Selkoe, 2012). During the development of AD, the ratio of A $\beta_{40}$ /A $\beta_{42}$  changes, A $\beta_{42}$

concentration initially increases in the CSF, next it falls and A $\beta_{42}$  begin to rise in the brain (Steinerman et al., 2008; Shaw et al., 2009). A $\beta$  can aggregate into several forms that coexist in the AD brain, the most studied forms are oligomers, composed by 2 to 6 peptides, and fibrils which fold into  $\beta$ -pleated sheets forming insoluble fibres. Neuritic plaques, one of the two main lesions present in AD brains, are formed by extracellular deposits of filamentous A $\beta$  protein, mostly the A $\beta_{42}$  longer form, but also A $\beta_{40}$  (Selkoe, 2001). Such plaques are associated with axonal and dendritic injuries, dystrophic neurites, activated microglia and reactive astrocytes. Preamyloid deposits or diffuse plaques are considered to be precursors of neuritic plaques, they have an amorphous, non-fibrillar appearance and they are composed exclusively by A $\beta_{42}$  peptides (Selkoe, 2001). Several studies have demonstrated that extracellular A $\beta$  depositions are preceded by an increased accumulation of intracellular A $\beta_{42}$  proteins which contribute to AD progression before amyloid plaques appear (Gouras et al., 2000; Oddo et al., 2003a; Casas et al., 2004; LaFerla et al., 2007; Wirths et al., 2009). Moreover soluble A $\beta$  oligomers and pre-fibrillar deposits are the most deleterious forms of A $\beta$  (Walsh and Selkoe, 2007; Shankar et al., 2008). A $\beta$  peptides not only form senile plaques in the brain parenchyma, but they also accumulate in the vessel walls giving rise to the cerebral amyloid (or congophilic) angiopathy which is the cause of lobar hemorrhages in AD. Interestingly, the more soluble A $\beta_{40}$  peptide is the major constituent of cerebral amyloid angiopathy and it accumulates in the intersitium between the smooth muscle cells of the tunica media of leptomeningeal arteries and cortical capillaries, small and medium size arteries (Serrano-Pozo et al., 2011).

The APP is a single-pass transmembrane protein, type I oriented, with the amino terminus in the lumen/extracellular space and the carboxyl terminus within the cytosol (Kang et al., 1987; O'Brien and Wong, 2010). The specific physiological role of APP in the CNS is still unknown, several studies have demonstrated that during development it could modulate cell growth, motility, neurite outgrowth and synaptic pruning (Young-Pearse et al., 2007), while in the adult brain it could regulate the proliferation, survival and maturation of neurons in the two neuronal stem niches, the subventricular zone (SVZ) and the subgranular zone (SGZ). This

influence has been shown to be positive or negative depending on the area and the neuronal subtype (Wang et al., 2016).

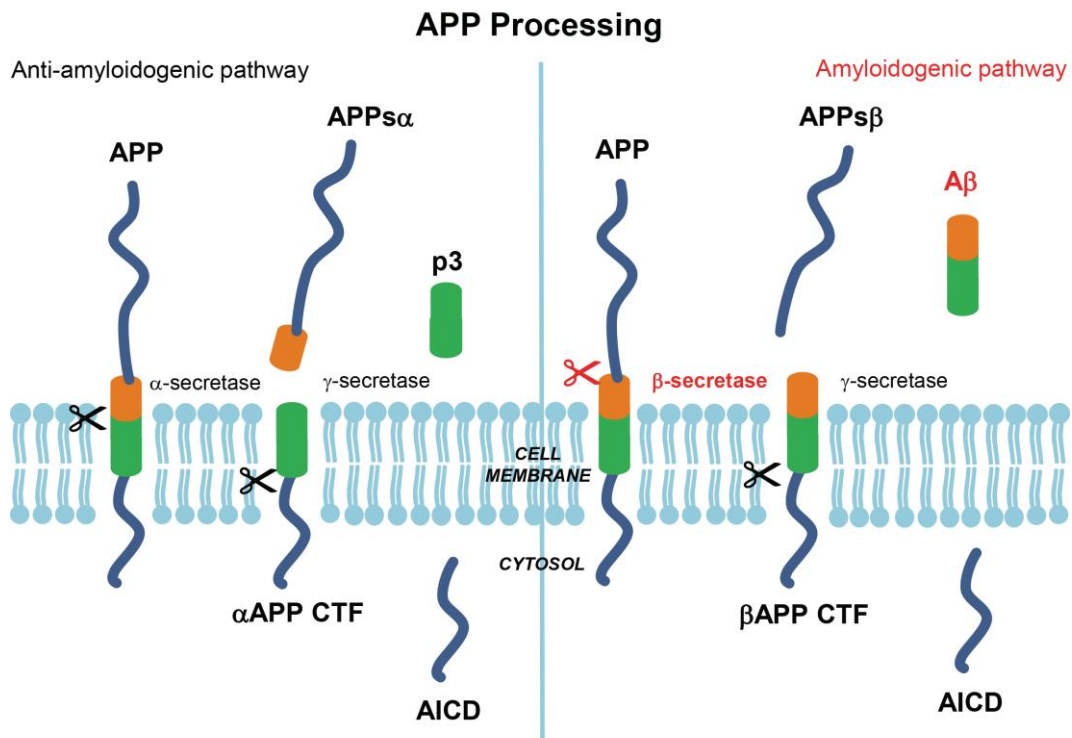


**Figure 1.3 The pathways of APP processing.** The anti-amyloidogenic pathway is mediated by  $\alpha$ -secretase and  $\gamma$ -secretase and determine the extracellular release of APPs $\alpha$  and p3 fragments and the intracellular release of the AICD. The anti-amyloidogenic pathway is initiated by  $\beta$ -secretase (BACE1) with the extracellular release of APPs $\beta$  fragment, later the transmembrane fragment  $\beta$ APP CTF is cleaved by  $\gamma$ -secretase producing A $\beta$  peptides, which will be released in extracellular environment, and the cytosolic fragment AICD (Gardenal, E. personal drawing).

APP can undergo two principal proteolytic pathways: the amyloidogenic pathway, which leads to the production of the A $\beta$  peptide, and the anti-amyloidogenic pathway, which does not generate A $\beta$  (O'Brien and Wong, 2010). Through clathrin-associated vesicles, APP can be transported from the Trans-Golgi network (TGN) to the cell surface or to an endosomal compartment (O'Brien and Wong, 2010). The amyloidogenic pathway occurs in the endosome where APP is first cleaved by the  $\beta$ -secretase enzyme (BACE1,  $\beta$ -site APP cleaving enzyme-1) generating two fragments: the APPs $\beta$ , which is shedded in the lumen, and the carboxy terminal  $\beta$ -CTF or C99 which is subsequently cleaved by the  $\gamma$ -secretase enzyme. Hence,  $\gamma$ -secretase proteolysis of  $\beta$ -CTF produces the A $\beta$  peptide that is then released in the extracellular space through vesicle recycling or degraded in lysosomes and the amyloid intracellular domain (AICD) which is released into the



cytosol and is targeted to the nucleus where it may activate signaling transcription (Fig. 1.3). In the anti-amyloidogenic pathway, APP is processed at the cell surface and is proteolysed in the middle of A $\beta$  region by the  $\alpha$ -secretase enzyme. This cleavage produces the APP $\alpha$  ectodomain fragment, that is released in the extracellular space, and the  $\alpha$ -CTF or C83 carboxy terminal fragment. C83 is then digested by  $\gamma$ -secretase with the release of the extracellular p3 peptide and the AICD (Fig. 1.3 O'Brien and Wong, 2010).

#### *1.1.5.1. $\beta$ -secretase*

The  $\beta$ -secretase enzyme, also called BACE1, is a type-I transmembrane aspartyl protease, it presents its active site in the lumen/extracellular space and it is highly expressed in the brain. It is the enzyme that initiates the amyloidogenic pathway by cleaving APP at the +1 or +11 sites of A $\beta$ . Although a homologous protease, BACE2, was identified, BACE1 is the principal  $\beta$ -secretase in the brain, indeed knock-out mice for BACE1 don't produce A $\beta$  (Cai et al., 2001). For this reason, BACE1 is considered as an important therapeutic target and its inhibition allow to reduce also the production of  $\beta$ CTF fragments which include the A $\beta$  domain and whom accumulation seem to contribute to toxic effects (Citron, 2004; Schenk et al., 2012). The physiological role of this secretase is still under study, in the peripheral nervous system BACE1 contribute in the myelination process after birth, but this function hasn't been confirmed for the CNS yet. A loss of function of BACE1 is related to memory impairment and changes in spontaneous activity, moreover it has also been demonstrated its involvement in the regulation of voltage-dependent sodium channels (Haass et al., 2012a).

#### *1.1.5.2. $\gamma$ -secretase*

The  $\gamma$ -secretase enzyme is a protease complex formed by four essential subunits: presenilin (PS) 1 or 2, nicastrin (NCT), anterior pharynx defective (APH)-1a or APH-1b and the PS enhancer (PEN)-2. PS is a polytopic protein composed by 9 transmembrane domains (TMD) with the two catalytic aspartyl residues localized within TMD 6 and TMD 7; its endoproteolitical cleavage occurs in the same just

mentioned TMDs and it is likely to stabilize the conformation of the active-site aspartates (Steiner et al., 2008). The biological function of the other essential subunits is still not clear. NCT is a type I membrane glycoprotein and it seems to be a selective substrate receptor for the  $\gamma$ -secretase; PEN-2 is required for the endoproteolysis of PS and its stabilization in the protease complex; so far, APH-1 role is poorly understood (Steiner et al., 2008; Zhang et al., 2014).  $\gamma$ -secretase substrates are cleaved several times within their TMDs. The final  $\gamma$ -cleavage of APP is not precise and can generate A $\beta$  peptides of 40 or 42 aminoacids. A $\beta$ <sub>42</sub> peptides aggregate more easily and are believed to have a toxic role in the AD brain (Haass et al., 2012b).

#### *1.1.5.3. $\alpha$ -secretase*

The  $\alpha$ -secretase activity is attributed to several zinc metalloproteinases that belong to the “a disintegrin and metalloprotease” (ADAM) family.

The  $\alpha$ -secretase digest APP within the A $\beta$  portion, at the residue +17, resulting in the anti-amyloidogenic APP processing. In the brain the main  $\alpha$ -secretase activity is due to ADAM10, increased expression of ADAM10 results in a decrease of A $\beta$  deposition, this make ADAM10 a potential therapeutic target for AD (Postina et al., 2004).

#### *1.1.6. Tau structure and function*

The protein tau is one of the first microtubule associated proteins (MAPs) to be characterized (Weingarten et al., 1975). Its hyperphosphorylated, aggregated and insoluble form is the principal component of the neurofibrillary tangles (NFTs), which are one of the main hallmarks of Alzheimer’s disease. Many neurodegenerative disorders have been linked to tau gene mutations and protein alterations, for this reason they are called “tauopathies” (Morris et al., 2011; Arendt et al., 2016).

In the CNS, tau is mostly expressed in neurons, where it is found mainly in the axons (Kempf et al., 1996), but it locates also in the somatodendritic compartments (Tashiro et al., 1997); in addition, it is expressed in oligodendrocytes and astrocytes (Arendt et al., 2016).

Tau protein is formed by four regions: an N-terminal “projection domain”, that projects away from the microtubules, a “proline-rich domain”, a “microtubule-binding domain” (MBD) and a C-terminal domain (Mandelkow and Mandelkow, 2011).

Alternative splicing of exons 2, 3 and 10 can generate six isoforms of tau proteins that differ by the number of microtubule binding repeat sequences expressed and by which N-terminal exons are included (Mandelkow and Mandelkow, 2011).

Tau is physiologically unfolded and has a disordered structure due to its hydrophilic character, which confers to the protein a high flexibility and mobility. The most known function of tau is to stabilize microtubules, probably acting as a spacer through the N-terminal projection domain that is negatively charged and keep microtubules apart via electrostatic repulsion. However, several other functions of tau are under study, since it can interact with many other binding partners. The proline-rich domain is supposed to have a role in cell signaling through the binding and modulation of Src family kinases as Fyn, Fgr and Lck. Tau can also bind to and bundle actin filaments, moreover it interacts with a numerous set of kinases as for instance GSK3 $\beta$ , cdk5, MAP kinase and with other proteins. Also DNA, RNA and lipids have been demonstrated to be tau binding partners (Morris et al., 2011).

Tau is subjected to several post-translational modifications that regulate its function and localization. Phosphorylation is the most studied modification of tau since it is strictly related to the pathogenesis of several neurodegenerative disorders. Most of the phosphorylated sites are localized in the regions flanking the microtubule-binding repeats, the phosphorylation of tau was found to decrease its affinity for microtubules and to regulate its subcellular localization and the interaction with molecules involved in the regulation of axonal transport, cargo delivery to dendritic spines, its association with plasma membrane, apolipoprotein E, Src kinases and other proteins (Arendt et al., 2016). Tau is physiologically highly phosphorylated during fetal brain development (Yu et al., 2009), hibernation (Arendt et al., 2003) and in response of stressor events like head trauma, hypothermia and experimental insulin-dependent diabetes (Planel et al., 2007). In cell cultures, the exposure of neurons to A $\beta$  oligomers or toxic

treatments as hypoxia, glucose, serum deprivation and hydrogen peroxide increased the hyperphosphorylation of tau which in turn detach from microtubules and membranes (Morris et al., 2011).

Hyperphosphorylation of tau is likely the result of an altered activity of tau kinases and phosphatases. When hyperphosphorylated, tau proteins detach from microtubules and deposit in pre-tangles, subsequently this non fibrillary form of tau changes conformation and forms  $\beta$ -sheet aggregates. However, despite being NFTs a typical hallmark of AD, there is evidence that tau is more deleterious in its soluble prefibrillar oligomeric state than in the aggregated form (Arendt et al., 2016).

#### ***1.1.7. Amyloid hypothesis and tau hypothesis***

The most supported hypothesis of AD pathogenesis sustains that the accumulation of the amyloidogenic protein  $A\beta$  is the cause of AD (Glennner & Wong, 1984). Although there is still a strong skepticism about this hypothesis, many studies have been conducted on the basis of this pathogenic mechanism. Indeed, the transgenic animal models of AD developed by far are characterized by the expression of mutant forms of amyloid precursor protein that give rise to an increased production of toxic  $A\beta$ , hence most of the recent therapeutic efforts aim to reduce the overproduction of  $A\beta$  in the brain.

The first evidence of  $A\beta$  dyshomeostasis role in giving rise to AD was the finding that mutations causing familial AD affect the APP gene and Presenilin 1 and 2 genes which encode for the catalytic subunit of  $\gamma$ -secretase and cause an increase in the production of  $A\beta_{42}$  peptides (Scheuner et al., 1996). Moreover, individuals with Down's syndrome, the trisomy of chromosome 21, bear three copies of APP gene, produce more  $A\beta$  and develop AD (Hof et al., 1995). Interestingly, some subjects who have a micro-duplication of chromosome 21 only in the region of APP gene do not develop Down's syndrome but develop AD in their mid-50s (Rovelet-Lecrux et al., 2006). Conversely, protective mutations that decrease the APP cleavage by  $\beta$ -secretase are associated with a lower risk of cognitive decline and AD (Jonsson et al., 2012). Some other genes related to an increased risk of AD are linked to  $A\beta$  dyshomeostasis. For instance, Apolipoprotein E4 (ApoE4)

isoform has been shown to decrease A $\beta$  clearance respect the other Apolipoprotein isoforms (Castellano et al., 2012). The risk genes CR1, CD33 and TREM2, which are component of innate immunity, are probably implicated in maintaining the microglia ability of phagocyte A $\beta$  in AD (Jones et al., 2010). Lastly, after the identification of the AD correlation with genes involved in endosomal vesicle recycling, it has been demonstrated that some of these genes, like SORL1 and PICALM are directly involved in the processing of APP. Moreover, PICALM was also demonstrated to regulate the transport of A $\beta$  across the blood brain barrier (Jones et al., 2010; Selkoe and Hardy, 2016; Zhao et al., 2016).

The causality of A $\beta$  in AD is supported also by studies demonstrating that A $\beta$  oligomers damage synaptic structure and function and impair LTP. What is generally considered the “Achilles heel” in the amyloid hypothesis is the fact that many people who have A $\beta$  plaques don’t develop AD. A study has isolated soluble A $\beta_{42}$  oligomers and amyloid plaques from AD brains and demonstrated that the diffusible A $\beta$  oligomers impair long term potentiation (LTP) and reduce dendritic spine density in normal rodent hippocampus, while insoluble A $\beta$  plaques do not, unless they are previously solubilized to release A $\beta$  dimers (Shankar et al., 2008). Thus the presence of amyloid plaques in normal brains might not cause AD because the more toxic A $\beta$  dimers are not released. The amyloid hypothesis is endorsed also by the *in vivo* temporal appearance of the AD biomarkers before any other pathological feature. In fact, the A $\beta_{42}$  levels in CSF and the deposition of A $\beta$  in the brain cortex seem to appear respectively 25 and 15 years before the symptom onset (Bateman, 2012).

The real validity of the amyloid hypothesis will probably be proved or rejected after the current clinical trials targeting A $\beta$  production will be concluded (Selkoe and Hardy, 2016).

Nevertheless, as previously described, A $\beta$  depositions are not the unique characteristics of AD, since tau pathology has an important role in the pathogenesis of this form of dementia (Braak and Del Tredici, 2013). An interesting debate has recently emerged about moving the causality of AD into a “tau hypothesis”. This hypothesis has arisen by observations that despite being

A $\beta$ <sub>42</sub> present in the CSF several years before the onset of clinical symptoms, intraneuronal tau accumulations appear decades before the deposition of amyloid plaques in the brain (Braak et al., 2013). Moreover, several studies have recently demonstrated that tau alterations start to appear in subcortical regions such as the *nucleus basalis of Meynert*, the *locus coeruleus* and the *raphe nuclei* in early pathology (Braak stages 0 or I). The study of brains from different ages showed that tau lesions are present also in the midbrain of 30 years of age subjects bringing attention to the possibility that tau pathology may begin even much earlier than previously thought (Braak et al., 2011; Attems et al., 2012; Arendt et al., 2016).

## **1.2. THE HIPPOCAMPAL FORMATION: BRAIN AREAS INVOLVED IN MEMORY FORMATION**

### ***1.2.1. Memory formation***

One of the first symptoms to be reported by patients affected by Alzheimer's disease is the loss of memory (Jahn, 2013). Memory can be classified into short-term memory vs. long-term memory and the latter is commonly distinguished into implicit memory vs. declarative memory. These different categories have also neuroanatomical and neurophysiological characteristics. The short-term memory lasts only seconds or minutes and the brain areas mainly related to it are situated in the frontal and parietal lobes. On the contrary, long-term memory could hypothetically have unlimited duration since it determines a *de novo* synthesis of proteins in the cortical areas involved in the specific types of memory. Declarative memory, which is a long-term conscious memory, can be subdivided into episodic and semantic memory. Episodic memory refers to the storage of information related to a specific context of time and place, in other words autobiographical events. Semantic memory corresponds to the storage of information not related to a context, but to general knowledge accumulated during life (Jahn, 2013). In AD, the first impairment involves the semantic memory, mainly affecting verbal fluency and naming (Verma and Howard, 2012). Different regions of the medial temporal lobe have been demonstrated to contribute to the formation and storage of long-term declarative memory, these structures are the hippocampal formation and the entorhinal, perirhinal and parahippocampal cortices (Scoville and Milner, 1957; Suzuki and Eichenbaum, 2000; Suzuki and Amaral, 2004). In addition, the hippocampus and the entorhinal cortex have been demonstrated to be critically involved in spatial navigation and memory, explaining the orientation difficulties of AD patients (Witter and Moser, 2006; Strange et al., 2014). Furthermore, AD patients progressively show impairment in working memory, a kind of short-term memory characterized by the ability to remember information for a short period with the purpose of processing and manipulate them and by its importance for the formation of long-term memory. The pre-frontal cortex is the brain region usually associated to working memory functioning, even if other cortical areas are also

involved. Accordingly, the deterioration of pre-frontal cortex is related to deficits in attention, problem solving, decision making and behaviour (Jahn, 2013).

### ***1.2.2. Histological description of the memory-related regions early affected in AD***

The entorhinal cortex is commonly considered the first affected area in AD, followed by hippocampus and associative and executive cortical areas, but several studies have demonstrated that neurofibrillary tangles appear very early in the nucleus basalis of Meynert (nbM) even before the involvement of the entorhinal cortex (Arendt et al., 1983; Sassin et al., 2000; Mesulam et al., 2004).

#### ***1.2.2.1. The nucleus basalis of Meynert***

The nucleus basalis of Meynert, which is located in the basal forebrain, is a cholinergic nucleus since 90% of the magnocellular neurons in the nbM are cholinergic and belong to the Ch4 group (Mesulam et al., 1983). The Ch4 neurons of nbM project to amygdala and to the entire cortex (Mesulam et al., 1983). In human, these Ch4 neurons permit to topographically divide the nbM into six different regions: the anteromedial, anterolateral, anterointermediate, intermediodorsal, intermedioventral and the posterior (Mesulam and Geula, 1988). Each one of these sectors projects to a different area: the anteromedial projects to medial cortical regions including the cingulate cortex and the anterolateral projects to fronto- parietal opercular regions and amygdala; the anterointermediate part projects to the frontal cortex, the parietal cortex and the temporal cortex, and finally, the posterior region of the nbM sends cholinergic projections to the superior temporal cortex (Mesulam et al., 1983). Although the nbM projects to the entire cerebral cortex, it receives cortical projections only from limbic and paralimbic regions of the brain, including the amygdala. The hippocampus doesn't receive cholinergic innervation from the nbM but from the medial septal nucleus and the vertical limb of the diagonal band nucleus (Mesulam et al., 1983).

The early lesions and neuronal loss in the nbM support the cholinergic hypothesis, which proposes that a cortical cholinergic deficit cause cognitive decline in AD,



since the concentrations of acetylcholine and choline acetyltransferase are remarkably reduced in the cerebral neocortex and hippocampus of AD brains (Bartus et al., 1982; Liu et al., 2015).

The present work is focused mainly in the study of alterations in the hippocampus and entorhinal cortices, which are histologically described more in detail in the next paragraph.

The *hippocampal formation* is a C-shaped elongated structure localized in the medial temporal lobe composed by several adjacent cortical regions which are the *dentate gyrus*, the *proper hippocampus*, the *subiculum*, *presubiculum*, *parasubiculum* and the *entorhinal cortex* (Fig. 1.4A-D). Most of mammals have two hippocampal formations, one in each side of the brain (Amaral and Lavenex, 2007).

#### 1.2.2.2. *The Dentate Gyrus*

The Dentate Gyrus (DG) is formed by three layers: the molecular layer (ML), the granule cell layer (GCL) and the hilus (Fig. 1.4 B, C). This trilaminar structure is present in all the studied species. The molecular layer is mostly occupied by projections, while relatively few cells are present. The projections are composed by the axons that form the perforant pathway and arrive from the entorhinal cortex, and by the dendrites of the granule cells, pyramidal basket cells and hilar cells (Amaral et al., 2007). Two kinds of interneurons were described in the molecular layer: the MOPP cells (molecular layer perforant path-associated cells) (Han et al., 1993), which are multipolar aspiny cells that innervate the outer two thirds of the ML and a type of axo-axonic cells that are located in the inner molecular layer, next to the granule cells, and make synapses with the initial portion of granule cell axons (Soriano and Frotscher, 1989).

The granule cell layer is occupied mainly by tightly packed granule cell bodies. The granule cells are excitatory cells and seem to use glutamate as principal neurotransmitter. They have a cone-shaped tree of spiny apical dendrite that extend through the entire molecular layer and stop at the hippocampal fissure or at the ventricular surface. The unmyelinated axons that originate from the granule

cells are called mossy fibres. The mossy fibres form synapses with the mossy cells, the pyramidal basket cells and other cells of the polymorphic layer and with the pyramidal cells of the hippocampal CA3 (Amaral et al., 2007). At the boundary of the granule cell layer and the hilus, the pyramidal basket cells are located. These cells are inhibitory interneurons, they have a pyramidal-shaped cell body that is larger than the granule cells, a single aspiny apical dendrite that extend to the molecular layer and several aspiny basal dendrites directed to the polymorphic cell layer. The pyramidal basket cells form inhibitory synapses mainly on the cell bodies and dendrites of the granule cells (Amaral et al., 2007).

The hilus, or polymorphic layer, is occupied mainly by the mossy cells, which are innervated by the mossy fibres of the granule cells. The mossy cells have triangular or multipolar cell bodies as large as the basket cells and several thick spiny dendrites, which project distally to the granule cell layer and to the inner third of the molecular layer. In addition to the mossy cells, more types of cells are present in the hilus, the most well described are the HIPP cells (hilar perforant path-associated cell, (Amaral, 1978; Han et al., 1993). HIPP cells are multipolar cells with long spines, their axons extend to the outer two-third of the molecular layer forming symmetrical inhibitory synapses on the dendrites of the granule cells thus being responsible for local inhibition.

#### 1.2.2.3. *The Cornu Ammonis or proper hippocampus*

The *Cornu Ammonis* (CA), so called because the shape resembles the ram's horn of the Egyptian God "Ammon", is subdivided in three areas: the CA1, CA2 and CA3 (Fig.1.4). The CA is characterized by the presence of a single layer of pyramidal neurons, which terminates at the border with the *hilus* of *dentate gyrus*. The pyramidal cell layer (PCL) or *stratum pyramidale* is a compact accumulation of the somas of the pyramidal neurons, but also some interneurons are present such as basket, axo-axonic, bistratified and radial trilaminar cells. The basal dendrites of the pyramidal cells extend in the deep layer called *stratum oriens* (Str Or), while the apical dendrites protrude into the *stratum radiatum* (Str Rad) and terminate in the *stratum lacunosum-moleculare* (Str Lac Mol). The stratum oriens and radiatum are occupied also by horizontal trilaminar cells, basket and

bistratified cells (Witter and Amaral, 2004). In the CA3 region an extra layer is present, the *stratum lucidum* (Str Luc), which locates between the PCL and stratum radiatum and is formed by the mossy fibres arriving from the DG (Amaral and Witter, 1989). The stratum lucidum of CA3 receives the projections from granule cells of the DG and CA3 pyramidal neurons send their projections to CA1 subfield through the Schaffer collaterals (Amaral and Witter, 1989).

#### 1.2.2.4. *The Entorhinal Cortex*

The Entorhinal Cortex (EC) corresponds to the Brodman area 28 and it is so called for being bordered by the rhinal sulcus (Brodman, 1909). It is part of the posterior temporal cortex and is strongly connected with the hippocampus.

The EC is generally subdivided into two subfields: the lateral entorhinal cortex (LEC, Brodman area 28a), which occupy a rostrolateral position in the EC and the medial entorhinal cortex (MEC, Brodman area 28b) that occupy a caudomedial position. The EC lamination is characterized by three superficial layers (I, II and III), the *lamina dissecans* and two deeper layers (V and VI). Layer I or the molecular layer is formed by a compact band of transversely oriented fibres and is almost devoid of neurons, indeed only two types of neurons were described in this layer, horizontal cells and multipolar neurons (MPNs), both of which are GABAergic. Layer II presents mainly principal neurons and large stellate neurons, more distributed in the MEC, and pyramidal-like cells; but also several kind of interneurons are present. Layer III is a wide layer rich of pyramidal cells and less stellate cells and interneurons. Next to the superficial layers there is the *lamina dissecans* that is the cell-sparse fibre layer, it is occupied by occasional pyramidal-shaped neurons and it is better developed in the MEC. Layer V presents three sublayers, the Va layer with large to medium size pyramidal cells and layers Vb and Vc with small and less densely packed pyramidal cells. In this layer are found also horizontal cells and polymorphic MPNs. The last layer, layer VI, is delineated by the white matter and is occupied by pyramidal cells. LEC and MEC are occupied by different types of interneurons and in some layers the principal neurons differ in their morphology and electrophysiologically (Canto et al., 2008).

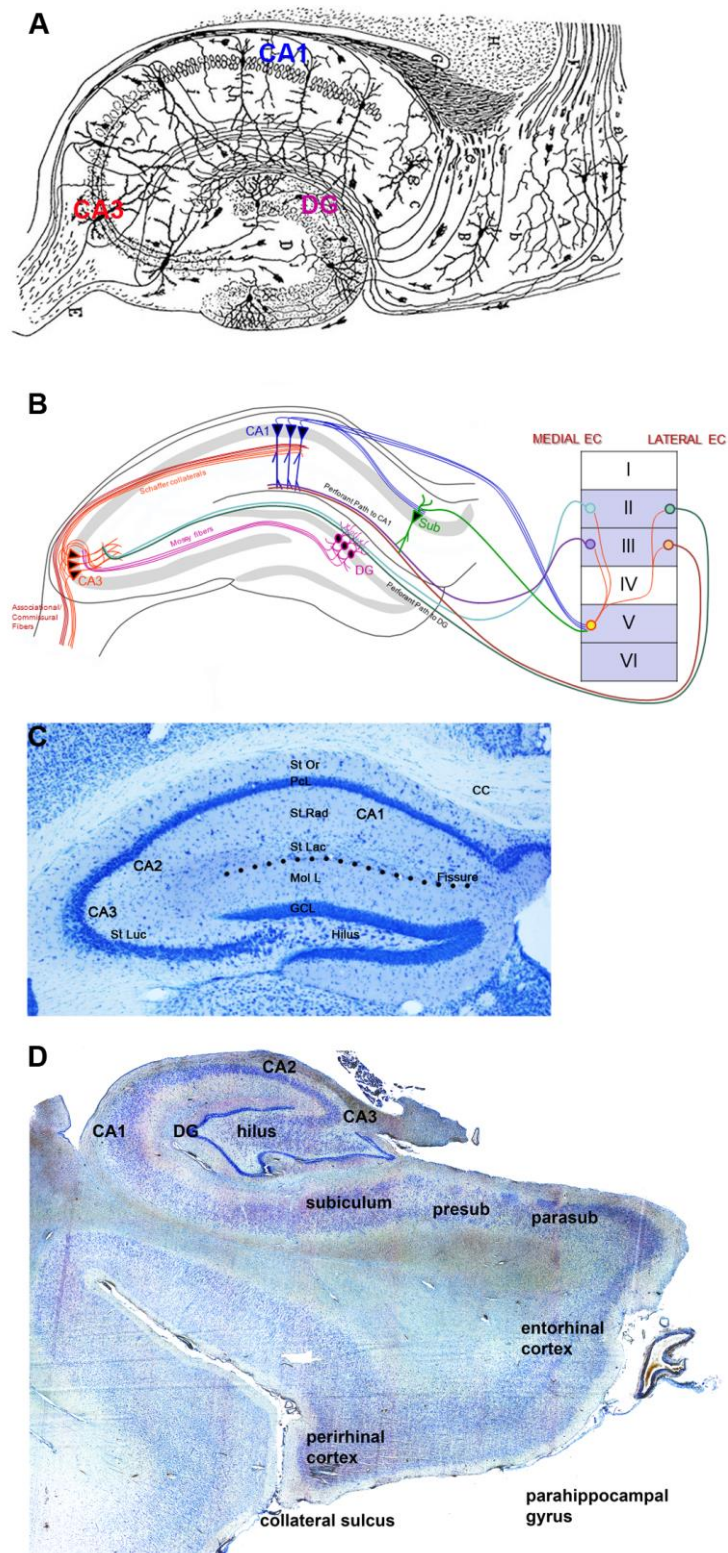


**Figure 1.4 Representation of hippocampal anatomic structure and entorhinal connections.** (A) Drawing of Cajal of a rabbit hippocampus. (B) Representation of the hippocampal loop and the connections between hippocampus and entorhinal cortex. (C) Toluidine stained section of the mouse hippocampus showing the hippocampal subfields and layers (personal picture of Rodríguez J.J.). (D) Toluidine stained section representative of the anatomical subdivisions of the human hippocampal formation (Gardenal E. personal unpublished image).

### 1.2.3. *Hippocampal connectivity*

The connections between the different areas of the hippocampal formation are generally simplified and described as the “trisynaptic circuit” (Fig. 1.4B). The projections start from the entorhinal cortex and extend unidirectionally in a sort of circuit composed by three sets of subsequent links: the perforant pathway projections to the dentate gyrus and CA1, the mossy fibres projections from the dentate granule cells to the CA3 pyramidal cells and the Schaffer collaterals of CA3 pyramidal cells directed to the CA1 pyramidal cells. Subsequently to the trisynaptic circuit, the connections extend from the CA1 back to the subiculum and the EC. This description of the hippocampal connections is largely simplified and a complex intrinsic and extrinsic organization has emerged (Amaral, 1993; Witter et al., 2000).

The EC projects to all hippocampal CA1, CA2, CA3 areas, the dentate gyrus and the subiculum. The connection between the entorhinal cortex and the hippocampus is called *perforant pathway*. Specifically, the projection of neurons from layer II of the EC innervate the outer two-thirds of the dentate molecular layer and the outer portions of stratum lacunosum-moleculare of CA3 and CA2 (Witter, 2007). Neurons of layer III of the EC project to the stratum lacunosum-moleculare of CA1 and to the molecular layer of the subiculum. The fibres from layer II and III distribute along the longitudinal axis in the same way, the cells of the lateral part of entorhinal cortex project to the rat septal hippocampus (caudal level for the monkey), while neurons of the medial part of the entorhinal cortex terminate in the rat temporal hippocampus (rostral level for the monkey) (Witter and Amaral, 1991; Amaral, 1993). The perforant pathways of the lateral entorhinal cortex and medial entorhinal cortex present a different distribution along the transversal axis of hippocampus. Neurons from layer II of the LEC project to the outer third of the dentate molecular layer and CA3 stratum lacunosum-moleculare, while axons originating from layer II of the MEC extend to the middle one third of these layers. Layer III cells from the LEC project to the distal part of the CA1 and the proximal part of the subiculum, whereas the cells from the MEC project to the proximal CA1 and the distal subiculum (Amaral, 1993; Witter et al., 2000; van Groen et al., 2003).

The superficial layers II and III of perirhinal and postrhinal cortices also project to specific areas of the hippocampal formation, which are the molecular layer of CA1 and the subiculum. These connections have a different distribution in the transversal axis of CA1 and subiculum similarly to the LEC and MEC topographical organization (Suzuki and Amaral, 1990; Witter et al., 2000; Naber et al., 2001).

The return projections from the CA1 to the parahippocampal region show a transverse topographical organization similar to the connections from the parahippocampus to the CA1 and subiculum. Axons coming from a specific point of CA1 target approximately one third of the transverse extent of the subiculum, moreover neurons from the proximal CA1 project to the distal subiculum and vice-versa the distal part of CA1 extend to the proximal part of subiculum. Projections from CA1 terminate in the pyramidal cell layer and in the molecular layer.

Projections from the CA1 and the subiculum to the EC terminate in the lamina dissecans and in layer V over the full transverse extent of the EC. The same projections reach also the superficial layers, mainly layer III. The connections to the EC are organized in a similar way to the perforant pathway, but they are also divergent, since the return projection from the CA1 and subiculum to the EC rarely terminate in the originating part of the EC (Witter et al., 2000).

### 1.3. ANIMAL MODELS

So far, several animal models have been used and created through different approaches to study dementia and cognitive decline (Neha et al., 2014). Being memory loss one of the most important features of old age, spontaneous aged models were the first used to study memory deficits and dementia. Aging animals are good models for general cognitive research since they have no central neurochemical manipulations. They exhibit not only neurochemical and morphological alterations, but also cholinergic hypofunction similarly to the pathogenesis of AD (Sherman and Friedman, 1990; Neha et al., 2014).

#### *1.3.1. Chemically induced animal models for AD*

Memory loss and pathophysiological alterations typical of AD can be induced by manipulating neuronal and neurotransmitter pathways with several different chemical compounds.

Scopolamine is an anti-cholinergic drug which can induce aspects of dementia like memory loss and disorientation (Riedel et al., 2009). Colchicine, a microtubule-disrupting agent, causes the loss of cholinergic neurons and pathways determining memory loss and behavioural changes (Kumar et al., 2007). A phenotype similar to dementia can be induced also by increasing L-methionine, which produces endothelial dysfunction as homocysteine level is increased (Koladiya et al., 2009), or by administering sodium azide, which inhibits the mitochondrial respiratory chain, produces free radicals and causes excitotoxicity followed by neurodegeneration and altered processing of APP (Henriques et al., 2005; Luques et al., 2007; Neha et al., 2014). In addition, infusion of A $\beta$  peptides in the brain induces memory loss, A $\beta$  plaques formation and neurodegeneration (Yamada and Nabeshima, 2000).

A valid model of lesion of nbM is the injection of ibotenic acid, which is an N-methyl-D-aspartic acid (NMDA) receptor agonist that leads to neuronal toxicity by overloading calcium into the neurons (Zhang et al., 2013). Some similar neurotoxins and cholinotoxins causing lesions of the forebrain with memory loss are kainic acid (Park et al., 2012), quisqualic acid (Toledano and Bentura, 1994)

and quinolinic acid (Beninger et al., 1986; Yamada et al., 1991). Cholinergic neurons lesions are induced also by the administration of the specific cholinergic toxin AF64 and antibodies against neurotrophic factors (Toledano and Alvarez, 2004).

All the models illustrated above are very good to test drugs effect on memory impairment and cognitive deficits, but they don't develop the two main pathological hallmarks of AD, that are the senile plaques and neurofibrillary tangles. Hence, transgenic mouse models have been generated to study the pathophysiology of AD typical lesions (Gotz et al., 2004).

### ***1.3.2. Transgenic animal models for AD***

#### ***1.3.2.1. Single and double transgenic mouse models of AD***

Transgenic animal models have been created to simulate amyloidogenesis and tau pathology on the basis of genetic mutations related to FAD (Table 1.1). The mouse is the specie commonly used to generate an AD model and several transgenic models have been created so far (Gotz et al., 2004; Cavanaugh et al., 2014; Neha et al., 2014).

Games et al. (1995) developed the first mouse model of amyloidosis by inserting the transgene of mutant APP V717F under the platelet-derived growth factor promoter (PDAPP). This model develops extracellular thioflavin-S-positive A $\beta$  deposits, neuritic plaques, synaptic loss, astrogliosis and microgliosis (Games et al., 1995). Other single transgenic mouse models of amyloidosis developed later and commonly used are the Tg2576 and the APP23 mouse models. The Tg2576 mice express the human APP695 containing the Swedish double mutation K670N/M671L and exhibit an impairment in spatial memory and learning from 9 months of age accompanied by an increased production of A $\beta$ <sub>40</sub> and A $\beta$ <sub>42/43</sub> and deposition of A $\beta$  plaques, in addition gliosis and neuritic dystrophy (Hsiao et al., 1996). The APP23 mice bear the Swedish mutation in the APP751 isoform under the control of the Thy-1 promoter and show a reduced number of neurons in the CA1 region of hippocampus, amyloid plaques, inflammatory processes, neuritic and synaptic degeneration and tau hyperphosphorylation (Sturchler-Pierrat and Staufenbiel, 2000). Other APP mutant mice model bearing the Swedish mutation



are the C3-3 mice (Borchelt et al., 1997) and TgCRND8 mice, the latter is a double mutant for APP since it carries also the V717F mutation (Chishti et al., 2001). Single transgenic mice were generated also with familial mutations of the Presenilin 1 (PS1) gene. The knock-in mouse model bearing a mutated PS1 gene which substitute the endogenous gene shows increased levels of A $\beta$ <sub>42/43</sub> peptides (Nakano et al., 1999).

Double transgenic mice were obtained by crossing APP<sub>Swe</sub> transgenic animals with the mutant presenilin 1 M146L animals to obtain the PSAPP mice (McGowan et al., 1999) or with the PSEN1 A246E (Borchelt et al., 1997). These double mutant APP/PSEN1 mice develop more pronounced and diffuse fibrillary A $\beta$  deposits at younger age (Holcomb et al., 1999) than single mutant and prominent gliosis (McGowan et al., 1999), but they don't show any tau pathology. A mouse model obtained by crossing the APP<sub>SL</sub> mice, which carry the Swedish and the London (V717I) mutations, with the PS1 knock-in mice bearing the M233T and L235P mutations, show a massive neuronal loss in the CA1/CA2 pyramidal neurons, accompanied with a high amount of intracellular A $\beta$  accumulation, but no extracellular A $\beta$  plaques (Casas et al., 2004). All these single and double transgenic mice are good models to study the amyloidogenic pathogenesis but they don't have tau pathology and they don't develop AD pathogenesis.

Several animal models have been developed to create tau pathology so far. The first transgenic mouse model for tau was created by expressing the longest human tau isoform under the control of the Thy1 promoter. These mice exhibit somatodendritic localization and hyperphosphorylation of tau, but they don't have NFTs (Götz et al., 1995). The establishment of a mouse model bearing the mutated tau P301L, typical of frontotemporal dementia, under the Th1.2 promoter showed a stronger pathologic phenotype with accumulation of hyperphosphorylated tau, which is translocated to the somatodendritic compartments and is accompanied by astrogliosis, neurodegeneration and formation of tau abnormal filaments (Götz et al., 2001).

A quintuple transgenic mouse model carries 5 familial AD mutations in APP and PS1/2 genes with the result of a rapid early intracellular A $\beta$  accumulation and extracellular amyloid deposition inducing the death of many pyramidal cortical and subiculum neurons and memory impairment (Oakley et al., 2006).

So far, the only transgenic mouse model exhibiting both amyloid pathology and NFTs similarly to human AD is the triple transgenic mouse model (Oddo et al., 2003a, 2003b).

#### *1.3.2.2. The 3xTg-AD mouse model*

The triple transgenic mouse model of AD was generated by co-injecting the human APP<sub>Swe</sub> and tau<sub>P301L</sub> transgenes into single-cell embryos derived from homozygous mutant PS1<sub>M146V</sub> knocked in (PS1-KI mice). The APP and tau transgenes co-integrated at the same site and the M146V mutation was knocked in to the endogenous PS1 locus, for this reason these mice breed as a “single” transgenic line and it is unlikely that APP and tau transgenes assort independently in the subsequent breeding. The hemizygous mice were also crossed and homozygous mice for all three transgenes were obtained (Oddo et al., 2003b). The penetrance of the phenotype is 100% and the pathology evolve equally in both male and female.

The 3xTg-AD mice exhibit a regional dependent A $\beta$  deposition related with age progression. These mice start to show intraneuronal A $\beta$  immunoreactivity between 3 and 4 months of age in neocortical regions and at 6 months of age in the CA1 area of hippocampus. In 6 months old mice, A $\beta$  proteins begin to accumulate also extracellularly in the frontal cortex and by 12 months of age A $\beta$  extracellular deposits are present also in other cortical areas and in the hippocampus (Oddo et al., 2003a, 2003b).

Tau changes start to appear in the hippocampus of the 3xTg-AD mice around 12 months of age when an intense immunoreactivity for human tau can be detected in the CA1 pyramidal neurons, especially in the somatodendritic compartments. Later, the tau pathology expands to the cortical regions. The 3xTg-AD mice show also immunoreactivity for the antibodies specific for the conformational changes

of tau, as MC1 antibody, and its phosphorylated form, such as AT180, AT8 and PHF1 antibodies.

The 3xTg-AD mice show the same temporal and regional pattern of distribution of A $\beta$  and tau alterations in human AD, moreover the early accumulation of A $\beta$  prior to tangle formation is consistent with the amyloid cascade hypothesis (Oddo et al., 2003a, 2003b).

As in the human AD pathogenesis, this mouse model exhibits an impairment in the basal synaptic transmission and in long-term potentiation (LTP) which is detectable already at 6 months of age when intraneuronal A $\beta$  appears in the CA1 pyramidal neurons suggesting a direct correlation between A $\beta$  intracellular accumulation and synaptic dysfunction (Oddo et al., 2003b). Moreover behavioural tests with the Morris water maze (MWM) showed that this animal model exhibit long-term memory retention starting in parallel with intracellular A $\beta$  accumulation and prior to amyloid plaques and tau pathology (Billings et al., 2005).

The 3xTg-AD mice show also an age-dependent reduction of neurogenesis in the dentate gyrus and in the subventricular zone. This impaired cell proliferation parallels the rise in the number of A $\beta$  positive neurons in the hippocampus and the deposition of amyloid plaques (Rodríguez et al., 2008, 2009b). Changes in astrocytic and microglial morphology were detected in this mouse model. Astrogliosis was observed mainly around amyloid plaques while in general astroglial activation or atrophy were observed with a specific regional pattern in hippocampus and cortical regions (Oddo et al., 2003a; Mastrangelo and Bowers, 2008; Rodríguez et al., 2008). Furthermore, increased microglia activation was detected in the hippocampus parallel with A $\beta$  plaques deposition and increased density of resting microglia was found even before extracellular amyloid deposition (Mastrangelo and Bowers, 2008; Rodríguez et al., 2010, 2013).

<b>Transgenic animal model</b>	<b>Neuropathology</b>	<b>Reference</b>
PDAPP	A $\beta$ deposits	(Games et al., 1995)
APP <sub>Swe</sub>	Plaques	(Hsiao et al., 1996)
APP <sub>Swe</sub> x PS1 <sub>A246E</sub>	Plaques	(Borchelt et al., 1997)
APP23	Plaques	(Sturchler-Pierrat et al., 1997)
PSAPP	Plaques	(Holcomb et al., 1998)
Tg-CRND8 (APP <sub>Swe</sub> /APP <sub>V717</sub> )	Plaques	(Chishti et al., 2001)
PS1 <sub>M146L</sub>	Diffused plaques	(Blanchard et al., 2003)
BACE x APP <sub>Swe</sub>	Plaques	(Mohajeri et al., 2004)
APP <sub>SL</sub> PS1 <sub>ki</sub>	Plaques	(Casas et al., 2004)
APP <sub>Swe</sub> /PS1 <sub>dE9</sub>	Plaques	(Savonenko et al., 2005)
Alz7 (4R tau)	Hyperphosphorylated tau	(Götz et al., 1995)
Tau <sub>P301L</sub>	Tangles	(Lewis et al., 2000)
P301L	Tangles	(Götz et al., 2001)
JNPL3 (4R+P301L)	Tangles	(Lewis et al., 2000; Arendash et al., 2004)
rTg4510 (P301L; Tet-off)	Tangles	(Ramsden et al., 2005)
Tg2576 x JNPL3	Plaques + Tangles	(Lewis et al., 2001)
Tg2576 x VLW (tau <sub>vlw</sub> )	Plaques + Tangles	(Ribé et al., 2005)
3xTg-AD (APP <sub>Swe</sub> + PS1 <sub>M146V+P301L</sub> )	Plaques + Tangles	(Oddo et al., 2003a, 2003b)
5xFAD	Plaques	(Oakley et al., 2006)

**Table 1.1 Summary of the most used transgenic mouse models of AD.**

## 1.4. CALCIUM SENSING RECEPTOR IN AD

### *1.4.1. Calcium Sensing Receptor structure and dimerization in the brain*

The calcium sensing receptor (CaSR) is a G protein-coupled receptor (GPCR) and more specifically it belongs to the subfamily C, which is formed by three distinct groups of receptors. Group I includes the metabotropic glutamate receptors, mGluRs 1–8, which are receptors for the excitatory neurotransmitter glutamate and are widely expressed in the brain. Group II consists of several types of receptors including the CaSRs and the VRs (vomeronasal receptors). The latter are expressed in neurons of the vomeronasal organ of the rat and are pheromones receptors. Group III contains a subfamily of receptors, the  $\gamma$ -aminobutyric acid (GABA)<sub>B</sub> receptors, that bind and are activated by the inhibitory neurotransmitter GABA (Brown and MacLeod, 2001).

The CaSR consists of a large NH<sub>2</sub>-terminal extracellular domain (ECD), a transmembrane domain (TMD) and a COOH-terminal intracellular domain (ICD). The ECD is also called the VFT domain because its bilobed structure resembles a Venus Flytrap. Its proper glycosylation is necessary for its expression in the plasma membrane, moreover it is important for the protein folding and dimerization. The VFT domain is responsible for the binding of Ca<sup>2+</sup>, the CaSR's primary agonist, even if also the TMD might bind Ca<sup>2+</sup>. Other molecules can bind and activate the CaSR through the ECD and TMD such as divalent and trivalent cations (Mg<sup>2+</sup>, Gd<sup>3+</sup>), cationic compounds (neomycin) and organic polycation compounds (spermine, polyamine, amyloid- $\beta$ -peptide, poly-L-arginine). The TMD is formed by 7 transmembrane  $\alpha$ -helices, it is essential for the protein processing, expression in the plasma membrane and stability and it permits the signal transmission along the receptor. It is the binding domain for the "calcimimetics" (NPS R-568, NPS R-467), which are molecules that interact allosterically with the receptor and increase the CaSR affinity for Ca<sup>2+</sup>. The ICD is required for the interaction with G-proteins and the activation of the intracellular cascade of signal transduction, it is also involved in the dimerization of the CaSR (Fig. 1.5) (Msaouel et al., 2004).

The CaSR can be found intracellularly in its immature form or in the plasma membrane after its glycosylation and processing. It is constitutively present in the membrane as a dimer, probably because its dimerization confers more stability, but it can be functional also when expressed as a monomer (Brown and MacLeod, 2001; Gama et al., 2001).

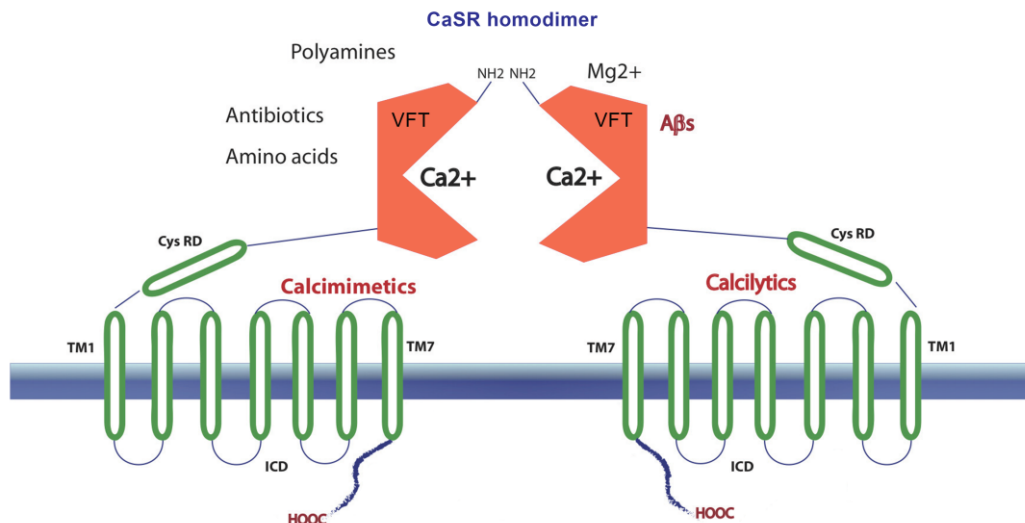


**Figure 1.5 Representation of the CaSR domains and their ligands specificity.** Adapted from Dal Prà et al., 2014.

Interestingly, the CaSR can form heterodimers with Group I metabotropic glutamate receptors (mGluR1a) in hippocampal and cerebellar neurons, but they are expressed differently in other brain regions. The CaSR, when present as heterodimers with mGluR1a, become sensitive to glutamate-mediated internalization, suggesting a role in the regulation of the neuronal function (Gama et al., 2001). The CaSR was demonstrated to co-localize with GABA<sub>B</sub> receptors (R1 and R2) in cultured mouse hippocampal neurones and also co-immunoprecipitate with GABA<sub>B</sub>R1 from brain lysates. The expression of CaSR is increased in GABA<sub>B</sub>R1 knock-out mouse brains and it is suppressed when the GABA<sub>B</sub>R1 was overexpressed in HEK 293 cell culture with a consequent inhibition of phospholipase C activation in response to high extracellular [Ca<sup>2+</sup>] (Chang et al., 2007). On the contrary, co-expression of CaSR with GABA<sub>B</sub>R2 in HEK 293 causes CaSR hyperexpression (Chang et al., 2007). These studies have

pointed out a very complex mechanism of functioning of CaSRs related to their ability of forming homodimers and heterodimers with other GPCRs that seems to be very important for their trafficking to the membrane, their ligand binding sensitivity and thus the regulation of signalling responses (Chang et al., 2007).

#### ***1.4.2. Regional and cellular distribution of the CaSR in the brain***

The CaSR is widely expressed in the body, especially in the parathyroid cells, C cells, kidney cells, intestine, placenta and bone cells (Msaouel et al., 2004).

The study of CaSR expression in rat showed that it is widely distributed throughout the CNS and the regions with highest CaSR cells density are those implicated in fluid and mineral homeostasis, hence CaSR could be important for maintaining such homeostasis. The subfornical organ is the brain region with highest expression of CaSR, which could have an important role in sensing the systemic fluid  $\text{Ca}^{2+}$ , owing to the absence of blood brain barrier in this region. CaSR is also abundantly expressed in the hippocampus, where its distribution is similar to that of mGluRs and iGluRs. It is also present in the olfactory bulb, striatum, cingulate cortex, cerebellum, ependymal zones of the cerebral ventricles and perivascular nerves around cerebral arteries, some CaSR expressing cells were found also in rat dorsal root ganglia (Ruat et al., 1995; Yano et al., 2004). The CaSR has been found abundantly expressed in neurones (mostly in projections and terminals) and in oligodendrocytes *in vivo* (Ruat et al., 1995; Chattopadhyay et al., 1998; Ferry et al., 2000); *in vitro* studies demonstrated its expression also in human primary astrocytes and in rat microglia (Chattopadhyay et al., 1999a; Dal Pra et al., 2005).

#### ***1.4.3. Functions of CaSR in the nervous system***

CaSR is known to be involved in the systemic  $[\text{Ca}^{2+}]$  homeostasis in organs like parathyroid glands, kidneys, bone and gut where it is abundantly expressed. However, its function in the brain is still not totally understood. Local small changes of extracellular ionized  $[\text{Ca}^{2+}]$  occur also in the brain during physiological activities like synaptic transmission, development and sleep. These

fluctuations in extracellular  $[Ca^{2+}]$  are detected by CaSR which can activate specific responses (Ruat and Traiffort, 2013).

Numerous functions have been assigned to CaSR expressed by neurons in the CNS from regulation of neuronal growth and migration, to the role in neurotransmission and synaptic plasticity.

The study of CaSR transcripts expression in mouse sympathetic neurons of the superior cervical ganglion (SCG) demonstrated a role of CaSR in enhancing axon growth and branching to distal targets, but not in the early axonal outgrowth. Indeed, the sympathetic axons ramify to their distal targets and broadly branch in the immediate perinatal period when also CaSR mRNAs noticeably increase. This finding was proved both using calcimimetic and calcilytic modulators of CaSR and expressing wild-type and dominant-negative CaSR protein in SCG neurons. Also the comparison of sympathetic neurons from wild-type and CaSR-deficient mice confirmed the direct involvement of CaSR in neurite growth in this specific developmental window (Vizard et al., 2008). CaSR expression level has been demonstrated to increase also in rat hippocampal pyramidal neurons several days after birth. In detail, CaSR proteins rise markedly at 10 days postnatally and last until 30 days, when their expression begins to diminish to reach the lower adult levels. In this time frame, long-term potentiation is first induced and the development of hippocampus proceeds most rapidly supporting the idea that the CaSR may have a role in the functional maturation of hippocampus and other brain regions (Chattopadhyay et al., 1997). Furthermore, Vizard et al. found that the CaSR takes part also in the regulation of dendritic growth in hippocampal pyramidal neurons in postnatal mice, therefore it may contribute to the mechanisms of learning and memory formation (Vizard et al., 2008).

The involvement of CaSR in cell migration has been proposed in a study on neurons synthesizing gonadotropin-releasing hormone (GnRH). Elevated extracellular  $[Ca^{2+}]$  stimulated chemotaxis of GnRH neurons from the basal forebrain to the preoptic area of anterior hypothalamus, this mechanism was mediated by CaSR with a partial contribution of the monocyte chemoattractant protein-1 (MCP-1) (Chattopadhyay et al., 2007). The hypothesis that CaSR might be involved in neurotransmission and synaptic plasticity was first advanced after



the finding of CaSR expression in nerve terminals (Ruat et al., 1995). Extracellular  $\text{Ca}^{2+}$  is necessary for synaptic transmission. When an action potential invades a nerve terminal,  $\text{Ca}^{2+}$  channels in the presynaptic terminal open and allow the transient entrance and increase of intracellular  $\text{Ca}^{2+}$ .  $\text{Ca}^{2+}$  triggers synaptic vesicle exocytosis, thereby releasing the neurotransmitters contained in the vesicles and initiating synaptic transmission (Katz and Miledi, 1967).

Several studies have demonstrated that CaSR can activate Nonselective Cation Channels (NSCC) when stimulated by its polycationic agonists or after falls in extracellular  $[\text{Ca}^{2+}]_o$  (Chen et al., 2010). It has been proposed that the decrease in  $[\text{Ca}^{2+}]_o$  in the synaptic cleft may act as feedback to presynaptic CaSR and the associated increased activity of NSCCs may increase action potential duration; in this way CaSR may influence synaptic transmission through a homeostatic pathway to prevent synaptic failure when  $[\text{Ca}^{2+}]_o$  falls (Ye et al., 1996).

Activation of CaSR was demonstrated to induce also a distinct form of spontaneous glutamate release independent on  $\text{Ca}^{2+}$  influx, that could be important for the formation of new synaptic connections (Vyleta and Smith, 2011).

*In vitro* studies conducted in the human astrocytoma cell line U87, and primary cultures of rat microglia and oligodendroglia showed that CaSR stimulates  $\text{Ca}^{2+}$ -activated  $\text{K}^+$  channels, contributing to local ionic homeostasis following the lowering of  $[\text{Ca}^{2+}]_o$  due to increased neuronal activity; it has been hypothesized that CaSR could play a role in microglia activation, but this hasn't been demonstrated yet (Chattopadhyay et al., 1998, 1999a, 1999b). The CaSR expression was found at high levels in oligodendrocyte progenitor cells (OPCs) until the pre-myelinating stage and decreased by several folds in the mature oligodendrocytes (Chattopadhyay et al., 2008). High  $[\text{Ca}^{2+}]_o$  acting via CaSR promoted the proliferation of oligodendrocyte progenitor cells and stimulated the increase of the mRNA levels of myelin basic protein in preoligodendrocytes. In addition, myelin basic protein levels were significantly reduced in the cerebellum of CaSR-null mice during development. The study of a case of neonatal hyperparathyroidism due to homozygous inactivating mutations of the CaSR showed a decrease in white matter associated with delayed myelination (Ward et al., 2004). Finally, the analysis of CaSR mRNA revealed that it co-localizes with

the myelin basic protein in rat brains during the first weeks after birth and also in mature oligodendrocytes (Ferry et al., 2000). This confirms that the CaSR is probably involved in the development and function of oligodendrocytes (Ruat and Traiffort, 2013).

#### ***1.4.4. CaSR role in the pathogenesis of AD***

The first evidence of CaSR correlation with AD was given by a study that reported the direct activation of CaSR by  $\beta$ -amyloid in rat hippocampal neurons (Ye et al., 1997). It was demonstrated that the exposure of neurons to A $\beta$  produces a CaSR mediated activation of NSCC, indeed these channels are not activated by A $\beta$  in neurons from mice with disrupted CaSR<sup>-/-</sup> (Ye et al., 1997). Nevertheless, the molecular mechanism of A $\beta$  interaction with CaSR is not clear. Some hypothesis sustain that it is possible that either  $\beta$ -amyloid fibrils or variously sized oligomers, having regular positive charges, mimic CaSR agonists, or hydrophobic interactions between  $\beta$ -amyloid and CaSR may take place (Ye et al., 1997). Furthermore, a genotyping study demonstrated a direct correlation between CaSR and AD, and confirmed that the CaSR can be activated by A $\beta$  as well as by apoE (isoforms 3 and 4) (Conley et al., 2009). The direct interaction of CaSR with A $\beta$ <sub>42</sub> and the formation of A $\beta$ •CaSR complexes was demonstrated in normal human cultured astrocytes by the utilization of *in situ* Proximity Ligation Assay (Söderberg et al., 2006; Dal Prà et al., 2014).

Several studies conducted on human cortical primary astrocytes demonstrated, for the first time, the real pathogenic involvement of CaSR in AD. The first experiments on the CaSR in normal adult human astrocytes showed that it has a role in the activation of NOS (Nitric Oxide Synthase)-2 enzyme. Astrocytes, when activated by pro-inflammatory cytokines, present increased expression and activation of NOS-2. This enzyme is responsible for NO production, which contributes to the killing of neurons in several neuropathology. It has been shown that treating activated astrocytes with a calcilytic stops their production of NO (Dal Pra et al., 2005). This interesting finding was further studied combining the treatments of astrocytes with soluble A $\beta$ -peptide and myelin basic protein (MBP). All these substances were able to induce a higher release of NO thus to enhance

the effect caused by pro-inflammatory cytokines (Chiarini et al., 2005). These studies pointed out the possibility to use CaSR antagonist to prevent the death of neurons in inflammatory conditions.

But the most important finding related to CaSR was the discovery that its altered activation is related with the increased production and spread of A $\beta$  peptides. First, it was found that the treatment of cortical astrocytes with an A $\beta_{42}$  surrogate induces the production of VEGF-A mediated by the nuclear translocation of the hypoxia-inducible factor (HIF)-1 $\alpha$  and  $\beta$  complexes (Chiarini et al., 2010). The same mechanism induces also a rise in the expression and activity of  $\beta$ -secretase in the first place and then of  $\gamma$ -secretase activity with the result of an increased production and secretion of A $\beta$  peptides (Dal Prà et al., 2011). Interestingly, the treatment of neurons with A $\beta$  is toxic and triggers their progressive death, while astrocytes don't die but start to produce A $\beta$ , promoting the death of the surrounding neurons. Finally, it was proven that the administration of the CaSR antagonist NPS2143 to astrocytes treated with A $\beta$  can block this mechanism of A $\beta$  self-induction and prevent the neuronal death (Armato et al., 2013). The research work described in this thesis demonstrates an increased expression of the CaSR in the hippocampus of the 3xTg-AD animal model, this hyperexpression is specific of the subfields first affected by A $\beta$ -plaques deposition. Hence, an alteration of CaSR related to AD hallmarks is demonstrated also *in vivo* (Chapter 3, Gardenal et al., 2017).

## 1.5. CALCIUM BINDING PROTEINS IN AD

Calcium binding proteins (CaBPs) like calmodulin, calretinin (CR), parvalbumin (PV) and calbindin-D28K are small intracellular proteins diffused in the central nervous system and expressed by specific subtypes of neurons. These CaBPs are able to sense intracellular  $\text{Ca}^{2+}$  and are supposed to play an important role in buffering excess of cytosolic  $\text{Ca}^{2+}$  (Baimbridge et al., 1992). Calcium dyshomeostasis is considered a valid hypothesis of AD pathogenesis and for this reason the study of CaBPs changes in AD could reveal important information on this subject. CaBPs are considered neuroprotective and their reduction in the neurons seem to render them more vulnerable. In particular, PV-positive interneurons are responsible for gamma oscillatory activity, which is reduced during epileptiform discharges, a cognitive dysfunction typical of AD. The restore of the normal function of PV-interneurons demonstrated to be effective in increase gamma activity, decrease epileptiform activity and reduce learning and memory deficits in a mouse model of AD (Verret et al., 2012). An impairment of PV-cells has been demonstrated also in other disorders associated with altered network activity like schizophrenia and autism (Sohal et al., 2009; Fazzari et al., 2010).

Furthermore, the immunolabelling of different CaBPs in the brain is used to distinguish different populations of GABAergic inhibitory interneurons since they are expressed in specific subtypes of interneurons without overlapping each other (Del Río and DeFelipe, 1996; Jinno and Kosaka, 2002, 2006; Maccaferri et al., 2003). Hence, the labelling of interneurons with CaBPs immunoreactivity is considered an extremely reliable biomarker to evaluate possible distinct vulnerability of different GABAergic interneurons subpopulations in specific brain regions. Neuronal network dysfunction and excitability is thought to play an important role in AD pathogenesis, the specific dysfunction of inhibitory interneurons may be the cause of neuronal hyperexcitability which is deleterious for neuronal survival.

The present work specifically focuses only on PV and CR since we have observed significant alterations of these proteins in the hippocampus of the 3xTg-AD mice

(Chapter 4, Zallo et al. in preparation). Here is reported a summary of the alterations in PV and CR expression and cell density in AD human brains and in AD animal models.

#### ***1.5.1. Hippocampal features and distribution of parvalbumin neurons***

The cell bodies of PV interneurons are generally larger than those of other interneurons and they localise mainly in the stratum pyramidale and oriens of the cornu ammonis and in the stratum granulare and the hilus of the dentate gyrus. About 20-24% of the GABAergic neurons contain parvalbumin in the hippocampus. Interestingly, the PV neurons present a weaker staining of GABA than the others GABAergic cell bodies lacking this calcium binding protein (Kosaka et al., 1987; Freund and Buzsáki, 1996; Jinno and Kosaka, 2006). The dendrites of the PV cells spread in all layers and are radially oriented in parallel with the principal cells dendrites, their staining of their arborisation become weaker in the stratum lacunosum moleculare of cornu ammonis and in the molecular layer of dentate gyrus. The majority of PV dendrites present varicosities, but they normally don't have spines. All PV-positive neurons can be classified as basket cells or chandelier cells (also called axo-axonic cells), even if the opposite is not true (Freund and Buzsáki, 1996; Jinno and Kosaka, 2006) and they are responsible for perisomatic inhibition (soma, axon initial segment, proximal dendrites) of principal cells (Freund and Buzsáki, 1996).

#### ***1.5.2. Hippocampal features and distribution of calretinin neurons***

CR-positive neurons are distributed in all layers of hippocampus and they can be differentiated in two main categories on the basis of dendritic morphology and distribution: the spiny CR-immunoreactive neurons and the spine-free CR-immunoreactive neurons.

The spiny CR interneurons are mainly distributed in the hilus and in the stratum lucidum of CA3, the regions rich of mossy fibres. Both somata and dendrites are full of long hairlike spines that form synapses with the mossy fibres, while the axons are not visible with immunostaining being strongly myelinated. The dendrites never enter the stratum granulare or pyramidale. These interneurons

receive inputs from mossy fibres and innervate principal cells dendrites. It is still not clear whether or not they are GABAergic neurons (Freund and Buzsáki, 1996).

The spine-free CR interneurons represent a large group of GABAergic cells which form multiple synapses with other interneurons, in particular they strongly innervate calbindin D28K interneurons, VIP-basket cells and other CR-positive cells, but they don't converge into PV basket and axo-axonic cells (Gulyás et al., 1996). Thus, the spine-free CR neurons are interneurons specialized to innervate other interneurons and because of these peculiar connections they have probably a role as disinhibitory interneurons and they might be involved in the generation of synchronous, rhythmic hippocampal activity (Freund and Buzsáki, 1996; Gulyás et al., 1996). These interneurons are widely distributed in all hippocampal areas and layers and they are usually characterised by axons with numerous varicosities in stratum radiatum and axons that form a horizontal plexus at the border between the stratum oriens and the alveus (Gulyás et al., 1996).

Finally, other CR interneurons are horizontal neurons localized near the hippocampal fissure, their soma is located on either side of the fissure and they seem to be Cajal-Retzius cells (Freund and Buzsáki, 1996).

### ***1.5.3. Parvalbumin alterations in Alzheimer's disease***

#### *1.5.3.1. PV alterations in the hippocampus:*

The hippocampal PV-positive neurons were studied in both AD mouse models and in human Alzheimer's disease brains.

In the APP<sup>SL</sup>/PS1KI double mutant mouse model a regional specific age-related loss of PV-positive neurons were found within the hippocampus. The number of PV neurons was significantly decreased in the stratum pyramidale of CA1 and CA2 in the mice 10 months old respect to the mice 2 months old (Takahashi et al., 2010). This loss in the PV-immunoreactive neurons was explained by the presence of the mutated PS1 gene, since PS1KI mice presented the same alterations, while the APP<sup>SL</sup> mice displayed no differences in the number of PV-positive neurons. The same authors found no differences in the density of PV-

positive neurons in the dentate gyrus of post-mortem human brains (Takahashi et al., 2010).

A study of calcium binding proteins reactivity in the dentate gyrus of the APP<sup>Swe</sup>/PS1<sup>A246E</sup> mouse model found a decrease in the immunoreactivity of PV which was extended in both the granular cell layer and hilus (Popovi et al., 2008). The analysis of parvalbumin-positive neurons in the TgCRND8 mouse model of AD at 6 months of age revealed a significant decrease only in the stratum oriens of CA1 and CA3 hippocampal areas (Albuquerque et al., 2015). This apparent resistance of PV cells in this AD model could be due to the age of the mice investigated, which are younger than in other studies (Takahashi et al., 2010) or it may be related to the different genetic characteristics of this mouse model. Indeed, these mice bear a mutation in the A $\beta$  precursor gene and Takahashi et al. pointed out that in their work PV vulnerability may be due mainly to PS1 mutation.

Conversely, the study of calcium binding proteins in the APP<sup>Swe</sup>/PS1dE9 mouse model exhibited no neuronal loss in transgenic mice 12 months old respect to their controls at the same age and to the 3 months old mice. In addition, the PV immunoreactivity resulted increased in the CA1 and CA3 at 3 months of age and in CA1, CA3 and DG at 12 months of age (Verdaguer et al., 2015). While the increase at 3 months occurred in all sublayers of CA1 and CA3 respect to the control mice, the increase at 12 months was apparent especially in the dendritic projections layers of stratum oriens and radiatum, of hilar and granular cells and of the Inner Molecular Layer (Verdaguer et al., 2015).

In the hippocampal formation of human AD brains a significant reduction of approximately 60% of PV interneurons was observed in both dentate gyrus and Cornu Ammonis areas, while the subiculum and presubiculum didn't show any vulnerability. In the dentate gyrus the alteration affected all layers and was accompanied also by a decreased immunoreactivity of the neuropils. In the Cornu Ammonis the neuronal loss was detected in CA1 and CA2, while CA3 showed only a modest decrease in the density of PV-stained processes (Brady and Mufson, 1997).

#### *1.5.3.2. PV alterations in the entorhinal cortex:*

The analysis of the entorhinal PV-containing neurons in human Alzheimer's disease brains revealed a dramatic alteration in layer II where there was a clear reduction in the immunostaining of both soma and dendrites and in the number of PV neurons. In some cases, also layer IIIb was affected with a decrease in the immunoreactivity and in its width, while the cell density was not altered. Interestingly, the layers II and IIIb didn't exhibit any neurons containing both neurofibrillary tangles and PV (Solodkin et al., 1996; Mikkonen et al., 1999).

#### *1.5.3.3. PV alterations in other cortical areas:*

Studies on cortical areas different from the hippocampal formation and the entorhinal cortex pointed out a different reaction of PV neurons to AD. In the frontal cortex of the double mutant APP<sup>SL</sup>/PS1KI no alteration of PV-positive neurons was found, while the PV cell density resulted increased in the APP and PS1KIho mice (Lemmens et al., 2011). The study of frontal cortex in human AD cases by Arai et al. revealed a vulnerability in PV positive cells that were reduced in number and size (Arai et al., 1987). However other authors found no alterations in PV neurons in the frontal lobe (Ferrer et al., 1993).

A decrease in the levels of PV was found also in the olfactory cortex and olfactory bulb of APP<sup>Swe</sup>/PSEN1De9 mice (Saiz-Sanchez et al., 2012, 2013), while in the piriform cortex of human brains with AD PV-positive cells were found to be increased (Saiz-Sanchez et al., 2014).

A relatively resistance of PV interneurons to degeneration in AD was demonstrated in human neocortex by studies on temporal cortex where only chandelier cells presented dystrophic neurites and sprouting (Ferrer et al., 1991; Fonseca et al., 1993), prefrontal cortex (Hof et al., 1991), superior frontal gyrus (Sampson et al., 1997) and visual cortex (Leuba et al., 1998). Finally, a study on human parahippocampal gyrus demonstrated a reduction in the expression of PV in the AD brains (Inaguma et al., 1992).



#### ***1.5.4. Calretinin alterations in Alzheimer's disease***

##### *1.5.4.1. CR alterations in the hippocampus:*

CR-positive neurons were numerically reduced in the stratum granulare and hilus of the dentate gyrus in the APP<sup>SL</sup>/PS1KI mouse model of AD and also in the PS1KI<sub>ho</sub> mice at 10 months of age respect to 1 month old mice, supporting the assumption that the neuronal loss in the double mutant mouse model may be due mainly to the presence of the mutated PS1 gene (Takahashi et al., 2010). It should be considered that this study only compares transgenic mice of 10 and 1 months of age without considering the wild-type mice, which should be included in the study in order to understand if any alteration at older age may be due to an age effect instead of a pathogenic process. Despite this consideration, Takahashi et al. found the same differences of CR-immunoreactive neurons in the dentate gyrus of Alzheimer's disease patients compared to control subjects (Takahashi et al., 2010).

The study of CR interneurons in the APP<sup>Swe</sup>/PS1<sup>A246E</sup> mice described a trend similar to the model used by Takahashi. Indeed, the numerical density of the CR cells was found decreased in the hilus and in the inner molecular layer of the dentate gyrus (Popovi et al., 2008).

As for the PV analysis, the APP<sup>Swe</sup>/PS1dE9 exhibited a different trend in CR expression respect to the other double mutant mouse model mentioned above. The number of CR-positive cells in the subgranular zone of the dentate gyrus decreased at 12 months of age respect to 3 months of age mice, but this reduction occurred in both mutant and wild-type mice. Interestingly, the numerical density at 3 months of age showed a significant difference in the subgranular zone between the mutant and wild type mice. On the contrary, at 12 months an increase in the CR neurons in the hilus was detected. No differences were found at any age analysed in the CA1 (Verdaguer et al., 2015).

##### *1.5.4.2. CR alterations in the entorhinal cortex:*

In the human brains of severely affected cases of Alzheimer's disease the radial organization of the multipolar and bipolar neurons was disappeared in many

subfields and the dendrites in layers II and III were curled and reduced in length. The clustered fibre staining normally visible around cell islands of layer II was not apparent. In the most severe cases the CR cell density seems to be affected also in layer V compared to control tissues (Mikkonen et al., 1999). In the study of Brion and Résibois in human entorhinal cortex, the CR-positive neurons had a reduced dendritic tree (Brion and Résibois, 1994).

#### *1.5.4.3. CR alterations in the other cortical areas:*

In the frontal cortex of the APP<sup>SL</sup>/PS1KI mouse model of AD no changes were found in the calretinin positive neurons (Lemmens et al., 2011) as previously observed in human AD brains where both prefrontal cortex and temporal cortex didn't exhibited any changes in CR neurons density and characteristics (Hof et al., 1993; Fonseca and Soriano, 1995).

CR-positive neurons were reduced in the olfactory cortex, olfactory bulb, anterior olfactory nucleus and tubercle of APP<sup>Swe</sup>/PS1dE9 mice (Saiz-Sanchez et al., 2012, 2013) and in the piriform cortex of AD cases (Saiz-Sanchez et al., 2014).

CR cell density was found increased in the superior frontal gyrus (Sampson et al., 1997), while no alterations in the CR number were found in the visual cortex (Leuba et al., 1998).

## **1.6. ASTROCYTES AND THEIR INVOLVEMENT IN ALZHEIMER'S DISEASE**

The functional role of astroglia in the brain and its involvement in the pathogenesis of Alzheimer's disease are described in details in several reviews and books (Heneka et al., 2010; Verkhratsky et al., 2010; Kettenmann and Ransom, 2013; Verkhratsky and Butt, 2013; Rodríguez-Arellano et al., 2015; Filous and Silver, 2016). Here there is a brief description of both healthy function and pathologic dysfunction of astrocytes in AD.

### ***1.6.1. Physiological functions of astrocytes***

For a long time, astrocytes were considered as mere supportive cells for neurons, but nowadays we know that they have several different functional roles in the nervous system.

Astrocytes constitute a metabolic link between neurons and blood vessels. Astrocyte endfeet, which were first discovered by Camillo Golgi (Golgi, 1903), embrace brain vasculature and induce the formation of tight junctions in the endothelial cells of the BBB. The tight junctions are important to limit the passive diffusion of substances between the blood and the CNS thus to maintain a strict control of what can enter in the CNS. Following the alterations of the neural activity, astrocytes are able to modulate blood flow by using their perivascular processes to induce vasoconstriction or vasodilatation (Zonta et al., 2002).

Neurons seem to achieve metabolic support from astrocytes through a mechanism called "astrocyte-neuron lactate shuttle". In this model, the glutamate released because of synaptic activity is re-uptaken by the astrocytes by means of a sodium-coupled mechanism of transport. The so caused increase of sodium inside the astrocytes activates the recruitment of glucose and its glycolytic processing, which results in the synthesis and release of lactate to fuel neurons during synaptic transmission (Magistretti, 2006).

The recovery of the glutamate released during the synaptic transmission is carried out mainly by astrocytes via the "glutamate-glutamine shuttle" mechanism, which is of noteworthy importance. Indeed, if glutamate remain in the extracellular fluid too long it will trigger excitotoxic neuronal death. Glutamine synthetase, an

enzyme expressed almost exclusively by astrocytes (Martinez-Hernandez et al., 1977), converts the glutamate into the non-toxic glutamine. The latter is then transported back to neurons through the extracellular space (Danbolt, 2001).

Astrocytes accomplish the control of the extracellular ionic homeostasis necessary for the maintenance of neuronal excitability. This activity requires the transport of ions and a parallel coordinated movement of water that occurs through aquaporins channels present in the perisynaptic and perivascular astrocytic processes.

Synaptic transmission is regulated also by astrocytes which, together with pre- and post-synaptic neuronal terminal, form the tripartite synapse (Araque et al., 1999). Astrocytes express neurotransmitter receptors that can sense the transmitters released by neurons in the synaptic cleft and induce astrocytic excitability. This signaling stimulate the astrocytic release of neurotransmitters such as glutamate, GABA, ATP and D-serine that can modify the synaptic strength and function. Astrocytes can virtually express every kind of neurotransmitter receptor, however different brain regions are endowed with distinct receptors (Lalo et al., 2006, 2008; Jabs et al., 2007; Verkhratsky and Kirchhoff, 2007).

Finally, astrocytes participate also in synaptogenesis, in synaptic maturation and maintenance, moreover they secret factors like thrombospondin that promote post-lesion synaptic plasticity and recovery (Christopherson et al., 2005).

#### ***1.6.2. Astrocytic physiological alterations in Alzheimer's disease animal models and cell cultures***

Glia has started to be considered as an active participant of Alzheimer's disease only recently, but the first evidence of its involvement in AD was already described by A. Alzheimer who reported also glial cells alterations in the brain of his patient (Alzheimer, 1907; Stelzmann et al., 1995).

More recently, several studies have showed that rat astrocytes specifically react to A $\beta$  exposure changing their morphology and activity with dramatic consequences on the functioning of the other cells and the worsening of the disease. Astrocytes were demonstrated to reduce the clearance of A $\beta$  by preventing its phagocytosis by microglial cells (Dewitt et al., 1998). However, human astrocytes also

exhibited a modest activity of A $\beta$ <sub>42</sub> phagocytosis and accumulation by themselves that often result in their lysis with eventual deposition of small plaques throughout the entorhinal cortex of AD patients (Nagele et al., 2003). On the contrary, *in situ* experiments with cultured adult mouse astrocytes incubated on APP mouse brain sections showed that astrocytes can reduce overall A $\beta$  levels in these slices. The endogenous astrocytes incapability of removing A $\beta$  may suggest the hypothesis that a dysregulation of A $\beta$  clearance by astrocytes may cause the accumulation of A $\beta$  in AD (Wyss-Coray et al., 2003).

Some studies have shown impairment in the glutamate-glutamine shuttle activity of astrocytes. Treatment of rat cultured astrocytes with A $\beta$ <sub>1-40</sub> induced a reduction in the uptake of glutamate through GLT-1 due to its activity inhibition mediated by oxidative stress and the altered activity of MAP kinases (Matos et al., 2008). The expression analysis of GLT-1 in the triple transgenic mouse model of AD showed that its level is unchanged in the mPFC during the pathogenesis of AD, while glutamine synthetase level is significantly reduced. In addition, the numerical density of GS positive astrocytes appear to be decreased respect to the non-transgenic mice in their early age. This disruption may affect glutamate homeostasis resulting in the failure of synaptic connectivity therefore to cognitive decline (Kulijewicz-Nawrot et al., 2013).

Both *in vitro* and *in vivo* amyloidosis models demonstrated alterations also in astrocytic calcium homeostasis (Vincent et al., 2010). The treatment of co-culture of rat astrocytes and neurons with A $\beta$  seems to stimulate an increase in the intracellular Ca<sup>2+</sup> signal in astrocytes, but not in neurons. The Ca<sup>2+</sup> signal disruption induces a transient depolarization in mitochondria accompanied by a slow collapse of potential that leads to oxidative damage due to the activation of NADPH oxidase and the depletion of glutathione. Neurons depend on astrocytes for antioxidant support, thus this mechanism brings to neuronal death (Abramov et al., 2003, 2004). A study on cultured rat astrocytes demonstrated that the transient rise of intracellular [Ca<sup>2+</sup>], stimulated by A $\beta$ , probably derive from intracellular Ca<sup>2+</sup> stores and it is intensified by a reduced extracellular [Ca<sup>2+</sup>], which bring to the hypothesis of involvement of receptors that sense extracellular Ca<sup>2+</sup> (Stix and Reiser, 1998). On the other side, A $\beta$  reversibly interrupts

intracellular  $[Ca^{2+}]$  oscillations induced by P2 receptors (Stix, 1998). *In vitro* rat astrocytes exposure to A $\beta$  alters also intercellular calcium waves, which travel faster, further and with a higher amplitude, furthermore, the astrocytic propagation of intercellular calcium signals specifically induced by A $\beta$  apparently requires the opening of gap junctions between astrocytes and the release of ATP (Haughey and Mattson, 2003). *In vivo* multiphoton imaging analysis on mice expressing mutated APP and PS1 proteins showed a global increase of resting calcium waves and more frequent and synchronized calcium transients in astrocytes, also rare intercellular calcium waves between astrocytes were observed (Kuchibhotla et al., 2009). Finally, a two-photon imaging study on different mouse models of AD revealed an increase in spontaneous astrocytic  $Ca^{2+}$  signaling in reactive astrocytes associated with instability of the vasculature tone in the early stages of disease (Takano et al., 2007).

The rapid effect of A $\beta$  in the induction of calcium signaling alterations support the hypothesis that astrocytes may be involved in the early stages of pathogenesis of AD.

### ***1.6.3. Astrocytic morphological and numerical alterations in ageing and Alzheimer's disease mouse models***

During the last decade several morphometric studies have tried to elucidate the astrocytic modifications related with normal ageing and Alzheimer's disease. These studies revealed a complex morphological reaction of astrocytes to age-dependent cognitive decline and AD pathogenesis that appears as concomitant gliosis and atrophy with a specific regional pattern.

Astrocytic morphological analyses have been performed by labelling the cells with specific astrocytic markers, which are the glial fibrillary acidic protein (GFAP), glutamine synthetase (GS) and S100 $\beta$ .

GFAP is a type III intermediate filament protein and it is mainly expressed in reactive astrocyte (Eng et al., 1971, 2000). Glutamine synthetase is an enzyme that catalyzes the condensation of glutamate and ammonia into glutamine allowing neurotransmitter recycling and ammonia detoxification (Albrecht et al., 2010; Rose et al., 2013). S100 $\beta$  is a calcium-binding protein with neurotrophic

functions at low nanomolar concentrations and inflammatory and neurotoxic effects at higher micromolar concentrations (Yardan et al., 2011).

The characterization of these markers in SV129/C57BL6 mice 24 months old demonstrated a structural atrophy of the EC, where the surface area, cell volume and body volume of GFAP-positive cells are reduced respect to 3 months old mice, even though GS-positive cells don't show any change while the profiles of S100 $\beta$  consistently increase. Conversely, the hippocampus showed different alterations, GFAP-positive astrocytes appear hypertrophic, whereas GS profiles decrease in both DG and CA1. S100 $\beta$ -positive cells showed a moderate increase in DG and no differences in CA1 (Rodríguez et al., 2014).

GFAP- and GS-positive profiles were analyzed in the EC, hippocampal formation and mPFC of 3xTg-AD mice and their correspondent non-transgenic mice (Olabarria et al., 2010, 2011, Yeh et al., 2011, 2013, Kulijewicz-Nawrot et al., 2012, 2013).

In the EC, GFAP-IR astrocytes of 3xTg-AD animals showed a morphological atrophy with a significant decrease in the total surface and volume and in the somata volume from 1 months of age, this reduction was sustained through all ages analyzed, however, from 9 months of age onwards the difference between the transgenic animals and their control became almost null because of the parallel age effect in the normal mice. The early changes were more pronounced in the superficial layers, while the alterations at 12 months were evident only in the deeper layer VI. Post-mortem studies revealed astrocytic gliosis only in the intralaminar astrocytes, while the interlaminar astrocytes appeared to be disrupted. In this AD mouse model neither A $\beta$  depositions and senile plaques triggered astrogliosis in any layer of the entorhinal cortex. This might be considered as an incapability of EC astrocytes to react to the pathogenesis and support the neurons, hence it may provide an explanation for the vulnerability of the EC. The GFAP-IR cells numerical density was unaltered in all layers at all ages investigated, neither ageing nor Alzheimer disease triggers cell loss (Yeh et al., 2011). The total expression of GS and the number of GS-IR positive cells were found to be constant between 3xTg-AD animals and their non-transgenic counterpart from 1 to 12 months of age. GS/GFAP-IR morphologic analysis demonstrated that these

cells, despite having GFAP atrophy, are not affected in the intracellular distribution of GS (Yeh et al., 2013).

In the mPFC, the analysis of GFAP-positive profiles of the 3xTg-AD mouse model showed a significant decrease in their cytoskeletal surface area and volume respect to the non-transgenic mice. This reduction was already evident at 3 months of age in the pre-symptomatic and pre-pathological stage and was sustained until 18 months of age. A $\beta$  intracellular accumulation starts to occur in the mPFC of the 3xTg-AD mice at about 6 months of age and increases with disease progression, however extracellular plaques appear only at 18 month of age. These neuropathological alterations were not associated with the presence of GFAP positive astrocytes.

The total number of GFAP-positive astrocytes was constant at every age and didn't show any difference between the 3xTg-AD mice and the control group (Kulijewicz-Nawrot et al., 2012).

GS-positive cells number as well as their cell bodies surface areas were decreased in the 3xTg-AD animals respect to their non-transgenic counterpart. The numerical density was significantly lower in the 3xTg-AD animals from already 1 month until 12 months of age, when the GS-positive astrocytes number started to decrease also in the control animals, reaching the same level of the transgenic mice (Kulijewicz-Nawrot et al., 2013).

In the hippocampus, GFAP-IR astrocytes of 3xTg-AD mice show both atrophic and gliotic morphology associated to different hippocampal subfields and to A $\beta$  plaques. In general, there is a significant reduction in the cell surface and volume and in somata volume in the DG at the early stage of the disease, beginning at 6 months of age and persisting and worsening until 18 months, whereas in the CA1 these atrophic profiles are evident only at 18 months of age. At 12 months of age, A $\beta$  plaques start to accumulate in the hippocampus of the 3xTg-AD animals affecting mainly the CA1, the DG starts to exhibit A $\beta$  plaques at 18 months of age. These plaques are surrounded by hypertrophic GFAP-positive astrocytes which associate also with A $\beta$  loaded blood vessels. To sum up, while atrophic GFAP-IR astrocytes appear at early stages of the pathology, the astrogliotic



astrocytes are exclusively associated with the A $\beta$  plaques and are detectable only in the middle-late stages of the disease (from 12 months onwards, Fig. 1.6).

The numerical density of the GFAP-IR astrocytes doesn't change in both DG and CA1 of 3xTG-AD animals respect to the non-transgenic and it is constant at all ages (Rodríguez et al., 2009a; Olabarria et al., 2010).

The hippocampus of 3xTg-AD mice showed alterations in the GS astrocytic expression and numerical density respect to the normal controls. The GS-IR astrocytes number started to decrease in the DG at 12 months and by 18 months both DG and CA1 showed a reduced numerical density. In parallel, GS expression showed a significant decrease with no regional differences at 18 months of age. GS-IR cells drop in CA1 area is more patent in the vicinity of neuritic plaques, demonstrating an association of GS-IR cell number with A $\beta$  deposit (Olabarria et al., 2011).

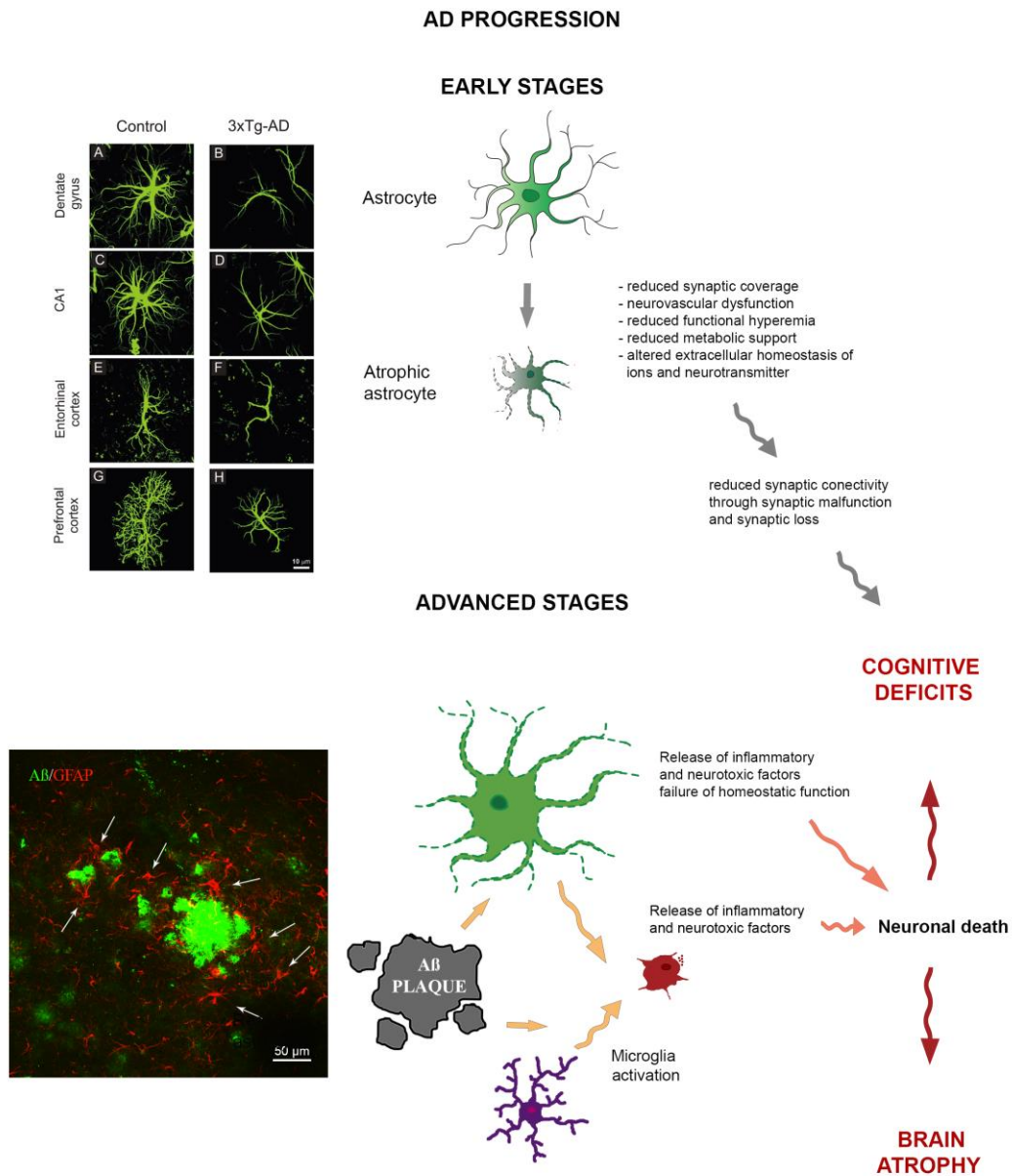


**Fig. 1.6 Drawing representing the astrocytic hypothesis of AD.** At early stages of AD, astrocytes are atrophic and unable to properly carry out their functions, inducing brain damage. At advanced stages of AD astrocytes associated to A $\beta$ -plaques become reactive and hypertrophic, triggering an inflammatory condition in the brain (adapted from Verkhatsky et al., 2010; Rodríguez-Arellano et al., 2015).

## Aim of the Thesis

The aim of this PhD thesis has been to characterize, through an *in vivo* immunohistochemical approach, different aspects of AD pathology in the hippocampus and entorhinal cortex of the 3xTg-AD mouse model, which are the memory-related areas early affected in the onset and progression of AD.

Considering the complexity of AD pathology and the enormous lack of knowledge that we still have regarding its cause and development it is necessary to perform extensive studies to characterize also the non-classical pathological mechanisms, which might have a key role for finding new and more efficient therapies. Therefore, in this work I have reported the immunohistochemical analysis of the hippocampal expression of the CaSR and the calcium binding proteins PV and CR, and the numerical density and morphometric profiles of S100 $\beta$ -positive astrocytes in the entorhinal cortex of 3xTg-AD mice.

In chapter 3, I aimed to study the alterations of expression of the CaSR in the hippocampal subfields affected during the stages of onset and progression of AD main hallmarks which correspond to 9, 12 and 18 months of age in the 3xTg-AD mice. This part of the thesis was thought to demonstrate the involvement of CaSR in the increase of A $\beta$  production and plaques deposition, since previous *in vitro* experiments have demonstrated that the CaSR is directly activated by A $\beta$  oligomers with a consequent increase of A $\beta$  peptides production and secretion and the rise of CaSR expression itself.

The target of chapter 4 was to elucidate the involvement of PV- and CR-positive interneurons in AD by means of an analysis of their expression level and numerical density in the hippocampus of the 3xTg-AD mice. This is the first study of this kind in this mouse model, which is the animal model that better resemble the human pathological hallmarks of AD whose characterization is necessary to get a clear idea of its neuronal networks alterations to allow its application in the evaluation of new drugs.

Lastly, in chapter 5, a numerical and morphometric characterization of astrocytes positive for S100 $\beta$  protein has been done with the aim of examining astrocytic

alterations in the onset and progression of AD. This part of the research had the purpose of clarifying how different subpopulations of astrocytes react and remodel during ageing and AD depending on the region affected and the stage of the disease. This research work had also the aim to demonstrate the correlation of an astroglial dysfunction with AD origin and development.

## Chapter 2

### Materials and Methods

#### 2.1. Animal model

*Chapters 3, 4 and 5*

All animal procedures were carried out in accordance with the United Kingdom Animals (Scientific Procedures) Act of 1986 under the license of the Home Office. All efforts were made to reduce the number of animals by following the 3R's.

The 3xTg-AD mice were generated at the Transgenic Mouse Facility at the University of California, Irvine and are derived from 129/C57/BL6 hybrid, with APP<sub>Swe</sub>, PS1<sub>M146V</sub> and Tau<sub>P301L</sub> mutations (Oddo et al., 2003a, 2003b; Billings et al., 2005; Rodríguez et al., 2008, 2009b). The 3xTg-AD mice progressively develop A $\beta$  plaques and neurofibrillary tangles, with a temporal and regional pattern that closely mimics their development in the human AD brain. In this AD model, A $\beta$  pathology precedes typical indications of tau pathology such as conformational or hyperphosphorylation changes in the tau protein in accord with the amyloid cascade hypothesis.

The non Tg mice were from the same strain with same genetic background. Mice were grouped by gender and genotype and housed under controlled temperature with a light–dark cycle of 12:12 h having ad libitum access to food and water.

#### 2.2. Animal perfusion

*Chapters 3, 4 and 5*

As described previously (Olabarria et al., 2010; Kulijewicz-Nawrot et al., 2012), 3xTg-AD and non Tg control mice of different age groups were intraperitoneally anesthetized with sodium pentobarbital (50 mg/kg). Mice were trans-cardially perfused with 4 % paraformaldehyde (PFA, Sigma, UK) and 0.1 M phosphate buffer (PB) at pH 7.4. Brains were removed and post-fixed in 4% paraformaldehyde overnight, then they were transferred in 0.1 M PB and cut into

4 - 5 mm coronal slabs of tissue containing the entire rostro-caudal extent of the hippocampus and entorhinal cortex, according to the mouse brain atlas of Paxinos and Franklin (2001). The tissues were transferred in a cryo-protectant solution containing 25% sucrose and 3.5% glycerol in 0.05 M PB at pH 7.4 and stored at -20°C. For the immunohistochemistry the tissues were further sectioned in 40-50 µm-thick slices with a vibrating microtome (VT1000S, Leica, Milton Keynes, UK). Free floating sections were collected in 0.1 M PB and stored in the cryo-protectant solution if not used immediately.

### **2.3. Antibodies**

#### *Chapters 3, 4 and 5*

A mouse monoclonal anti-Calcium Sensing Receptor antibody (anti-CaSR; Sigma-Aldrich, UK; C0493) was used for the determination of CaSR expression throughout the dorsal hippocampus. For the identification of intracellular  $\beta$ -amyloid deposits and plaques it was used a monoclonal mouse antibody that reacts with abnormally processed isoforms, as well as precursor forms of A $\beta$ , recognizing an epitope within amino acids 3–8 (EFRHDS; anti-A $\beta$  6E10 [SIG-39320] Signet Laboratories, Dedham, MA), for hyperphosphorylated tau it was used the mouse monoclonal antibody anti-PHF tau AT8 (Innogenetics, Gent, Belgium). For double immunostaining of CaSR with GFAP and A $\beta$ , a rabbit anti-GFAP (Sigma-Aldrich, UK; G9269) and a mouse anti-A $\beta$  Alexa 488 6E10 conjugated antibody (Covance, USA) were used.

For the OD measurement and cell counting of PV and CR neurons, a mouse monoclonal anti-parvalbumin antibody (Swant) and a rabbit polyclonal anti-calretinin antibody (Swant) were used.

For the astrocytes labelling in the entorhinal cortex a mouse monoclonal anti-GS antibody (clone GS6, Millipore), a rabbit polyclonal anti-GFAP antibody (Sigma-Aldrich, UK; G9269) and a rabbit polyclonal anti-S100 $\beta$  antibody (DAKO, Z0311) were used.

Antigen	Host	Type	Dilution	Source	Reference
CaSR	mouse	monoclonal	1:250	Sigma-Aldrich, UK; C0493	
A $\beta$ 6E10	mouse	monoclonal	1:1000	Covance, USA; SIG- 39320	Oddo et al., 2003a
A $\beta$ 6E10 Alexa488	mouse	monoclonal	1:1000	Covance, USA; SIG- 39347	Olabarria et al., 2011
PHF-tau	mouse	monoclonal	1:1000	Innogenetics; AT8	Oddo et al., 2003a Rodríguez et al., 2008
Parvalbumin	mouse	monoclonal	1:2000	Swant	
Calretinin	rabbit	polyclonal	1:2000	Swant	
GFAP	rabbit	polyclonal	1:20000	Sigma-Aldrich, UK; G9269	Olabarria et al., 2010 Yeh et al., 2011
GS	mouse	monoclonal	1:2000	Millipore, MAB301	Olabarria et al., 2011 Yeh et al., 2013
S100 $\beta$	rabbit	polyclonal	1:5000	DAKO, Z0311	Rodríguez et al., 2014

**Table 2.1 Summary of the primary antibodies used in this research work and their details.**

Secondary Antibody	Dilution	Source	Reference
Biotinylated goat anti-mouse	1:400	Vector Laboratories	Olabarria et al., 2010 Yeh et al., 2013
Biotinylated goat anti-rabbit	1:400	Vector Laboratories	Olabarria et al., 2010 Yeh et al., 2011
Alexa595 goat anti-mouse	1:200	Invitrogen; A11005	Olabarria et al., 2010
Alexa488 goat anti-rabbit	1:200	Invitrogen; A11008	Noristani et al., 2011

**Table 2.2 Summary of the secondary antibodies used in this research work and their details.**

## 2.4. Immunohistochemistry

### *Chapters 3, 4 and 5*

A minimum of three coronal sections at levels -1.58 mm/-2.46 mm (dorsal hippocampus, chapters 3 and 4) or -2.92/-3.88 mm (lateral entorhinal cortex, chapter 5) posterior to Bregma, were selected from each animal for immunohistochemistry according to the mouse brain atlas of Paxinos and Franklin (2004). The immunohistochemistry was done following this procedure:

1<sup>st</sup> part:

- To block endogenous peroxidase, the sections were incubated for 30 minutes in 30% methanol in 0.1M PB with 3% H<sub>2</sub>O<sub>2</sub>.
- Sections were rinsed with 0.1M PB for 5 minutes.
- To block aldehydes coming from the fixative that could cause autofluorescence and to help antigen retrieval, the sections were placed in 1% sodium borohydride in 0.1M phosphate buffer (PB) for 30 minutes, that was squirted over tissue during incubation.
- Sections were rinsed copiously with PB until no bubbles remain.
- Tissue was rinsed in 0.1M tris saline buffer (TS, 0.9% NaCl) 2 X 5 minutes.
- The sections were incubated in blocking solution (0.5% BSA and 0.25% Triton in 0.1M TS) for 30 min.
- Primary antibody was diluted at the proper concentration in 0.1% BSA and 0.25% Triton in 0.1M TS, for dual immunofluorescence a cocktail of the primary antibodies was prepared.
- Slices were transferred with a brush from crucibles to vials and they were incubated capped and shaking for the necessary time (from 24 to 72 hours) at room temperature.

2<sup>nd</sup> part:

- Slices were transferred back to crucibles and rinsed in 0.1M TS 2 X 15 minutes.

*Peroxidase reaction (chapters 3, 4)*

- Biotinylated secondary antibody was diluted in 0.1% BSA and 0.25% Triton in 0.1M TS in capped vials. Tissue was transferred to vials as previously and incubated shaking at room temperature for 1hr.
- During incubation, avidin-biotin peroxidase complex (ABC) solution was prepared by adding 2 drops of solution A and 2 drops of solution B for every 10 ml of antibody diluent (0.1% BSA and 0.25% Triton in 0.1M TS) and immediately vortexed. Then the solution was allowed to stand for 30



minutes prior to use (VECTASTAIN Elite ABC HRP Kit, PK-6100, Vector Laboratories, USA).

- Sections were rinsed in 0.1M TS 2 X 15 minutes.
- The sections were transferred to new vials containing the ABC solution and incubated for 30 minutes.
- The sections were transferred back to crucibles and rinsed in 0.1M TS twice for 15 minutes.
- During the washes the DAB solution was prepared by adding 22 mg of 3,3' diaminobenzidine for every 100 millilitres of 0.1M TS whilst stirring. Just prior to use, 10 µl of 30% H<sub>2</sub>O<sub>2</sub> were added per every 100 millilitres.
- Following rinses, tissues were incubated in DAB, time depending on reaction strength or previous experiment, squirting solution over the tissue.
- Sections were rinsed in 0.1 M TS 3 times per 2 minutes to stop the reaction, then 3 times per 5 minutes in 0.1 M PB.
- For light level examination of peroxidase reaction, the sections were mounted onto gelatinised slides and allowed to dry overnight.
- Sections were dehydrated by using increasing concentrations of ethanol, from 50% to 100%, finally into xylene.
- Coverslips were applied by using Entellan, air bubbles were removed and the slides were dried at least overnight.

#### *Immunofluorescence (chapters 3, 5)*

- Secondary antibodies for fluorescence were prepared in capped vials, diluted in 0.1% BSA and 0.25% Triton in 0.1M TS. Tissues were transferred to vials as previously and incubated shaking at room temperature for 1 hour.
- Sections were transferred back to crucibles and rinsed in 0.1M TS twice per 15 minutes.
- For dual immunofluorescence the sections were sequentially incubated in the 2<sup>nd</sup> secondary antibody shaking at room temperature for 1 hour.
- Sections were washed in 0.1M TS twice per 15 minutes, then in 0.1M PB 3 times per 5 minutes.

- Finally, they were mounted onto gelatinised slides, coverslipped using VECTASHIELD Antifade Mounting Medium (H-1000, Vector Laboratories, USA) and closed with nail polish.

## **2.5. Optical density measurement**

### *Chapter 3 and 4*

To perform the optical density measurement all images needed to be taken using standardized settings. A Nikon Eclipse 80i microscope coupled with an 8001 MicroFIRE camera was used equipped with the grey filters ND8 and ND32 and the blue filter NCB11. To exclude any experimental errors and/or bias, all images were taken at constant light intensity, with the same optical filters and at a magnification of 4X that permits to obtain a picture of the entire dorsal hippocampus. The software used for photomicrographs acquisitions is Neurolucida (MBF Bioscience).

The expression of CaSR, PV and CR was analysed by measuring their OD, as described by (Cordero et al., 2005; Noristani et al., 2010, 2012) using a computer-assisted imaging analysis software (ImageJ 2.0.0-rc-39/1.50b; NIH, USA).

In more detail this procedure was followed:

- Each picture was converted to 8-bit grayscale whose scale of intensity rank from 0 to 250, with a measurement of 250 corresponding to the area with very low expression of the target protein and 0 corresponding to the area with highest labelling.

The commands are: Image > Type > 8-bit

- Each layer of CA subfields (stratum pyramidale, stratum oriens, stratum radiatum, and stratum lacunosum-moleculare, including stratum lucidum for CA3) and of dentate gyrus (DG; granular cell layer, molecular layer, and hilus) was outlined using the polygon selection tool (Fig. 1.7), then area and mean grey values were measured through these commands:

1. Analyse > Set Measurements > tick Area and Mean Grey Value
2. Analyse > Measure > a windows opens with the measurements

The measurements were selected and copied into an excel sheet.

- The changes in the target proteins immunoreactivity were analysed against a constant control region that was established to be the Corpus Callosum (CC). 250 was divided by the intensity value of the control region and the obtained factor was multiplied by the region of interest in every given section. Inverse Optical Density (IOD) was obtained by subtracting the OD (after the control region normalisation) from 250. Values of IOD were taken and averaged in both the left and right hemisphere of each slice. The results are shown as Inverse Optical Density (IOD/pixel).

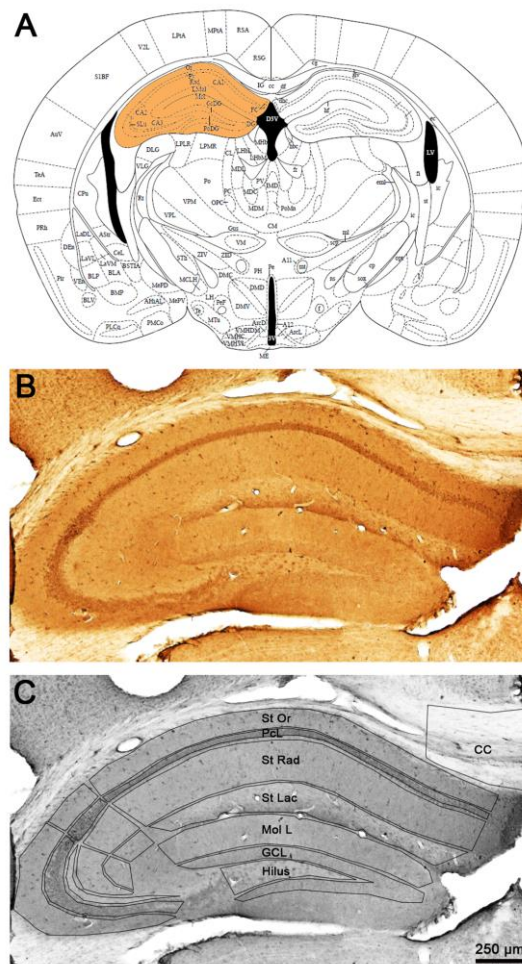


**Fig. 2.1: Schematic representation of mouse dorsal hippocampus selection for OD analysis.** (A) Representative drawing of the Bregma level of dorsal hippocampus used for analysis in chapter 3 and 4, adapted from Paxinos and Franklin, 2001. (B) Representative picture of a section of dorsal hippocampus stained with anti-CaSR antibody (Gardenal E. personal unpublished image). (C) Example of grayscale conversion and of the layers outlining conducted to analyse the OD in the immunolabelled sections in chapter 3 and 4.

## 2.6. Cell counting

### *Chapters 4 and 5*

To determine the numerical density (Nv, number/mm<sup>3</sup>) of immunolabelled cells in the dorsal hippocampus of 3xTg-AD mice respect to non Tg mice, 2 representative sections at the level -1.58/-2.46 mm posterior to Bregma were chosen and both hemispheres were used for the counting. To keep the counting bias to a minimum the counting was performed by two different observers and the mean of the two measurements was calculated. The counting was performed on each layer of the hippocampus in pictures taken at 4X magnification and using the software ImageJ with the following procedure: the area in mm<sup>2</sup> of each layer (region of interest) was determined after having outlined the perimeter of each layer, the area was then multiplied by the thickness of the section to obtain the volume of the layer measured in every specific section. Finally, the counted cell number was divided by the volume of the region of interest providing the Nv of every hemisphere analysed, the final Nv value was given by calculating the mean of all the hemispheres that were measured.

For the determination of the Nv of S100β-, GFAP- and GS-positive astrocytes in the entorhinal cortex, confocal z-stacks at 20X magnification were acquired in each hemisphere of three non-consecutive coronal sections at the level -2.92/-3.88 mm posterior to Bregma (lateral entorhinal cortex). Next, through the Leica software “LAS AF Lite” the acquisitions were converted into tiff pictures and by means of the software ImageJ each tiff z-stack was condensed into one picture with the command “max projections”. Then the procedure to calculate the Nv was the same as the neuron counting in mouse hippocampus: the area of the region of interest was measured in mm<sup>2</sup> and multiplied by the thickness of the section (20 μm) the number of cells counted in each picture was divided by the volume in mm<sup>3</sup> of the field analysed. The mean of the counting of all the sections per each animal was calculated.

## 2.7. Morphometric analysis

### *Chapter 5*

S100 $\beta$ -, GFAP- and GS-immunopositive astrocytes from the entorhinal cortex of both 3xTg-AD and non-transgenic animals were imaged using a Leica TCS STED CW SP8 microscope and a Leica 63X oil-immersion objective. Thirty to thirty-five astrocytes were acquired from 3 different slices from each animal. In relation to A $\beta$  plaques, all cells with somata within 50  $\mu$ m of distance from the plaque border were considered as plaque-associated astrocytes, while cells with somata positioned more far than 50  $\mu$ m from the plaques were considered as not associated.

Each astrocyte was sectioned along the vertical axis (z) into a uniformly spaced (0.3  $\mu$ m) set of two-dimensional parallel confocal planes, resulting in a stack of 70-90 consecutive images, each of which of 1024 x 1024 pixels in size.

Image processing and morphometric measurements were performed with the program CellAnalyst (Chvátal et al., 2007; Kulijewicz-Nawrot et al., 2012; Rodríguez et al., 2014). To improve the images, a series of digital filters based on convolution kernels were used: average 3 X 3, convolution and gauss 5 X 5; the filtering was then completed through the steps of despeckle and simple objects removal. Finally, to remove the background a threshold of 50, in a greyscale of 0-255, was applied. To perform the morphometric measurements, the related xyz values for each z-stack were given to the software. Cell volumes and somata volumes were calculated from a marked region of interest (ROI) using the Cavalieri method. The unit areas of each confocal plane represented by pixels were recalculated to real values in square micrometres, summed up and multiplied by the distance between two consecutive plans according to this equation:

$$V = T \cdot \sum_{i=1}^n U_i$$

where  $V$  is the cell volume,  $T$  is the distance between sections,  $U$  is the unit area, and  $n$  is the number of sections.

Cell surfaces were determined by using the isocontouring or isointensity contouring method with this equation:

$$S = \sum_{i=1}^n (K_i \cdot T + |U_{i-1} - U_i|)$$

where  $S$  is the cell surface area,  $K$  is the length of the isovalue edge,  $T$  is the distance between sections,  $U$  is the unit area, and  $n$  is the number of sections.

Changes in the complexity of the cells were determined by calculating the surface/volume ratio using this equation:

$$C = \sqrt[2]{S} / \sqrt[3]{V}$$

A sphere is the object with the lowest complexity and lowest S/V ratio, the more protrusions a cell has, the higher is the complexity.

## 2.8. Statistics

### *All chapters*

The statistical analysis was performed using the software GraphPad Prism (GraphPad, La Jolla, CA, USA).

To examine the differences in CaSR expression between the 3xTg-AD and non-transgenic animals considering the ageing of the mice from 9 months to 18 months of age a one-way Analysis Of Variance (ANOVA) with a *post-hoc* Tukey test was performed. The changes in CaSR expression at single time points were analysed using an unpaired *t*-test.

Calcium binding proteins changes of expression and Nv in 3xTg-AD respect to control animals were analysed with an unpaired *t*-test or Mann-Whitney test.

The morphological and numerical changes of S100 $\beta$ -positive astrocytes in 3xTg-AD mice compared to non-transgenic mice, as well as the differences in relationship with  $\beta$ -amyloid plaques were analysed through ANOVA or unpaired *t*-test. Difference among genotype and age groups were further analysed with a *post hoc* Bonferroni test.

Significance of results was accepted at  $p < 0.05$ .

All data are expressed as means  $\pm$  standard error of the mean (S.E.M.).

## Chapter 3

### **Calcium-Sensing Receptor Immunoreactivity is increased in the Hippocampus of the 3xTg-AD mouse model**

**Gardenal E**, Chiarini A, Armato U, Dal Prà I, Verkhatsky A and Rodríguez JJ (2017) Increased Calcium-Sensing Receptor Immunoreactivity in the Hippocampus of a Triple Transgenic Mouse Model of Alzheimer's Disease *Front. Neurosci.* 11:81.

CaSR expression was analysed in all hippocampal layers of the 3xTg-AD mice and the respective non Tg animals at 9, 12 and 18 months of age (respectively n = 5, 5, 4 for non Tg and 4, 5, 3 for 3xTg-AD).

The immunohistochemical labelling demonstrated that CaSR is present in the hippocampus of both 3xTg-AD and non Tg control animals at all ages with a rather homogeneous distribution throughout all hippocampal areas (Fig. 3.1 A and B). Punctate CaSR labelling is mainly present in pyramidal neurones of the different CA subfields and in granule cells of the DG as well as in the pleomorphic cells of the hilus, being more evident in the soma, nucleus excluded, although it is also detectable in the neuropil, including both dendrites and axons (Fig. 3.1 C-F). CaSR expression in astrocytes was rather rare and when detected was of very low intensity respect to neurons; appearing as puncta mainly restricted to the astrocytic soma (Fig. 3.1 K-P).

#### **3.1 CaSR expression is increased in 3xTg-AD animals**

Optical density analysis of CaSR staining in the hippocampus of the 3xTg-AD mice showed a significant increase in its expression in CA1 and DG subfields ( $F_{7,166}=11.32$ ,  $p < 0,0001$  and  $F_{7,166}=7.994$ ,  $p < 0,0001$ , respectively) at all ages (9, 12 and 18 months; Fig. 3.1, 3.2 and 3.3; Table 3.1). An increase in CaSR optical density of 23.44%, 17.62% and 20.09% at 9, 12 and 18 months of age respectively when compared to control non Tg animals was detected in CA1 area (Fig. 3.1 C and D; Fig. 3.2 A; Table 3.1). Similar increase in CaSR optical density was observed in DG: 17.82%, 14.74% and 20.74%, at 9, 12 and 18 months respectively in 3xTg-AD animals compared to non Tg (Fig. 3.1 E and F; Fig. 3.3A

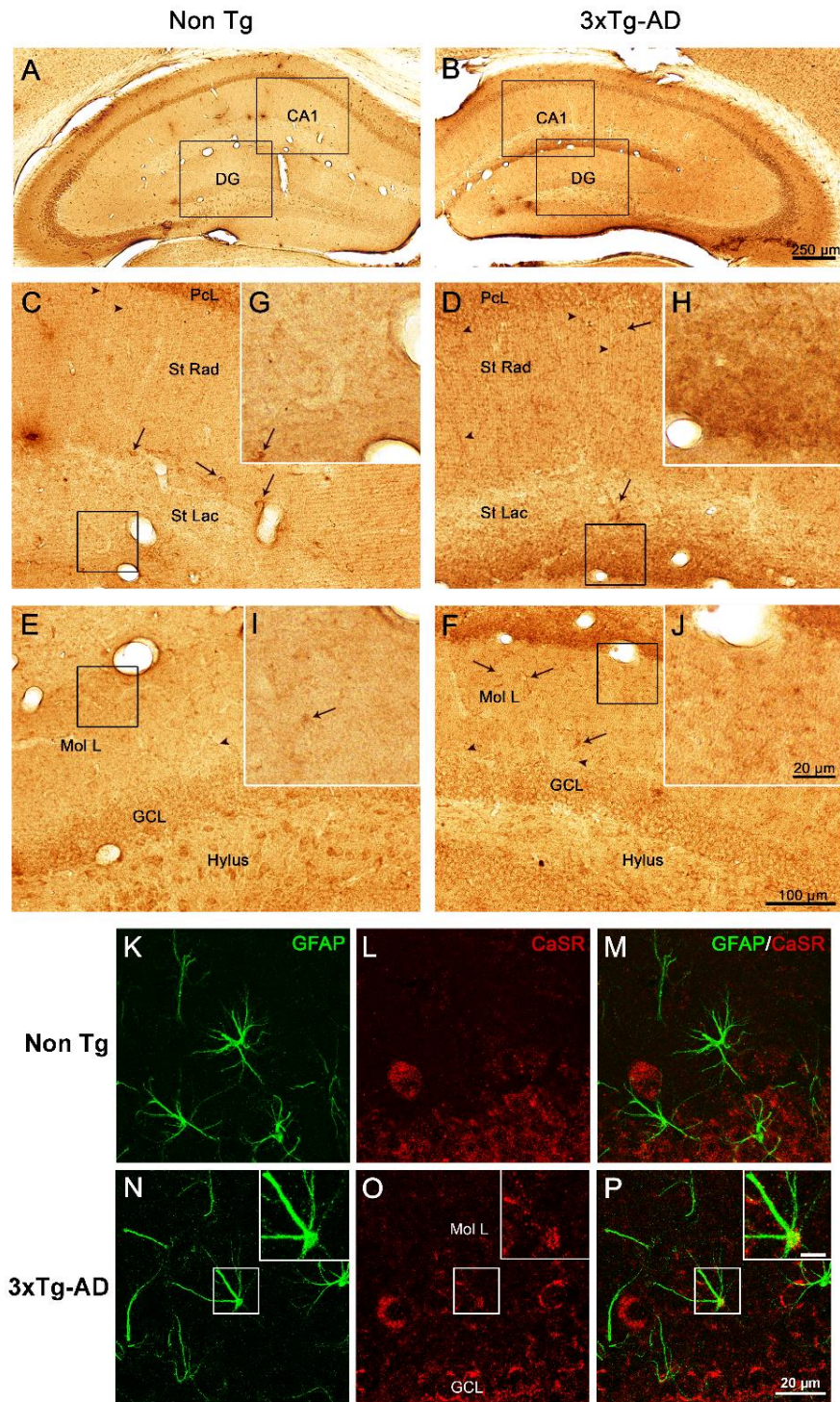


**Figure 3.1 CaSR expression and localization in mouse hippocampus.** Brightfield micrographs showing the distribution of CaSR-IR within the dorsal hippocampus of 18 months old Non Tg controls (A, C, G, E and I) and 3xTg-AD mice (B, D, F, H and J; arrowheads show neuropil elements, whilst full arrows indicate interneurons). Confocal micrographs showing the rare expression of CaSR (red) in GFAP-positive astrocytes (green), in both Non Tg (K, L, M) and 3xTg-AD mice (N, O, P). High magnification inserts are shown in the K, L and M panels. Scale bars: 250  $\mu\text{m}$  (A and B); 100  $\mu\text{m}$  (C-F); 20  $\mu\text{m}$  (G-J and K-P). CA1, Cornu Ammonis 1; DG, Dentate Gyrus; St Rad, Stratum Radiatum; St Lac, Stratum Lacunosum-Moleculare; Mol L, Molecular Layer; GCL, Granular Cell Layer.



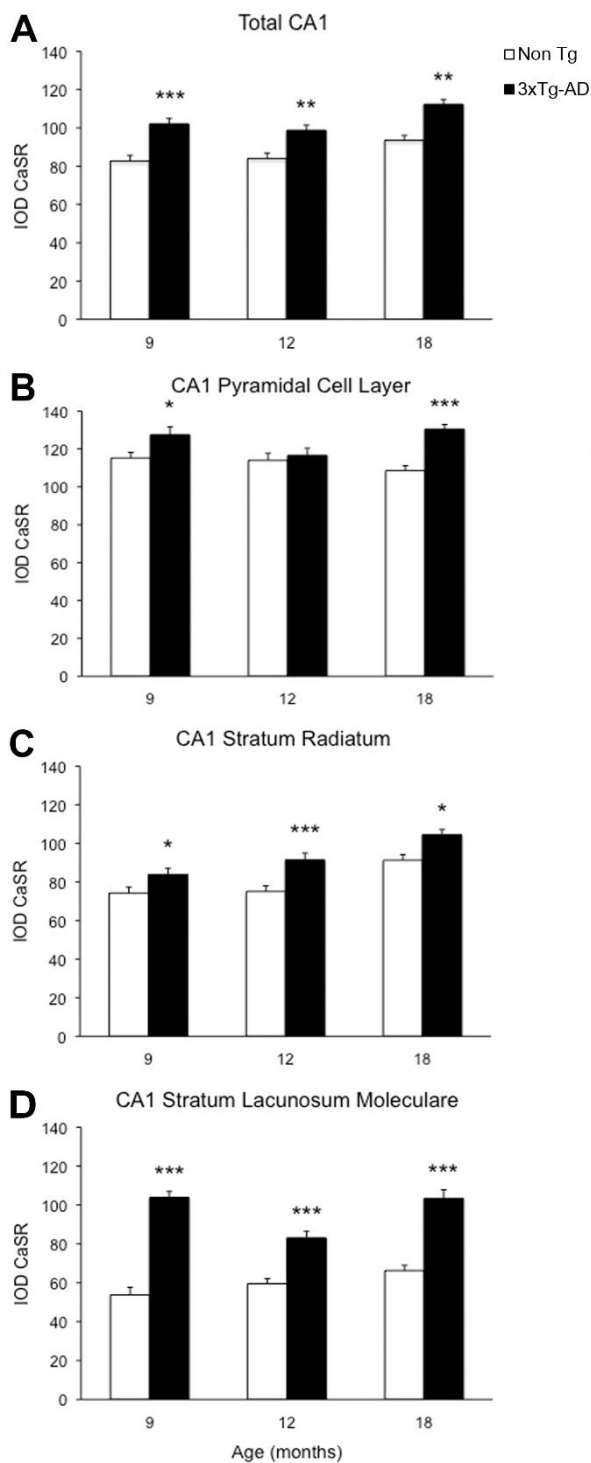


**Figure 3.2 Changes of CaSR expression in hippocampal CA1.**

Bar graphs illustrating CaSR-IR IOD within CA1 subfield of hippocampus between Non Tg controls and 3xTg-AD mice at 9, 12 and 18 months of age (Ns for non Tg = 5, 5, 4; ns for 3xTg-AD = 4, 5, 3, respectively; 3 slices have been analysed per each animal). (A) Total CA1, (B) CA1 Pyramidal Cell Layer, (C) CA1 Stratum Radiatum, (D) CA1 Stratum Lacunosum-Moleculare. Bars represent means  $\pm$  SEM (\*  $p \leq 0.05$ , \*\*  $p \leq 0.01$ , \*\*\*  $p \leq 0.001$ ).

and Table 3.1). No significant alterations in the optical density of CaSR were identified in the CA2 and in CA3 sub-fields.

Hipp area	Age	CaSR IOD	p-value	t
CA1	9 months non Tg	82.71 ± 2.98		
	9 month 3xTg-AD	102.1 ± 2.72	< 0.0001 ***	4.474
	12 months non Tg	83.92 ± 2.51		
	12 months 3xTg-AD	98.71 ± 2.56	0.0002 ***	4.117
	18 months non Tg	93.51 ± 3.39		
	18 months 3xTg-AD	112.30 ± 4.68	0.0022 **	3.342
DG	9 months non Tg	82.68 ± 3.11		
	9 month 3xTg-AD	97.41 ± 3.56	0.0039 **	3.051
	12 months non Tg	81.35 ± 3.33		
	12 months 3xTg-AD	93.34 ± 2.80	0.0079 **	2.773
	18 months non Tg	89.78 ± 4.75		
	18 months 3xTg-AD	108.40 ± 4.96	0.0119 *	2.676

**Table 3.1 CaSR IOD values of the hippocampal CA1 and DG subfields in both non Tg and 3xTg-AD mice at 9, 12 and 18 months of age.** Values are expressed as means ± SEM (\*  $p \leq 0.05$ , \*\*  $p \leq 0.01$ , \*\*\*  $p \leq 0.001$ ).

### 3.2 The increase of CaSR expression in CA1 and DG is layer-specific

The increase of CaSR expression in the CA1 area of 3xTg-AD animals mainly occurred in the pyramidal cell layer (PCL) (10.68% at 9 months, 2.28% at 12 months and 20.17% at 18 months; Fig. 3.2 B; Table 3.2), in the stratum radiatum (St Rad) (12.93% at 9 months, 27.71% at 12 months, 14.55% at 18 months; Fig. 3.2 C; Table 3.2) and in the stratum lacunosum moleculare (St Lac Mol) (93.19% at 9 months, 39.58% at 12 months, 56.08% at 18 months; Fig. 3.1 G and H; Fig. 3.2 D; Table 3.2).

CaSR expression increase in the DG was most prominent in the molecular layer (Mol L) of 3xTg-AD animals in respect to their controls (15.90% at 9 months, 12.32% at 12 months, 20.98%, at 18 months; Fig. 3.3 B; Table 3.3) and in the granular cell layer (GCL) (19.33% at 9 months, 10.68% at 12 months, 37.38% at 18 months; Fig. 3.1 I and J; Fig. 3.3 C; Table 3.3). The increase in the molecular layer was similar in all subdivisions; the inner, middle and outer molecular layers (data not shown).

CaSR hyperexpression in the projections layers above described doesn't appear to derive from neuronal somata, despite its presence in some interneurons cell bodies, but mainly from the neuropil comprising both dendrites and axons (Fig. 3.1 D and F).

CA1 Layer	Age	CaSR IOD	p-value	t
<b>PCL</b>	9 months non Tg	115.20 ± 3.78		
	9 month 3xTg-AD	127.50 ± 3.80	0.0351 *	2.177
	12 months non Tg	114.00 ± 2.49		
	12 months 3xTg-AD	116.60 ± 2.39	ns	0.7488
	18 months non Tg	108.60 ± 4.57		
	18 months 3xTg-AD	130.50 ± 3.40	0.001 **	3.659
<b>St Rad</b>	9 months non Tg	74.23 ± 2.91		
	9 month 3xTg-AD	83.83 ± 3.60	0.0451 *	2.066
	12 months non Tg	75.08 ± 2.85		
	12 months 3xTg-AD	91.38 ± 2.75	0.0002 ***	4.112
	18 months non Tg	91.23 ± 3.31		
	18 months 3xTg-AD	104.5 ± 5.99	0.0489 *	2.053
<b>St Lac Mol</b>	9 months non Tg	53.78 ± 2.60		
	9 month 3xTg-AD	103.9 ± 3.33	< 0.0001 ***	11.92
	12 months non Tg	59.53 ± 2.71		
	12 months 3xTg-AD	83.09 ± 4.41	< 0.0001 ***	4.46
	18 months non Tg	66.25 ± 5.31		
	18 months 3xTg-AD	103.4 ± 6.25	< 0.0001 ***	4.552

**Table 3.2 CaSR IOD values of the hippocampal CA1 layers with statistical significance between non Tg and 3xTg-AD mice at 9, 12 and 18 months of age.** Values are expressed as means ± SEM (\* p ≤ 0.05, \*\* p ≤ 0.01, \*\*\* p ≤ 0.001).

DG Layer	Age	CaSR IOD	p-value	t
<b>Mol L</b>	9 months non Tg	73.06 ± 3.16		
	9 month 3xTg-AD	84.68 ± 4.88	0.0424 *	2.094
	12 months non Tg	80.58 ± 4.18		
	12 months 3xTg-AD	90.51 ± 3.01	0.0547 *	1.953
	18 months non Tg	90.00 ± 4.11		
	18 months 3xTg-AD	108.8 ± 6.91	0.0203 *	2.45
<b>GCL</b>	9 months non Tg	98.30 ± 3.55		
	9 month 3xTg-AD	117.30 ± 4.27	0.0016 **	3.379
	12 months non Tg	87.76 ± 3.15		
	12 months 3xTg-AD	97.13 ± 2.78	0.0298 *	2.239
	18 months non Tg	82.18 ± 6.16		
	18 months 3xTg-AD	112.90 ± 3.54	0.0004 ***	4.001

**Table 3.3 CaSR IOD values of the hippocampal DG layers with statistical significance between non Tg and 3xTg-AD mice at 9, 12 and 18 months of age.** Values are expressed as means ± SEM (\* p ≤ 0.05, \*\* p ≤ 0.01, \*\*\* p ≤ 0.001).

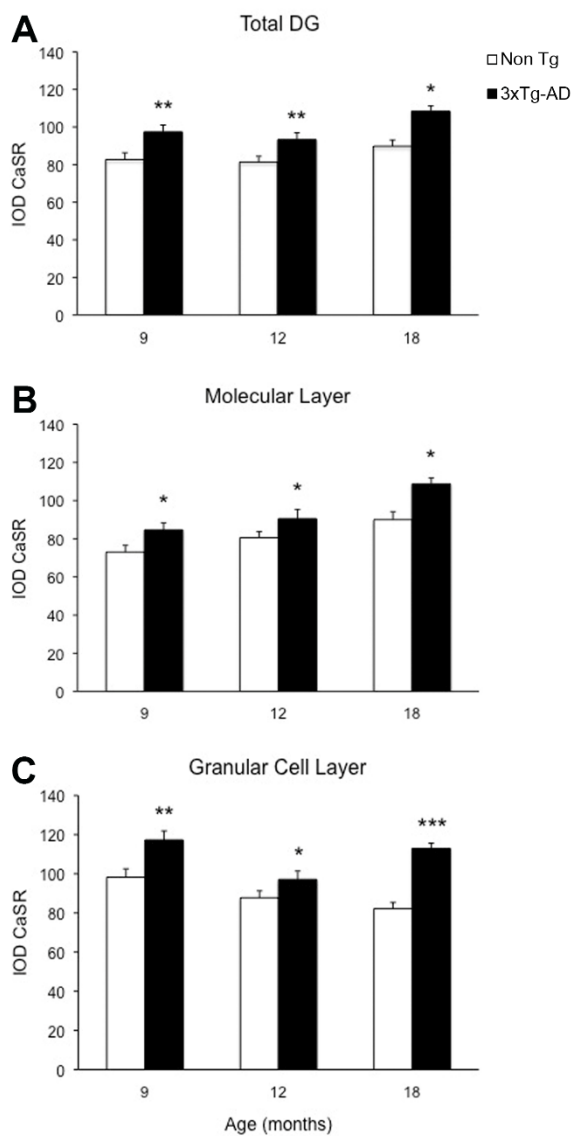


**Figure 3.3 Modification of CaSR expression in hippocampal DG.** Bar graphs illustrating CaSR-IR IOD within DG subfield between Non Tg controls and 3xTg-AD mice at 9, 12 and 18 months of age (Ns for non Tg = 5, 5, 4; ns for 3xTg-AD = 4, 5, 3, respectively; 3 slices have been analysed per each animal). (A) Total DG; (B) Molecular Layer; (C) Granular Cell Layer. Bars represent means  $\pm$  SEM (\*  $p \leq 0.05$ , \*\*  $p \leq 0.01$ , \*\*\*  $p \leq 0.001$ ).

### 3.3 CaSR increase in hippocampus occurs in the same areas affected by $\beta$ -amyloid accumulation

The increase of CaSR immunoreactivity in the CA1 region follows the same spatio-temporal pattern as that of  $\beta$ -amyloid deposition (Fig. 3.4 A-F), while in the DG it starts even before the accumulation of  $A\beta$  becomes evident. Indeed, intracellular  $A\beta$  appears in hippocampal neurones of 3xTg-AD mice between 4 and 6 months of age and reaches its maximum at 9 months of age (Fig. 3.4 G and H); extracellular  $A\beta$  depositions start to mount from 9-12 months, being maximal at 18 months. At 18 months the  $A\beta$  plaques are big and expanded through the

hippocampus mainly concentrating in the CA1 subfield (Fig. 3.4 E, F, I and J); with later appearance in the DG (Noristani et al., 2012; Rodríguez et al., 2013). In a similar way hyper-phosphorylated tau protein begins to be detectable in 3xTg-AD mice at 12 months causing the formation of tangles by 18 months, and it is also concentrated in CA1 region affecting all the layers (Fig. 3.4 K and L).

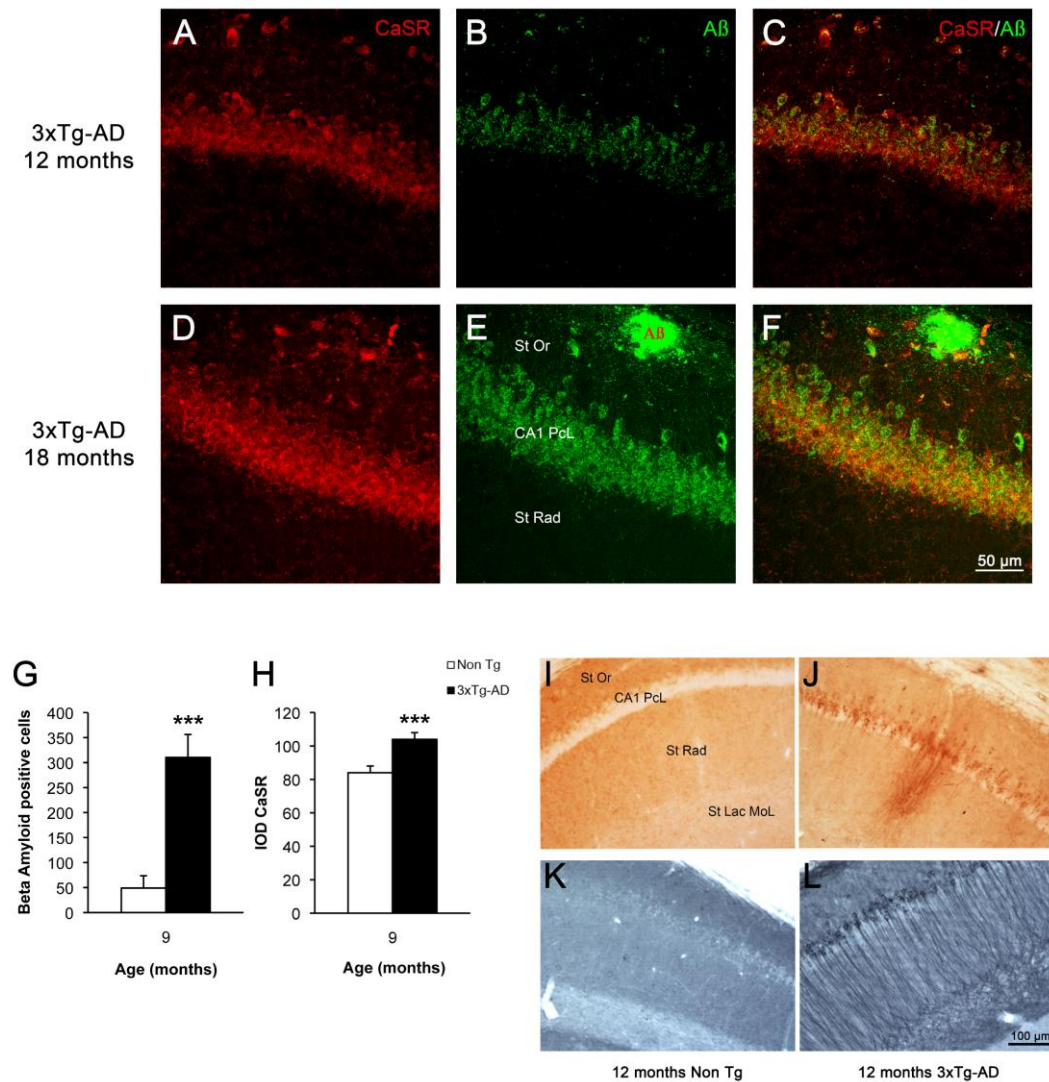


**Figure 3.4 CaSR and  $\beta$ -amyloid relationship in hippocampus during AD progression.** Confocal micrographs showing the overlapping expression of CaSR (red) with the accumulation of intraneuronal A $\beta$  (green, anti-A $\beta$  488) and the formation of plaques in hippocampal pyramidal neurons of 3xTg-AD mice of 12 and 18 months of age respectively. (A and D) CaSR-IR; (B and E) A $\beta$ -IR; (C and F) merge. St Or Stratum Oriens; CA1 PcL CA1 Pyramidal Cell Layer; St Rad Stratum Radiatum. Bar graphs illustrating the number of A $\beta$  positive cells within CA1 subfield of hippocampus between Non Tg controls (G) and 3xTg-AD mice (H) at 9 months of age (\*\*\*)  $p \leq 0.001$ ). Brightfield micrographs of CA1 areas of hippocampus of Non Tg and 3xTg-AD mice immunolabelled with anti-A $\beta$  (I and J) and anti-tau antibody (K and L) at 12 months of age. St Or, Stratum Oriens; CA1 PcL, CA1 Pyramidal Cell Layer; St Rad, Stratum Radiatum; St Lac Mol, Stratum Lacunosum Moleculare.

### 3.4 Discussion

This study in the 3xTg-AD mouse model conceptually complements the results previously obtained *in vitro* by Armato and colleagues (Armato et al., 2013).

*In vitro* exposure of human cortical astrocytes and neurons to a truncated form of  $\beta$ -amyloid, the A $\beta_{25-35}$  peptide, which binds and activates the CaSR (Dal Prà et al., 2014), stimulated the intracellular production and secretion of  $\beta$ -amyloid by both cell types with the subsequent death of a fraction of neurons (Armato et al., 2013). While neurons were vulnerable to toxic  $\beta$ -amyloid, the cultured astrocytes survived and they showed a transient increase of CaSR expression. These cytotoxic effects were fully inhibited following addition of CaSR antagonist NPS 2143 to the incubation media. Indeed, the NPS prevented the death of neurons and it deeply and steadily downregulated the receptor in the A $\beta$ -treated astrocytes, and besides blocked the A $\beta$  self-induction mechanism completely (Armato et al., 2013).

The results described in the present work further corroborate links existing between increases in CaSR expression and  $\beta$ -amyloid accumulation. In the 3xTg-AD mice, intraneuronal  $\beta$ -amyloid starts to accumulate in the CA1 pyramidal neurones at 4 to 6 months of age and extracellular  $\beta$ -amyloid deposits emerge from 12 months of age, in parallel with a clear and specific astrogliosis around the plaques despite the generalized hippocampal astrocytic atrophy and with an increase in the density of activated microglia and recruitment of new ramified microglial cells (Rodríguez et al., 2009a, 2010, 2013; Olabarria et al., 2010). Accumulation of tau that occurs later follows similar pattern. The 3xTg-AD mouse model not only develops the typical histopathological hallmarks of Alzheimer's disease, but also manifests synaptic dysfunction with impaired LTP (Oddo et al., 2003b; Rodríguez et al., 2008).

Interestingly, a study of acute hypoxia/ischemia in rats revealed that A $\beta$  overproduction due to hypoxic injury is mediated by CaSR hyperexpression (Bai et al., 2015). Experiments on rat hippocampal neurons demonstrated that hypoxia induces an up-regulation of CaSR which in turn promotes the elevation of cytosolic [Ca<sup>2+</sup>] thereby producing an increase of BACE1 expression that results

in the rise of A $\beta$ <sub>40</sub> and A $\beta$ <sub>42</sub> generation. In addition, specific block of CaSR with Calhex 231, an allosteric antagonist of CaSR, induced a decrease of BACE1 and A $\beta$  both *in vitro* and *in vivo* in hypoxic conditions (Bai et al., 2015). The dramatic effect of the increased expression and activity of CaSR in hippocampus is confirmed also by another work on a mouse model of acute ischemic injury where a transient global cerebral ischemia (TGI) was induced. In this model CaSR was overexpressed in parallel with GABA<sub>B</sub>R1 downregulation and was followed by neuronal death. The administration of the calcilytic compound NPS89636 through intracerebroventricular injections after the TGI specifically blocked the activity of CaSR, restored GABA<sub>B</sub>R1 expression and protected hippocampal neurons from cell death. Furthermore, the treatment of TGI mice with calcilytics significantly improved learning and memory (Kim et al., 2014).

Altogether these findings reveal the importance and the impact which CaSR's altered expression has on maintaining the normal brain function, supporting the idea that its changes could contribute to the development and progression of pathologies such as Alzheimer's disease and stroke. Our present data in an AD mouse model show that expression of CaSR is increasing while neuropathology progresses. Previous works demonstrated that the administration of A $\beta$ <sub>42</sub> oligomers to neuronal and astrocytic human cell cultures increases the endogenous A $\beta$ <sub>42</sub> production and secretion resulting in a progressive death of neurons. This mechanism of A $\beta$  self-induction, which determine the advance of AD, was demonstrated to be completely suppressed by adding a specific calcilytic like NPS 2143 to the cell culture (Armato et al., 2013; Dal Prà et al., 2015; Chiarini et al., 2016). It needs to be emphasized that the CaSR could be a promising target of investigation for not only further understanding AD pathology onset and spread but also for evaluating new therapeutic solutions.

## Chapter 4

### **Parvalbumin and Calretinin regional changes in the hippocampus of the 3xTg-AD mouse model**

Zallo F, Gardenal E, Verkhatsky A, Rodríguez JJ. (2017) Manuscript in preparation

#### **4.1 Parvalbumin optical density and cell numerical density in hippocampal CA1 and DG**

Parvalbumin (PV) is homogeneously expressed throughout the hippocampal Cornu Ammonis of the non-transgenic 18 months old mice. In this area a strong positivity is present in the soma of interneurons as well as in their processes; the positive interneurons appear highly ramified and with numerous axonal varicosities. The entire stratum pyramidale shows a high labelling, even though pyramidal cells are slightly less positive than interneurons present in this layer. The stratum lacunosum moleculare is completely devoid of labelling, a weak PV-immunoreactivity is visible only in the axon terminals. The dentate gyrus shows a similar labelling pattern with a strong reactivity in the soma and processes of some interneurons of the granular cell layer and hilus. Granular neurons are weakly labelled and the majority of the positivity is present in projections terminating in the outer part of the GCL and in the inner molecular layer, while the medium and outer molecular layers are completely devoid of labelling (Fig. 4.1 A, C, E and G).

In general, the 3xTg-AD 18 months old mice exhibit an interneurons' arborisation less clear than in the normal mice, the immunoreactivity appear to be more diffuse and cellular structures are more difficult to identify (Fig 4.1 B, D, F and I).

These mice show a decrease in the numerical density (Nv) of PV-positive interneurons (52%; Table 4.1; Fig. 4.1 C, D and I) as well as a lower PV optical density (13.8%; Table 4.2; Fig 4.1 C, D and J) in the CA1 hippocampal subfield. The decrease in the numerical density of PV-positive interneurons is specific of stratum oriens (46%) and stratum pyramidale (57%; Table 4.1; Fig. 4.1 E-H and I).



Hipp area	PV Nv in Non-Tg (cells/mm <sup>3</sup> )	PV Nv in 3xTg-AD (cells/mm <sup>3</sup> )	p-value	t
<b>Total CA1</b>	2962 ± 375.8	1423 ± 274.4	p < 0.05	3.307
<b>CA1 stratum oriens</b>	3245 ± 506.2	1754 ± 329.9	p < 0.05	2.467
<b>CA1 stratum pyramidale</b>	7742 ± 898.4	3316 ± 944.8	p < 0.05	3.235

**Table 4.1** Values of PV-positive cells Nv in the CA1 and the sublayers which show significant reduction in the 3xTg-AD mice respect to the non Tg mice. Values are expressed as means ± SEM.

Also PV optical density reduction is layer specific and follows the same pattern of Nv, thus the two layers that result statistically affected are the stratum oriens (16%) and the stratum pyramidale (23%; Table 4.2; Fig. 4.1 E-H and J).

Hipp area	PV IOD in Non-Tg	PV IOD in 3xTg-AD	p-value	t
<b>Total CA1</b>	84.49 ± 4.546	68.48 ± 4.9	p < 0.05	2.398
<b>CA1 stratum oriens</b>	88.2 ± 4.245	74.1 ± 4.399	p < 0.05	2.307
<b>CA1 stratum pyramidale</b>	145.7 ± 3.816	112.1 ± 3.125	p < 0.0001	6.787

**Table 4.2** Values of PV inverted optical density (IOD) in the CA1 and the sublayers which significant reduction in the 3xTg-AD mice respect to the non Tg mice. Values are expressed as means ± SEM.

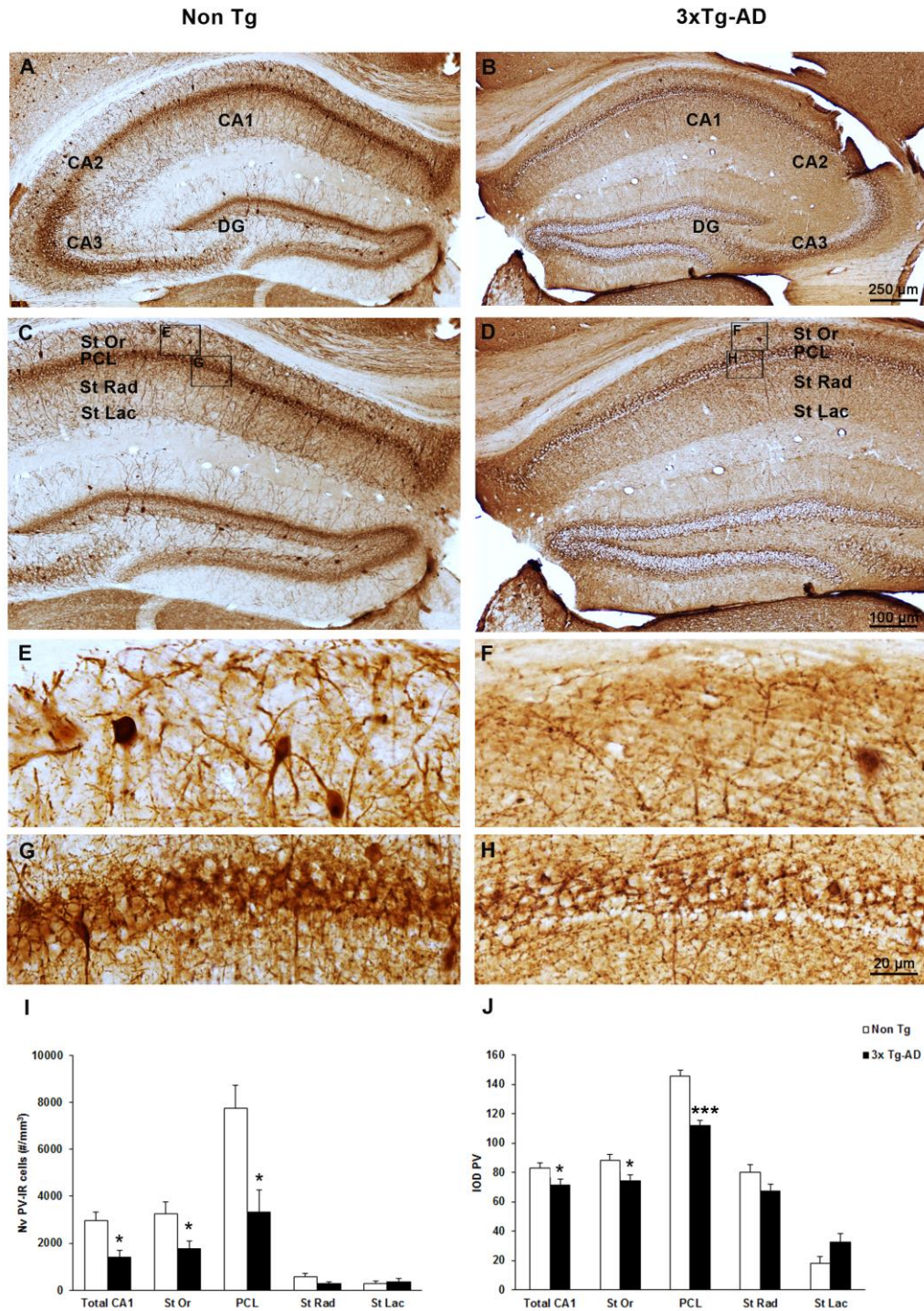


**Figure 4.1: Parvalbumin expression changes in mouse hippocampus with AD.** (A-H) Brightfield micrographs illustrating the distribution of PV-immunoreactive cells and its expression within the CA1 of 18 months old Non Tg controls (A, C, E and G) and 3xTg-AD mice (B, D, F and H). (I-J) Bar graphs showing the Nv (#cells/mm<sup>3</sup>; I) and the inverse optical density (IOD; J) of PV-IR cells in the hippocampal CA1 subfields between 18 months old Non Tg controls (n = 5) and 3xTg-AD mice (n = 5). Data represent mean ± SEM (\* p≤0.05, \*\* p≤0.01, \*\*\* p≤0.001). CA, Cornu Ammonis; DG, Dentate Gyrus; St Or, Stratum Oriens; PCL, Pyramidal Cell Layer; St Rad, Stratum Radiatum; St Lac, Stratum Lacunosum-Moleculare.

## 4.2 Calretinin optical density and cell numerical density in the hippocampus of the 3xTg-AD mice

Calretinin (CR) immunohistochemistry in the non-transgenic 18 months old mice shows a homogeneous expression of this protein among all the hippocampal subfields CA1, CA2 and CA3. A strong immunoreactivity is visible in the soma and varicose processes of a subpopulation of interneurons, whereas pyramidal cells are devoid of labelling. A high immunolabelling is also evident in projections at the border within the stratum radiatum and the stratum lacunosum moleculare. In the DG very few interneurons somas are positive for CR and they are mostly distributed in the hilus; the granular cells show no CR immunoreactivity, but positive projections are visible in the Subgranular Zone (SGZ). The inner part of the molecular layer is highly positive, however any neuronal soma result immunolabelled in this sublayer (Fig. 4.2 A, C, E and G).

The hippocampus of the 3xTg-AD 18 months old mice shows a general staining similar to its non-transgenic counterpart (Fig. 4.2 A and B). The measurement of CR optical density in all the hippocampal subfields has revealed no differences in the total protein expression (Fig. 4.2 I). In contrast, a significant decrease of CR positive interneurons has been identified in the CA1 area (33.7%; Table 4.3; Fig. 4.2 C, D and J). The loss of immunoreactive neuronal somas in the 3xTg-AD mouse model respect to the normal control is statistically significant in specific sublayers: the stratum radiatum (63.5%) and the stratum lacunosum moleculare (64.3%; Table 4.3; Fig. 4.2 E-H and J).

Hipp area	CR Nv in Non-Tg (cells/mm <sup>3</sup> )	CR Nv in 3xTg-AD (cells/mm <sup>3</sup> )	p-value	t
<b>Total CA1</b>	3390 ± 246.6	2248 ± 352.6	p < 0.05	2.656
<b>CA1 stratum radiatum</b>	1990 ± 399.4	726 ± 139	p < 0.05	2.989
<b>CA1 lacunosum moleculare</b>	2107 ± 157.1	751.6 ± 40.45	p < 0.0001	8.358

**Table 4.3 Values of CR-positive cells Nv in the CA1 and the sublayers which show significant reduction in the 3xTg-AD mice respect to the non Tg mice.** Values are expressed as means ± SEM.

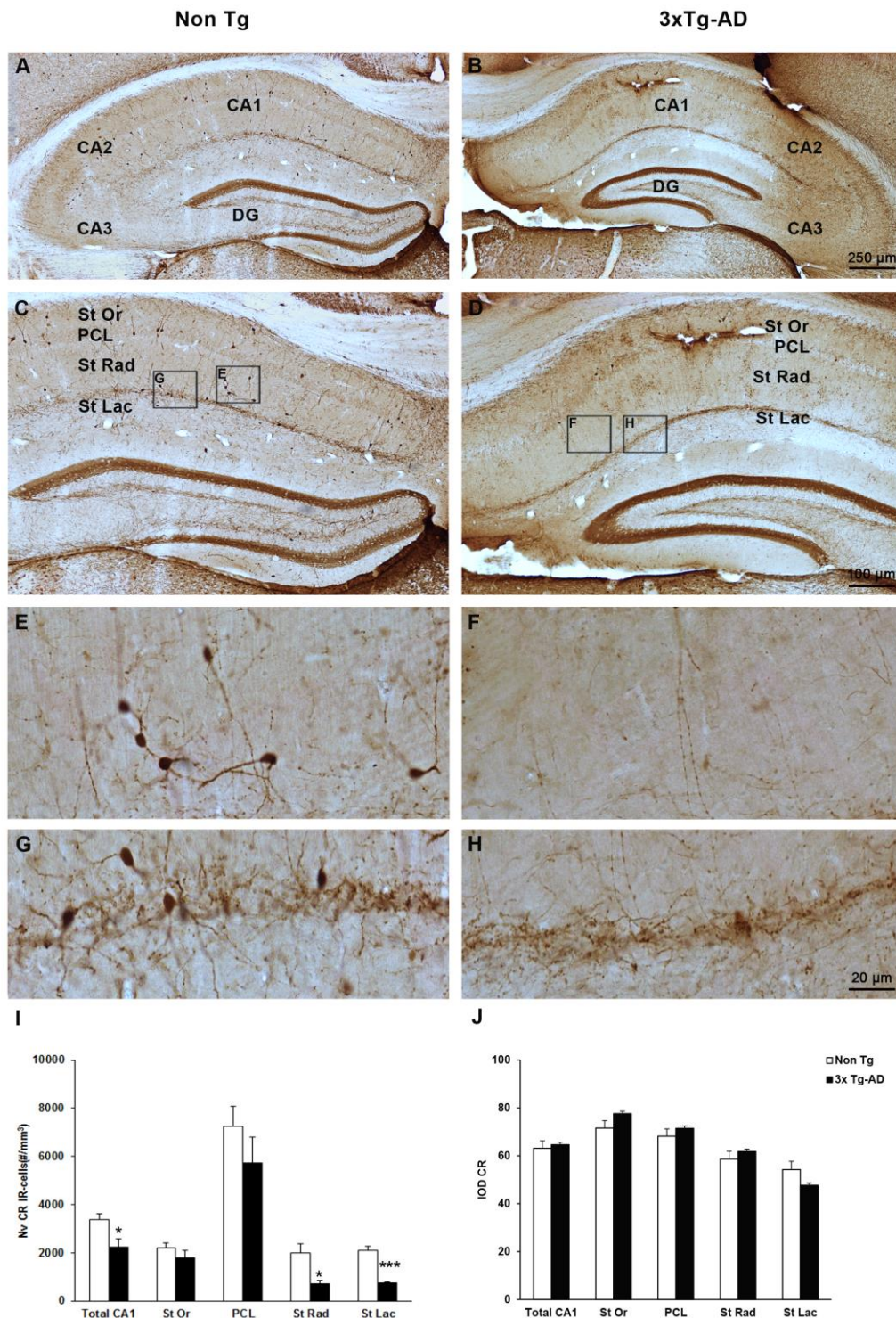


**Figure 4.2: Calretinin expression changes in mouse hippocampus with AD.** (A-H) Brightfield micrographs illustrating the distribution of CR-immunoreactive cells and its expression within the CA1 of 18 months old Non Tg controls (A, C, E and G) and 3xTg-AD mice (B, D, F and H). (I-J) Bar graphs showing the numerical density (Nv; #cells/mm<sup>3</sup>; I) and the inverse optical density (IOD; J) of CR-IR cells in the hippocampal CA1 subfields between 18 months old Non Tg controls (n = 5) and 3xTg-AD mice (n = 5). Data represent mean ± SEM (\* p≤0.05, \*\* p≤0.01, \*\*\* p≤0.001). CA, Cornu Ammonis; DG, Dentate Gyrus; St Or, Stratum Oriens; PCL, Pyramidal Cell Layer; St Rad, Stratum Radiatum; St Lac, Stratum Lacunosum Moleculare.

### 4.3 Discussion

In this work and for the first time, we have carried out an in depth analysis of parvalbumin and calretinin expression in the hippocampus of the 3xTg-AD mouse model. So far, calcium-binding proteins have been characterized in several mouse models of AD but all the models previously used bear mutations generating only A $\beta$  hyperexpression and amyloid plaques deposition, without any tau tangles presence. The 3xTg-AD mouse model is the unique animal model that closely mimics AD pathogenesis, since both A $\beta$  plaques and NFTs are present in the brain of these mice. The animals chosen for this work were 18 months old because this age resemble a late-stage of Alzheimer's disease comparable to human brains. In these animals PV and CR-positive interneurons showed a specific hippocampal regional vulnerability, since their numerical density was found significantly reduced, mainly in the CA1 subfield. Moreover, PV showed also a decrease of its optical density in the same hippocampal area. The alterations of the calcium binding proteins found in the 3xTg-AD animals are likely pathogenically related to AD, since CA1 hippocampal area is among the first regions to show intracellular and extracellular A $\beta$  depositions and neurofibrillary tangles formation in these mice.

In general, all the studies conducted on human AD hippocampal tissue demonstrated a reduced expression of PV and CR and/or a decrease in the number of interneurons positive for these calcium binding proteins (Tab. 4.4). The same vulnerability was demonstrated also in several AD mouse models which hyperproduce A $\beta$ . Only one mouse model, the APP<sup>Swe</sup>/PSEN<sup>1dE9</sup> exhibited an increase in PV expression in hippocampus (Verdaguer et al., 2015), but the mice used in this work were only 12 months old, thus they were at an earlier stage of the pathogenesis respect to our animals that were 18 months old. However, the same mouse model (APP<sup>Swe</sup>/PSEN<sup>1dE9</sup>) was studied by other research groups revealing a decrease of both CR and PV in the olfactory system areas, where PV seemed to be affected at an older age than CR. On the basis of this, it may be hypothesized that at early AD stages GABAergic interneurons are more resistant to toxicity and the expression of some calcium binding proteins like PV might show an increase in the attempt to compensate an initial brain dysfunction which

subsequently determine the significant decrease I have just described at later stages. In addition, these alterations, which have specific regional and temporal pattern, might be slightly different depending on the animal model used.

It should be noted that the analysis of PV and CR in human brains demonstrated a reduction in calcium binding proteins immunoreactivity in the areas early affected by AD, like EC, hippocampus and parahippocampal gyrus, while the regions affected at later stages showed lesser alterations of these proteins (Table 4.4). This observation supports the hypothesis mentioned above about a PV and CR vulnerability apparent only at late stages of AD.

The studies demonstrating a resistance of calcium binding proteins-positive interneurons to AD pathology sustain that the presence of calcium-buffering proteins including CR and PV, may offer neuroprotection by maintaining calcium homeostasis and more importantly, the lack of NFTs presence in PV interneurons seem to suggest that these neurons have distinct features that confer them resistance to AD pathological markers (Sampson et al., 1997). Indeed, it has been demonstrated that neurofilament triplet proteins are almost absent in the CBPs-positive interneurons which don't develop NFTs, suggesting that neurofibrillary pathology may arise only if axons contain neurofilament proteins (Vickers et al., 1994, 1996; Sampson et al., 1997).

However, GABAergic interneurons are also somehow vulnerable to AD pathology, indeed an interesting work has demonstrated that PV interneurons vulnerability is not associated to neurofibrillary tangle formation but to the loss of neuronal projections with which they are associated (Solodkin et al., 1996).

Since it is clear that different neuronal populations show distinct vulnerability to pathogenic factors and that they are involved in neuronal networks in different ways, it is extremely important to have a deep characterization of the neuronal loss or alteration during the pathology progression.

Spine-free CR-positive GABAergic interneurons (the most abundant CR cells in the hippocampal CA1) have been demonstrated to form synapses with other non-principal neurons and for this reason they are supposed to be disinhibitory cells participating in synchronizing the inhibition of principal cells (Gulyás et al., 1996; Del Rio and DeFelipe, 1997). PV-positive interneurons innervate principal cells

forming inhibitory synapses (Andressen et al., 1993). The dysfunction or loss of these inhibitory neurons might cause hyperexcitability of the target neurons with detrimental consequences on their viability.

To sum up, our results in the 3xTg-AD mice 18 months old demonstrate that the aggravation of symptoms during AD might be related to the loss of PV- and CR-positive interneurons, hence to the alteration of specific neuronal circuits, which might be important for the brain functionality. Indeed, this could be also an explanation of why severe symptoms appear only after many years of the onset of AD pathogenesis. In conclusion, the identification of all the neuronal populations that might be responsible of pathogenesis onset and progression during the entire development of the disease could be useful for a better understanding of the complexity of AD and for the investigation of therapies that are able to recover brain functionality by targeting specific cellular subsets.

Reference	Region	Markers	Outcome
(Hof and Morrison, 1991)	FC	CB	Preserved, reduced in layer III
(Ferrer et al., 1993)	FC	PV	Preserved
(Satoh et al., 1991)	FC, PC, OC	PV	Reduced (parahipp gyrus)
(Inaguma et al., 1992)	FC, PC, OC	PV	Reduced (parahipp gyrus)
(Arai et al., 1987)	FC, TC	PV	Reduced numbers and size
(Hof et al., 1991)	PFC, ITC	PV	Preserved
(Hof et al., 1993)	PFC, ITC	CR	Preserved
(Fonseca et al., 1993)	TC	PV	PV cells modified, dystrophic neurites and sprouting
(Ferrer et al., 1991)	TC	PV	Preserved
(Fonseca and Soriano, 1995)	TC	CR	Preserved
(Leuba et al., 1998)	VC	PV, CR, CB	Preserved
(Mikkonen et al., 1999)	EC	PV, CR, CB	PV and CB reduced
(Solodkin et al., 1996)	EC	PV	Reduced
(Brady and Mufson, 1997)	Hi	PV	Reduced
(Brion and Résibois, 1994)	Hi	CR	Dystrophic neurites (parahipp gyrus and subiculum)
(Popovi et al., 2008)	Hi	PV, CR, CB	Reduced
(Takahashi et al., 2010)	Hi	PV, CR	Reduced
(Albuquerque et al., 2015)	Hi	SOM, NPY, PV	SOM, NPY reduced, PV preserved
(Verdaguer et al., 2015)	Hi	PV, CR, CB	PV increased, CR preserved, CB reduced
(Lemmens et al., 2011)	FC	PV, CR	Preserved
(Saiz-Sanchez et al., 2012)	Olf C	SOM, CR, PV, CB	Reduced first SOM and CR, then PV and CB
(Saiz-Sanchez et al., 2013)	Olf System	SOM, CR, PV	Reduced first SOM and CR, then PV

**Table 4.4 Summary of published reports on PV- and CR-expressing neuronal subpopulations in AD**, adapted from Takahashi et al., 2010.

FC frontal cortex, PC parietal cortex, OC occipital cortex, TC temporal cortex, PFC prefrontal cortex, ITC inferior temporal cortex, VC visual cortex, EC entorhinal cortex, Hi hippocampus, Olf C olfactory cortex, PV parvalbumin, CR calretinin, CB calbindin, SOM somatostatin, NPY neuropeptide Y.



## Chapter 5

### **Characterization of S100 $\beta$ -positive astrocytes compared to GFAP and GS astrocytic markers in the entorhinal cortex during ageing and progression of Alzheimer's disease.**

Gardenal E, Zallo F, Terzieva S, Yeh CY, Verkhatsky A, Rodríguez JJ. (2017) Manuscript in preparation

#### **5.1 S100 $\beta$ -positive astrocytes Nv does not change during ageing and AD pathology, but GFAP and GS astrocytic populations show slightly alterations**

S100 $\beta$ -positive cells showed that they are equally distributed throughout the entire EC in non Tg and 3xTg-AD animals of different ages (Fig. 5.1 B, C, F, G and Fig. 1 D, E, H, I respectively) and neither Nv (number of cells/mm<sup>3</sup>) of S100 $\beta$ -positive astrocytes nor their distribution demonstrated significant changes in the EC of the aged or transgenic animal tissues (Fig. 5.1 A-I). The S100 $\beta$  positive astrocytes in the EC showed typical morphology of protoplasmic astrocytes, characterized with small and rounded somata, radially extending proximal processes and several distal processes branching in random fashion and forming the extended "spongiform" arborisation (Fig. 5.3).

The dual labelling of astrocytes in the EC of 18 months old mice with different astroglial markers has permitted to identify different astrocytic populations. S100 $\beta$  is expressed in the majority of astrocytes, if not almost all of them, while GS is slightly less expressed and GFAP is the marker less present in the EC (Fig. 5.2 A, B) of both aged and 3xTg-AD mice. The double labelling S100 $\beta$ /GFAP showed that most of S100 $\beta$ -positive astrocytes are negative for GFAP (77% in non Tg mice and 69% in 3xTg-AD mice), while all GFAP-positive astrocytes express also S100 $\beta$  (Fig. 5.2 A, C). The numerical density of total S100 $\beta$  and single S100 $\beta$ -positive astrocytes was not altered between non Tg and 3xTg-AD mice, but GFAP-positive astrocytes were found significantly increased in the 3xTg-AD animals 18 months old compared to the non Tg (Fig. 5.2 A, C).

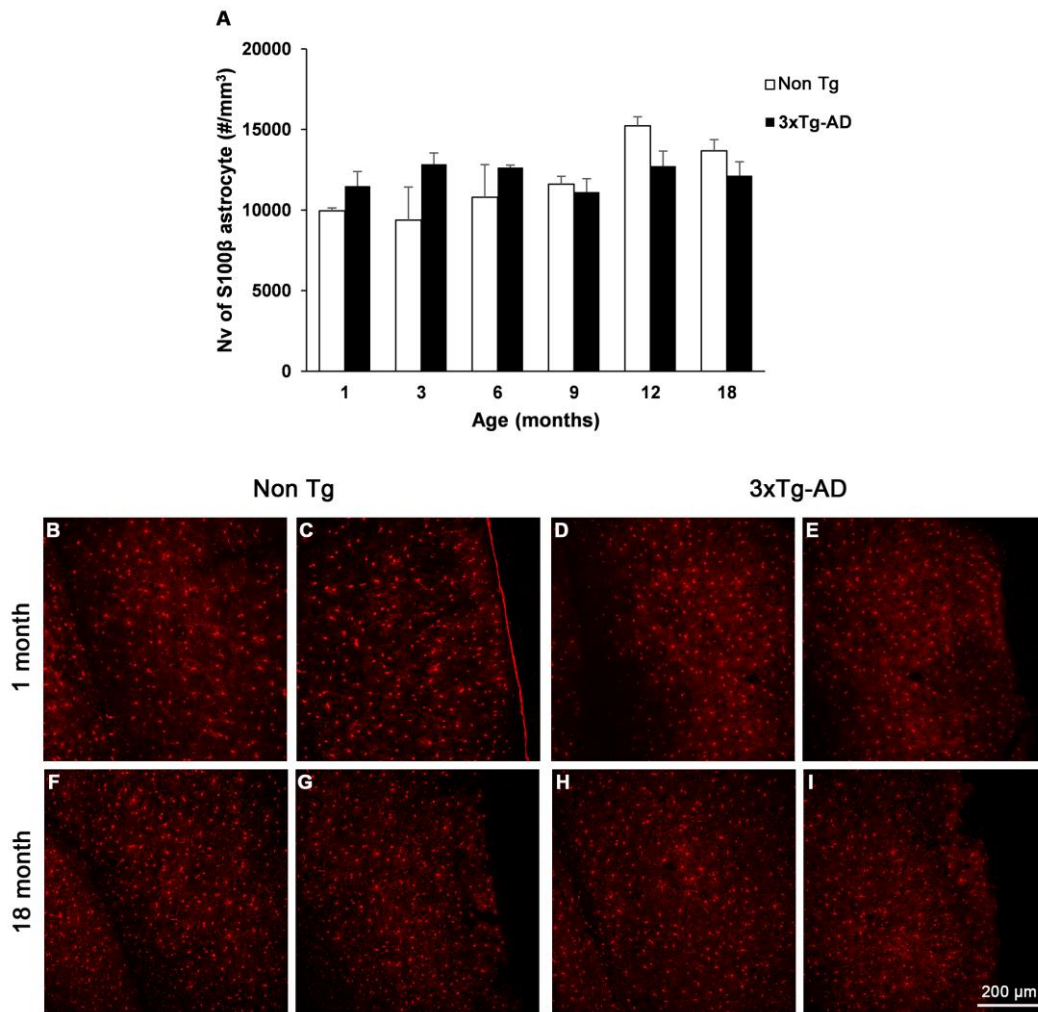


**Fig. 5.1: Nv of S100β-positive astrocytes in the EC is not altered during ageing between the 2 genotypes.** (A) Histogram showing the numerical density of S100β-positive astrocytes in the EC of 3xTg-AD mice compared with non Tg animals. Bars represent mean ± SEM. (B-I) Confocal images depicting cell density of S100β-IR cells in the deeper (D, H) and superficial (E, I) layers of EC of 3xTg-AD mice compared with deeper (B, F) and superficial (C, G) layers of EC of non Tg animals, at age of 1 and 18 months, respectively. N for 3xTg-AD are 3, 4, 4, 4, 3, 5 and n for non Tg are 4, 4, 3, 3, 5, 4 at respectively 1, 3, 6, 9, 12, 18 months of age.

The analysis of S100β/GS astrocytes demonstrated that the majority of S100β-positive astrocytes express also GS (50% in non Tg mice and 65% in 3xTg-AD mice; Fig. 5.2 B, D), however a big population of single S100β astrocytes is present (38% in non Tg and 31% in 3xTg-AD mice), whereas the single GS are the smallest population and they showed a significant decrease in 3xTg-AD animals respect to the non Tg mice (12% and 4% in non Tg and 3xTg-AD mice respectively; Fig. 5.2 B, D). Since the total numerical density of astrocytes is unchanged between non Tg and 3xTg-AD mice, the alteration found in GFAP- and GS- positive astrocytes suggest that during the pathogenesis astrocytes can

alter the expression of these proteins which probably are related with their specific function and reaction to brain damage.

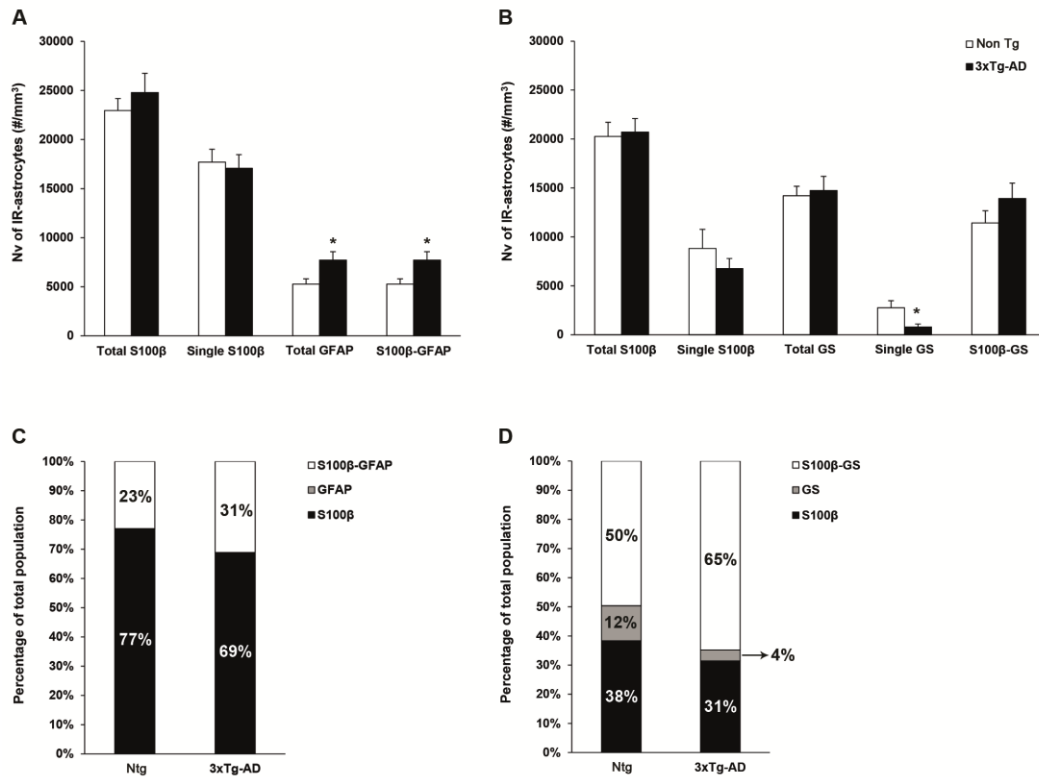


**Fig. 5.2 GS and GFAP positive astrocytes are less numerous and show alterations in their Nv in the EC of 3xTg-AD mice compared to the non Tg.** Bar graphs showing the Nv of double labelled S100β and GFAP astrocytes (A) as well as S100β and GS (B) in 18 months old 3xTg-AD mice compared to control mice. Data represent mean ± SEM (\* p ≤ 0.5). Bar graphs showing the estimated percentage of different astrocytic populations that are S100β and GFAP positive (C) and S100β and GS positive (D) in 3xTg-AD mice and their respective controls.

## 5.2 Age-dependent increase in S100β-positive profiles

S100β-positive astrocytes in the EC of the non-transgenic animals in ageing showed a statistically significant steady and continuous increase of their surface area and of their volume at 9 months of age. Compared to 1 month old mice, S100β profiles showed an increment of the surface area by 50.07% (p = 0.01) at 9 months of age, by 42.77% at 12 months (p = 0.05) and by 116,38% (~2 fold) at 18 months (p=0.005; Fig. 5.3 and 5.4 A and Table 5.1). However, the volume was significantly larger only at 18 months of age with a 117.98% increase (p=0.006) when compared with 1 month-old animals (Fig. 5.3 and 5.4 B and Table 5.1). Surface area and volume of the cell bodies showed no significant change at any age, whereas the S100β-positive processes were significantly increased; therefore,

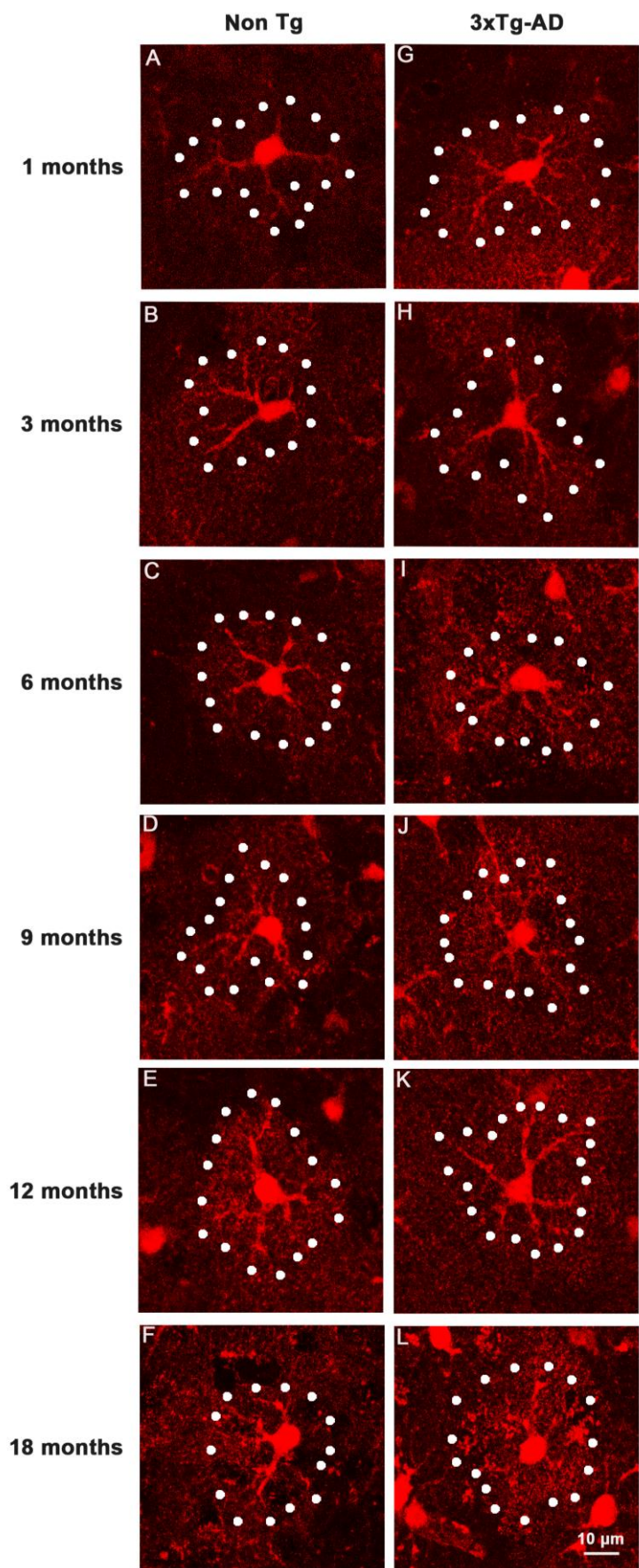


**Fig. 5.3: Changes in the S100 $\beta$ -positive profiles of astrocytes with age in non Tg and 3xTg-AD mice.** Representative confocal images of S100 $\beta$ -positive astrocytes in the EC of 3xTg-AD mice at age of 1, 3, 6, 9, 12 and 18 months (A, B, C, D, E and F, respectively) and their age-matched non Tg controls (G, H, I, J, K and L, respectively).

the general morphometric changes result exclusively from the enlargement of the processes and not the cell body (Fig. 5.3 and 5.4 C, D and Table 5.1). At 9 months of age, the surface area and the volume of astrocytic processes in the EC were increased by 164.49% ( $p = 0.004$ ) and 165.41% ( $p = 0.008$ ) when compared to 1 month old mice. At 12 months, the surface area was increased by 131.39% ( $p=0.04$ ), and the volume by 148.24% ( $p=0.05$ ), whereas at 18 months, the processes surface area was 375.46% larger ( $p=0.002$ ) and volume 417.57% larger ( $p=0.002$ ) (Fig. 5.4 E, F and Table 5.1).

S100 $\beta$ profiles	1 month	9 months	12 months	18 months
Cell surface in $\mu\text{m}^2$	507.25 $\pm$ 50.81	764.31 $\pm$ 28.23	724.22 $\pm$ 36.98	1097.58 $\pm$ 98.76
Cell volume $\mu\text{m}^3$	132.41 $\pm$ 31.36	177.12 $\pm$ 12.50	199.78 $\pm$ 7.51	288.63 $\pm$ 31.36
Processes surface in $\mu\text{m}^2$	147.48 $\pm$ 34.42	390.07 $\pm$ 21.72	341.25 $\pm$ 44.17	701.21 $\pm$ 77.18
Processes volume in $\mu\text{m}^3$	27.32 $\pm$ 7.48	72.51 $\pm$ 5.15	64.82 $\pm$ 8.61	141.40 $\pm$ 16.11
Somata surface in $\mu\text{m}^2$	359.77 $\pm$ 21.41	341.87 $\pm$ 31.02	464.88 $\pm$ 33.86	419.81 $\pm$ 46.58
Somata volume in $\mu\text{m}^3$	105.09 $\pm$ 21.70	97.93 $\pm$ 10.99	161.73 $\pm$ 11.04	156.10 $\pm$ 17.12

**Table 5.1 S100 $\beta$  morphometric values in the non Tg mice at 1, 9, 12 and 18 months of age.** Values are expressed as means  $\pm$  SEM.

### 5.3 S100 $\beta$ -positive astroglial profiles in 3xTg-AD

The morphological changes in S100 $\beta$ -positive astrocytes in the EC among the age groups of 3xTg-AD mice were less pronounced than the aged non transgenic mice and they reached statistical significance at 18 months of age. S100 $\beta$  positive profiles in 18 months old 3xTg-AD mice showed an increase of 150.71% ( $p=0.003$ ; Fig. 5.3 and 5.4 A) and 166.73% ( $p=0.006$ ; Fig 5.3 and 5.4 B and Table 5.2), in the surface area and volume, respectively, when compared to 1 month old 3xTg-AD mice. Similarly, the morphometric parameters of the cell compartments showed alterations only at age of 18 months. The surface area of the cell processes was increased by 281.16% ( $p=0.003$ ; Fig. 5.3 and 5.4 E and Table 5.2), and the volume by 343.16% ( $p=0.006$ ; Fig. 5.3 and 5.4 F and Table 5.2) when compared to their 1 month old 3xTg-AD mice. Moreover, the somata volume was increased by 54.06% ( $p=0.02$ ; and Table 5.2) whereas no significant alterations were found in the surface area, in the same age group.

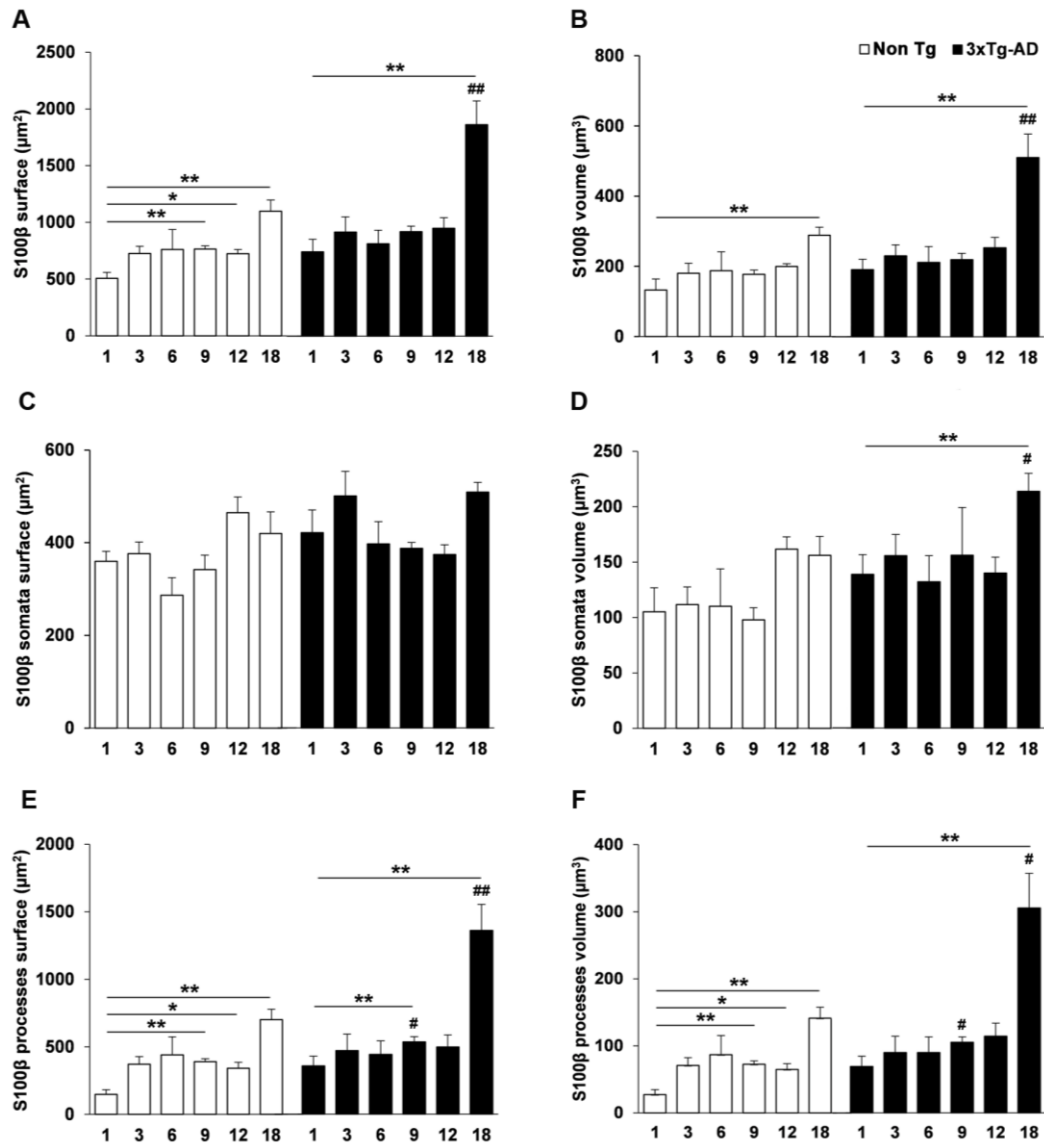


**Fig. 5.4: Increase of the s100β-positive astrocytes' surface area and volume in the EC of 3xTg-AD mice and the non Tg controls between the age of 1 and 18 months.** (A, C, E) Histograms showing surface area differences in the entire S100β-IR cells (A), their cell bodies (C) and processes (E) in the EC of 3xTg-AD and non Tg mice in the age between 1 and 18 months. (B, D, F) Histograms showing differences in the volume of the entire s100β-IR cells (B), their cell bodies (D) and processes (F) in the EC of 3xTg-AD and non Tg mice of age between 1 and 18 months. Bars represent mean ± SEM (\* p≤0.05, \*\* p<0.01, comparing with 1 month animals from the same genotype; # p≤ 0.05, ## p<0.01 comparing 3xTg-AD mice with their aged-matched non Tg control).

When comparing 3xTg-AD animals with their age-matched non Tg controls, an increment of the surface area and volume in 3xTg-AD mice was already evident at 1 month, but statistical significant differences were observed only at 18 months of age, when an increase of 69.74% in the surface area (p=0.01; Fig. 5.4 A) and 76.73% in the volume (p=0.01; Fig. 5.4 B) was detected (Fig. 5.3 and Table 5.2).

S100 $\beta$ profiles	1 month	9 months	12 months	18 months
Cell surface in $\mu\text{m}^2$	743.08 $\pm$ 110.32	919.84 $\pm$ 48.13	949.26 $\pm$ 94.05	1862.98 $\pm$ 208.83
Cell volume $\mu\text{m}^3$	191.24 $\pm$ 29.39	219.82 $\pm$ 17.69	253.46 $\pm$ 29.36	510.09 $\pm$ 67.59
Processes surface in $\mu\text{m}^2$	356.14 $\pm$ 72.23	532.68 $\pm$ 39.28	495.99 $\pm$ 89.11	1357.55 $\pm$ 193.35
Processes volume in $\mu\text{m}^3$	68.27 $\pm$ 15.19	104.22 $\pm$ 7.75	112.89 $\pm$ 19.54	302.28 $\pm$ 51.20
Somata surface in $\mu\text{m}^2$	421.00 $\pm$ 49.32	387.16 $\pm$ 13.02	374.21 $\pm$ 20.97	508.63 $\pm$ 21.08
Somata volume in $\mu\text{m}^3$	137.62 $\pm$ 17.67	154.71 $\pm$ 42.77	138.84 $\pm$ 14.26	212.02 $\pm$ 16.06

**Table 5.2 S100 $\beta$  morphometric values in the 3xTg-AD mice at 1, 9, 12 and 18 months of age.** Values are expressed as means  $\pm$  SEM.

The same animals were also characterised by enlarged somata with an increase in the volume of the cell body of 35.82% ( $p=0.04$ ; Fig. 5.4 D), whereas no significant alterations were detected in the surface area (Fig. 5.4 C and Table 5.2). In addition, differences in the morphometric parameters of the astrocytic processes in the 3xTg-AD mice were detected at 9 months of age when the surface area and the volume were increased by 36.56% ( $p=0.05$ ; Fig. 5.4E) and 43.73% ( $p=0.039$ ; Fig. 5.4F and Table 5.2), respectively, when compared with non Tg animals.

S100 $\beta$ profiles	18 months non-Tg	18 months 3xTg-AD
Cell surface in $\mu\text{m}^2$	1097.58 $\pm$ 98.76	1862.98 $\pm$ 208.83
Cell volume $\mu\text{m}^3$	288.63 $\pm$ 31.36	510.09 $\pm$ 67.59
Processes surface in $\mu\text{m}^2$	701.21 $\pm$ 77.18	1357.55 $\pm$ 193.35
Processes volume in $\mu\text{m}^3$	141.40 $\pm$ 16.11	302.28 $\pm$ 51.20
Somata surface in $\mu\text{m}^2$	419.81 $\pm$ 46.58	508.63 $\pm$ 21.08
Somata volume in $\mu\text{m}^3$	156.10 $\pm$ 17.12	212.02 $\pm$ 16.06

**Table 5.3 S100 $\beta$  morphometric values in the 3xTg-AD mice compared to the non Tg at 18 months of age.** Values are expressed as means  $\pm$  SEM.

No differences were found in the astrocytic processes at 12 months of age, while a maximal increase of 2 folds was detected in 3xTg-AD animals at age of 18 months both in the surface area (93.6%;  $p=0.013$ ) and volume (113.78%;  $p=0.017$ ; Fig. 5.4 E, F and Table 5.2, 5.3).

#### 5.4 Hypertrophy of S100 $\beta$ -positive astrocytes is associated with the presence of A $\beta$ plaques

Finally, an important analysis compared the S100 $\beta$ -positive profiles of astrocytes associated with  $\beta$ -amyloid plaques (with somatas placed within 50  $\mu\text{m}$  range from the plaque border) with astrocytes located further away from the plaques (Fig. 5.5 A-C and Table 5.4). Although the accumulation of A $\beta$  plaques in the EC starts at 12 months of age, the measurements were performed in 18 months old animals where the astroglial hypertrophy is maximal. The S100 $\beta$ -positive astroglial profiles associated with plaques were much larger than astrocytes distant to them: the surface area was 136.00% larger ( $p=0.05$ ; Fig. 5.5 D) and the volume 140.20% larger ( $p=0.06$ ; Fig. 5.5 E and Table 5.4). Surface area of somata of astrocytes associated with plaques was 54.90% larger ( $p=0.006$ ; Fig. 5.5 D), and their volume 66.34% larger (66.34%;  $p=0.004$ ; Fig. 5.5 E and Table 5.4). Processes of astrocytes associated with plaques were similarly larger when compared to distal astrocytes. The surface area and the volume of processes of cells located near plaques were 195.70% ( $p=0.06$ ; Fig. 5.5 D) and 231.57% larger ( $p=0.07$ ; Fig. 5.5 E and Table 5.4).

S100 $\beta$ profiles	18 months 3xTg-AD close to A $\beta$ plaques	18 months 3xTg-AD far from A $\beta$ plaques
Cell surface in $\mu\text{m}^2$	2891.19 $\pm$ 683.88	1225.10 $\pm$ 107.76
Cell volume $\mu\text{m}^3$	807.99 $\pm$ 206.73	336.38 $\pm$ 37.15
Processes surface in $\mu\text{m}^2$	2319.71 $\pm$ 662.92	784.48 $\pm$ 92.14
Processes volume in $\mu\text{m}^3$	545.57 $\pm$ 173.07	164.54 $\pm$ 21.43
Somata surface in $\mu\text{m}^2$	688.50 $\pm$ 53.62	444.47 $\pm$ 22.55
Somata volume in $\mu\text{m}^3$	292.04 $\pm$ 17.81	175.57 $\pm$ 17.87

**Table 5.4 S100 $\beta$  morphometric values in the astrocytes close to A $\beta$  plaques and far from A $\beta$  plaques in the 3xTg-AD mice at 18 months of age.** Values are expressed as means  $\pm$  SEM.

Astrocytes in the EC of 3xTg-AD mice located far from amyloid plaques showed no statistical significant differences in their morphometric values when compared with the astrocytes in the non-transgenic mice (Fig. 5.5 D, E).



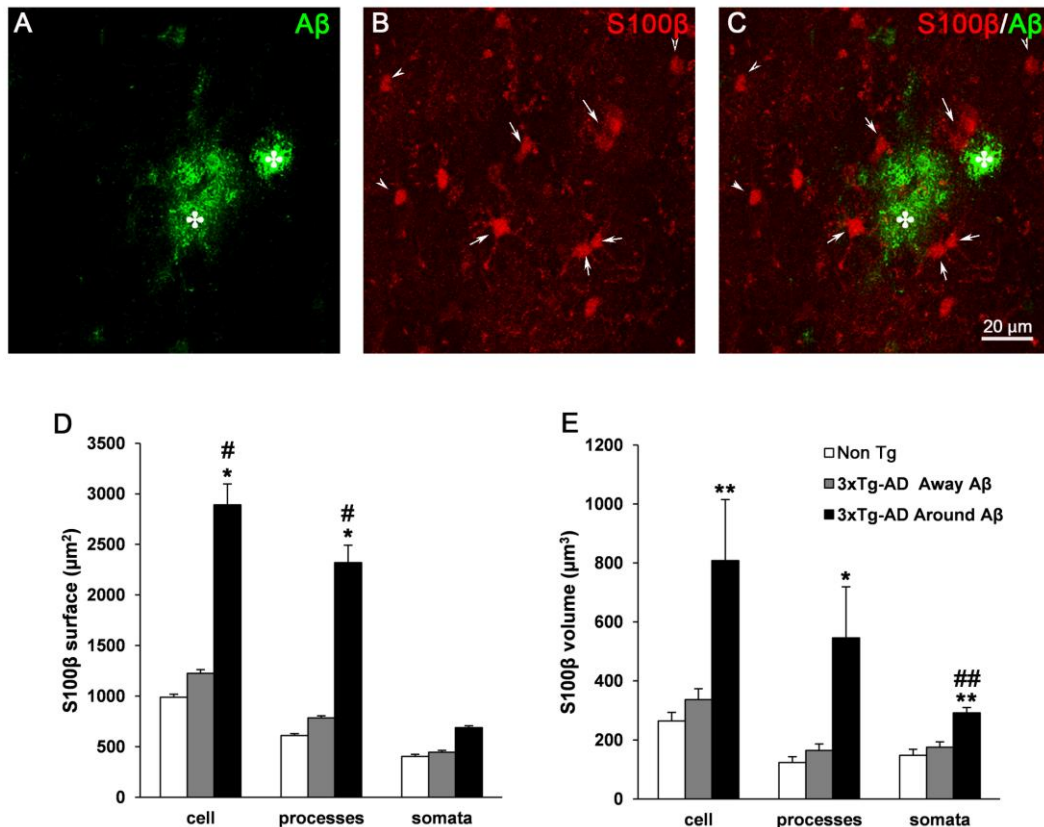


**Fig. 5.5: Increment in the surface area and volume of s100β-IR astrocytes in close vicinity to senile plaques in EC of 3xTg-AD mice at age of 18 months.** (A-C) Representative confocal images of Aβ (A, green) and S100β-positive astrocytes (B, red) dual labelling (C) showing the morphometric difference in the astrocytes distant from the plaques (indicated with arrowhead) and associated with the Aβ plaques (indicated with arrows). (D and E) Histograms showing the difference in surface area (D) and volume (E) between the S100β expressing astrocytes located around the senile plaques and those placed distant to the plaques in the EC of the 3xTg-AD, compared to S100β expressing astrocytes in the EC of the non Tg animals. Morphometric analysis was performed on the entire astrocyte, but also cells counterparts, the processes and the somata. Bars represent mean ± SEM (\* p<0.05; \*\* p <0.01 compared with astrocytes from non Tg mice; # p<0.05, ## p<0.01 comparing with the astrocytes away from the plaques).

### 5.5 Distinct astrocytic populations show different morphological alterations during AD progression

A preliminary morphological characterization was conducted on S100β/GFAP and S100β/GS astrocytes of non-transgenic and 3xTg-AD mice 18 months old. In general, S100β/GFAP positive astrocytes showed a decrease in the surface and volume of both S100β and GFAP profiles, even if this reduction was not significant (Fig. 5.6).

The analysis of S100β/GS positive astrocytes showed that both S100β and GS profiles are increased in 3xTg-AD mice 18 months old compared to the non-transgenic mice. The increase of GS profiles seem to be in discordance with

previous work (Yeh, 2013) that demonstrated GS is not altered in 3xTg-AD mice compared to non Tg, but we should bear in mind that this study was conducted on mice maximum 12 months old, thus a more aggravated stage of the disease might be the cause of an increase in the GS-profiles that we preliminary found in the present work. Indeed, S100 $\beta$ -positive profiles show an increase in 3xTg-AD mice only at 18 months of age when compared to non-transgenic animals. However, further experiments are necessary to better characterize these astrocytic sub-populations.

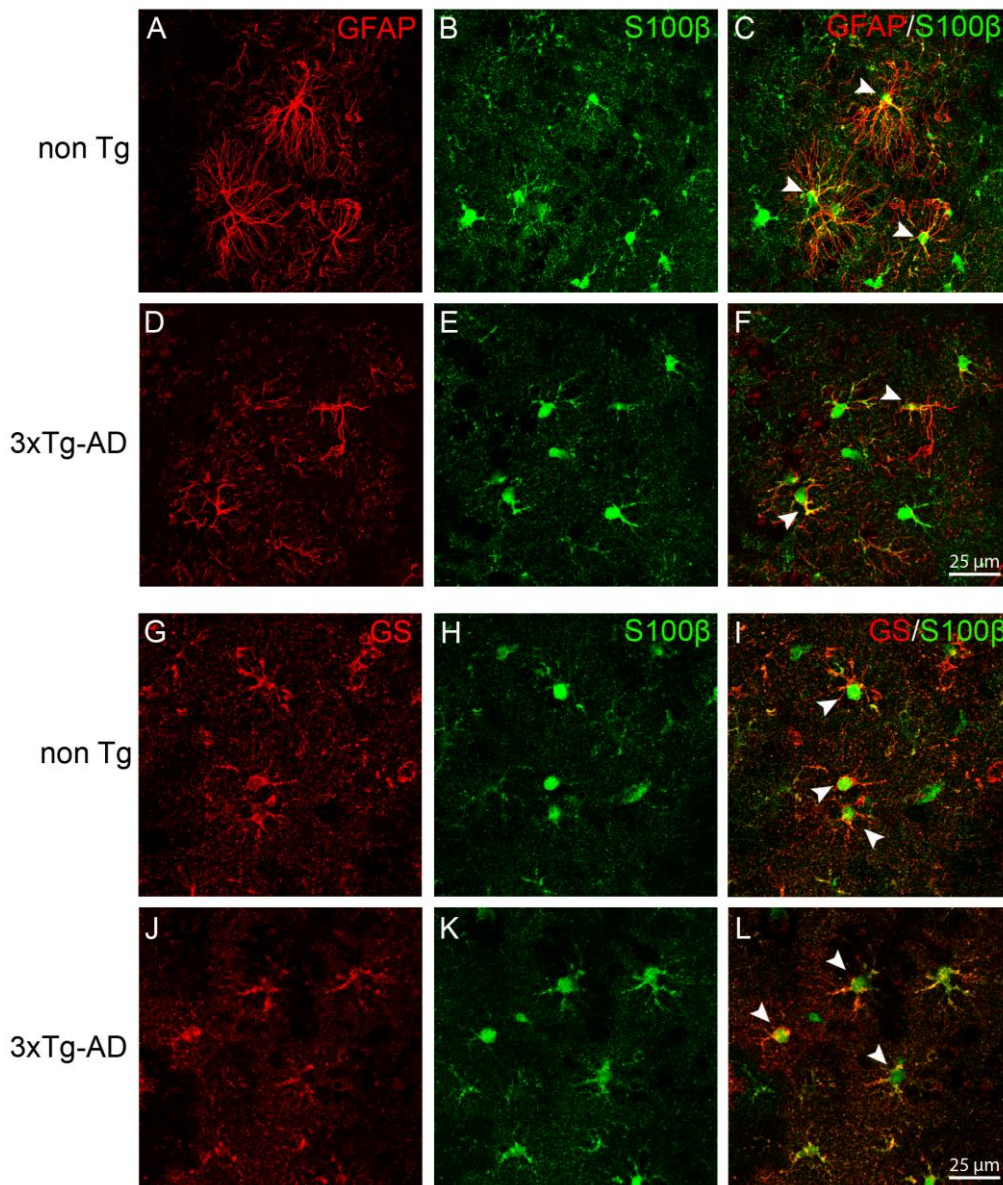


**Fig. 5.6: S100 $\beta$ , GFAP and GS differently label astrocytes.** Confocal micrographs showing in red the astrocytic labelling with GFAP (A, C, D, F) and GS (G, I, J, L) and in green the astrocytic labelling with S100 $\beta$  (B, C, E, F, H, I, K, L) in the EC of 18 months old non-transgenic mice compared with the 3xTg-AD mice. Scale bars: 25  $\mu$ m.

## 5.6 Discussion

The present study provides an astrocytic numerical analysis and morphological characterization of the entorhinal cortex of 3xTg-AD mice and their non-transgenic counterpart based on the trophic astroglial marker S100 $\beta$ . Different brain areas and regional subfields present astrocytes with distinct morphology and functional specialisation and their features and distribution can show a considerable divergence depending on the astrocytic marker utilised. Moreover, astrocytic heterogeneity is even more visible during pathogenesis, where different subsets of astrocytes respond with a different behaviour to CNS insults depending on the specific vulnerability or resistance of each brain region (Emsley and Macklis, 2006; Matyash and Kettenmann, 2010; Oberheim et al., 2012; Verkhratsky et al., 2013).

The S100 $\beta$  immunolabelling of astroglia in the entorhinal cortex reported in this study has displayed a highly numerous astrocytic population when compared to astrocytes labelled with other markers. Indeed, S100 $\beta$ -positive astrocytes occupy the entire extent of this cortical region and they are much more abundant than GS- and GFAP-positive astrocytes. Analogously, Savchenko et al. demonstrated a different distribution of S100 $\beta$ - and GFAP-positive astrocytes in the normal adult brain, in fact, GFAP stained more astrocytes in white matter than in grey matter and GFAP-positive astrocytes were approximately one-third that of S100 $\beta$ -positive astrocytes (Savchenko et al., 2000). Despite being S100 $\beta$  expressed also in some rat and mouse neurons and oligodendrocytes, its expression in these cells is very rare and concerns only some brain areas, thus the non-astrocytic cells S100 $\beta$ -positive can be considered negligible in quantitative studies. Therefore, since almost the entire cellular extent labelled with S100 $\beta$  is formed by astrocytes, S100 $\beta$  can be recognized as the chemical marker that label the largest population of astrocytes (Rickmann and Wolff, 1995; Ogata and Kosaka, 2002).

The counting of S100 $\beta$ -positive astrocytes in this work demonstrated that their numerical density was not altered in the 3xTg-AD mice, but the morphological analysis of their profiles showed a significant increase of volume and surface of the S100 $\beta$ -positive astrocytes at 18 months of age compared to the non Tg mice. An increased astrocytic expression of S100 $\beta$  was already associated with AD

pathogenesis and with cerebral amyloidosis and gliosis (Griffin et al., 1998; Mori et al., 2010), as well as its secretion in the CSF was related with AD severity (Whitaker-Azmitia et al., 1997; Jesse et al., 2009). Indeed, here we have also demonstrated that this increase is exclusive of A $\beta$  plaques-related astrocytes, while S100 $\beta$  astrocytic profiles of distant astrocytes were unchanged comparing to non Tg mice. It is noteworthy the observation that S100 $\beta$ -positive profiles are significantly higher at 18 months of age also in the non Tg mice compared to the younger animals, this means that there is also a component of age in the increase of S100 $\beta$ -positive profiles. Astrocytic relevance in AD is usually contemplated considering only astrogliotic reaction and production of inflammatory cytokines. However, what we have observed in the 3xTg-AD mice is that astrocytes become gliotic only at late stages of the pathogenesis and this reactivity is circumscribed to specific regions and in the vicinity of A $\beta$  plaques. The role that astrocytes might have in AD early stages, prior to A $\beta$  deposition, is almost unknown and underestimated. At these stages, we have observed a very small and non-significant increase in S100 $\beta$ -positive profiles in 3xTg-AD mice entorhinal cortex compared to the non Tg animals. In previous studies it was demonstrated an early astrocytic atrophy (already evident at 1 month of age and sustained, even if with a lesser extent, until 12 months of age) in the EC of the 3xTg-AD animal model by means of GFAP labelling, while GS-positive profiles showed no alteration in the same area (Yeh et al., 2011, 2013). An original work that analysed the S100 $\beta$  level in serum reported a positive correlation between S100 $\beta$  concentration in the serum and severity of the disease, but interestingly, the total AD group showed a lower serum level of S100 $\beta$  compared to the controls (Chaves et al., 2010). This finding suggest that initial astrocytic dysfunction might be characterized by an incapability to protect neurons, whilst their inflammatory activation is a late event that only favour the progression of the pathology.

In this study a significant increase of the S100 $\beta$ /GFAP positive astrocytes was found in the 3xTg-AD mice at 18 months of age comparing with the non Tg mice, but the profiles of these astrocytes were decreased. This finding is in line with our previous study which demonstrated GFAP atrophy in the entorhinal cortex (Yeh et al., 2011). The numerical density increase of S100 $\beta$ /GFAP positive astrocytes is

associated to a decrease in single GS astrocytes. We hypothesize that GS single astrocyte at late stages of AD might start to express S100 $\beta$  protein as a reaction to the amyloid pathology, but further experiments must be conducted to elucidate these preliminary data.

Altogether these findings demonstrate that distinct astrocytic populations in the EC probably have different functional properties and might respond in a diverse way during AD progression. We sustain that further studies should be conducted to better characterize astrocytic diversity and role in the different brain regions and a deep characterization of their role in AD should be studied at early stages when their behaviour doesn't resemble to be reactive and inflammatory but rather atrophic and insufficient to support and defend neurons from pathological conditions.

## Chapter 6

### Conclusions

This research work has had the aim to characterize three distinct aspects of AD pathogenesis in the 3xTg-AD mouse model: 1. The expression changes (increase) in the Calcium Sensing Receptor within the hippocampus during the progression of AD pathology; 2. The decreased expression of two calcium binding proteins, parvalbumin and calretinin, in the hippocampus at late stages of the pathology and 3. The determination and characterization of the numerical density, the distribution and the morphological profiles of astrocytes positive for the astrocytic marker S100 $\beta$  in the entorhinal cortex in relation with AD progression and comparing also to other astrocytic markers such as GFAP and GS.

In Chapter 3, the immunohistochemical analysis of the expression of the CaSR in 3xTg-AD animals compared to non-transgenic animals has revealed an increase of the expression of the CaSR in specific hippocampal subfields which are characterized by accumulation of intracellular and extracellular A $\beta$  and amyloid plaques depositions. This study has been performed on the basis of a new original hypothesis of pathological A $\beta$  hyperproduction and diffusion in the brain. Experiments conducted on human primary cortical astrocytes have demonstrated that there is a direct interaction between A $\beta$ <sub>42</sub> toxic oligomers and the CaSR, which can activate this receptor and induce an increased production and secretion of A $\beta$ <sub>42</sub> peptides. This mechanism has been demonstrated through the concomitant administration of exogenous A $\beta$  and a specific antagonist of CaSR, the compound NPS 2143, which is able to totally block A $\beta$  self-induction caused by the A $\beta$  and CaSR interaction (Armato et al., 2013). Therefore, this new pathological pathway has been proposed as a fundamental process of spread of the deleterious A $\beta$  peptides. After *in vitro* A $\beta$  stimulation, CaSR resulted also hyperexpressed. The finding here reported that CaSR has increased expression also in the 3xTg-AD mouse model compared to the non-transgenic mice is an interesting evidence

which permit to sustain the need to further investigate this pathological mechanism of increased amyloidogenesis due to CaSR direct activation. Future studies will aim to treat these animals with a calcilytic compound as NPS 2143 to test its possible therapeutical use in the treatment of AD.

In Chapter 4, PV- and CR-positive interneurons were analysed in the hippocampus of the 3xTg-AD mice to measure their numerical density alteration and the changes in the total expression of these two calcium-binding proteins. GABAergic interneurons immunoreactive for both PV and CR resulted numerically reduced in the CA1 area, which is strongly affected by A $\beta$  plaques deposition and NFTs formation and is strictly connected with entorhinal cortex and subiculum in the hippocampal-entorhinal circuit involved in memory formation. The labelling of these calcium-binding proteins showed a deterioration of the neurons that are still immunoreactive, and in addition also a decrease in the expression of PV, which was significantly evident in the CA1 area of the hippocampus. The dysfunction of inhibitory interneurons is believed to be extremely detrimental for the functionality of brain since it can alter the general function of entire complex networks and might be crucial for the appearance of symptoms. This was the first characterization of calcium binding proteins in the 3xTg-AD mouse model, the possible alterations of other subpopulations of inhibitory interneurons should be investigated in this mouse model in the future, as well as the age-related onset of these changes, in order to establish the exact relation with the progression of the disease.

In chapter 5, an extensive analysis of S100 $\beta$ -positive profiles confirmed our previous results, which showed an increase in their surface and volume on the entorhinal cortex of normal aged mice (Rodríguez et al., 2014). Moreover, in the present work the same analysis was conducted also in the 3xTg-AD animals and demonstrated that S100 $\beta$ -positive profiles are even more expanded than in the normal mice, with significant increase evident at 9 months of age, but massive difference only at 18 months of age. A deeper characterization showed that this significant increase is specific of astrocytes that localize close to A $\beta$ -plaques, while the more distant astrocytes have S100 $\beta$ -profiles similar to the non-transgenic animals. This evidence supports our hypothesis that astrocytic

hypertrophy is associated only to A $\beta$  plaques and become manifest only at late stages, whereas astrocytes that are not in close contact with neuritic plaques are not reactive and might be incapable to defend neurons from toxic agents such as the diffusible A $\beta$  oligomers.

Altogether these different works demonstrate that many pathways and cellular populations are affected with a different temporal and regional pattern during AD and they should be all clarified in a way to better understand the mechanism of onset and progression of AD. However, all the alterations that we have investigated are clearly related with amyloid and tau pathology, since the protein changes found appear in the areas where the AD hallmarks first accumulate. These alterations, even if in the 3xTg-AD mouse model are a consequence of A $\beta$  hyperproduction, concur to the progression of AD pathology and/or to the onset of symptoms and if considered in early stages of the disease they might be an efficient target to stop the progression of the pathology. Hence, a multi target approach might be more useful to the final purpose of preventing and treating AD.

Furthermore, all the proteins that we have investigated in this research work are somehow related to calcium signalling and/or homeostasis; and since calcium is extremely important for neuronal excitability and brain homeostasis, strong attention should be paid to these proteins whose alterations might have severe consequences and can reveal new disease progression mechanisms and potential treatment strategies.



## **Funding**

This research work was supported by the Ministry of Italian University and Research (MIUR), the Spanish Government Plan Nacional de I+D+I 2008-2011, and ISCIII Subdirección General de Evaluación y Fomento de la investigación co-financed by FEDER (grant number PI10/02738), the Government of the Basque Country (grant number AE-2010-1-28; AEGV10/16, GV2011111020), as well as by the Spanish Ministerio de Economía y Competitividad, RETOS Colaboración (grant number RTC-2015-3542-1 co-financed by FEDER).

## References

- Abramov AY, Canevari L, Duchen MR (2003) Changes in intracellular calcium and glutathione in astrocytes as the primary mechanism of amyloid neurotoxicity. *J Neurosci* 23:5088–5095
- Abramov AY, Canevari L, Duchen MR (2004)  $\beta$ -Amyloid Peptides Induce Mitochondrial Dysfunction and Oxidative Stress in Astrocytes and Death of Neurons through Activation of NADPH Oxidase. *J Neurosci* 24:565–575
- Albrecht J, Sidoryk-Węgrzynowicz M, Zielińska M, Aschner M (2010) Roles of glutamine in neurotransmission. *Neuron Glia Biol* 6:263–276
- Albuquerque MS, Mahar I, Davoli MA (2015) Regional and sub-regional differences in hippocampal GABAergic neuronal vulnerability in the TgCRND8 mouse model of Alzheimer's disease. 7:1–7.
- Alzheimer A (1907) Über eine eigenartige Erkrankung der Hirnrinde. *Allg Zeits Psychiatry Psych Y Gerichtl Med* 64:146–148.
- Alzheimer A (1910) Beiträge zur Kenntnis der pathologischen Neuroglia und ihrer Beziehungen zu den Abbauvorgängen im Nervengewebe. In: *Histologische und histopathologische Arbeiten über die Grosshirnrinde mit besonderer Berücksichtigung der pathologischen Anatomie der Geisteskrankheiten* (Nissl F, Alzheimer A, eds), pp 401–562. Jena: Gustav Fischer.
- Amaral DG (1978) A Golgi study of cell types in the hilar region of the hippocampus in the rat. *J Comp Neurol* 182:851–914
- Amaral DG (1993) Emerging principles of intrinsic hippocampal organization. *Curr Opin Neurobiol* 3:225–229.
- Amaral DG, Lavenex P (2007) Hippocampal Neuroanatomy. In: *The hippocampus Book* (Andersen P, Morris R, Amaral D, Bliss T, O'Keefe J, eds), pp 832. New York: Oxford University Press.
- Amaral DG, Scharfman HE, Lavenex P (2007) The dentate gyrus: fundamental neuroanatomical organization (dentate gyrus for dummies). *Prog Brain Res* 163:3–22.
- Amaral DG, Witter MP (1989) The three-dimensional organization of the hippocampal formation: a review of anatomical data. *Neuroscience* 31:571–591.
- American Psychiatric Association (2013) *Diagnostic and Statistical Manual of Mental Disorders, Fifth Edition*. American Psychiatric Association.
- Andressen C, Blümcke I, Celio MR (1993) Calcium-binding proteins: selective markers of nerve cells. *Cell Tissue Res* 271:181–208.
- Arai H, Emson PC, Mountjoy CQ, Carasso LH, Heizmann CW (1987) Loss of parvalbumin-immunoreactive neurones from cortex in Alzheimer-type dementia. *Brain Res* 418:164–169.
- Araque A, Parpura V, Sanzgiri RP, Haydon PG (1999) Tripartite synapses: Glia, the unacknowledged partner. *Trends Neurosci* 22:208–215.
- Arendash GW, Lewis J, Leighty RE, McGowan E, Cracchiolo JR, Hutton M, Garcia MF (2004) Multi-metric behavioral comparison of APP<sup>sw</sup> and P301L models for Alzheimer's Disease: Linkage of poorer cognitive performance to tau pathology in forebrain. *Brain Res* 1012:29–41.
- Arendt T, Bigl V, Arendt A, Tennstedt A (1983) Loss of neurons in the nucleus basalis of Meynert in Alzheimer's disease, paralysis agitans and Korsakoff's Disease. *Acta Neuropathol* 61:101–108.
- Arendt T, Stieler J, Strijkstra AM, Hut R a, Rüdiger J, Van der Zee E a, Harkany T, Holzer M, Härtig W (2003) Reversible paired helical filament-like phosphorylation

- of tau is an adaptive process associated with neuronal plasticity in hibernating animals. *J Neurosci* 23:6972–6981.
- Arendt T, Stieler JT, Holzer M (2016) Tau and tauopathies. *Brain Res Bull* 126:238–292.
- Armato U, Chiarini A, Chakravarthy B, Chioffi F, Pacchiana R, Colarusso E, Whitfield JF, Dal Prà I (2013) Calcium-sensing receptor antagonist (calcilytic) NPS 2143 specifically blocks the increased secretion of endogenous A $\beta$ 42 prompted by exogenous fibrillary or soluble A $\beta$ 25-35 in human cortical astrocytes and neurons—Therapeutic relevance to Alzheimer’s disease. *Biochim Biophys Acta - Mol Basis Dis* 1832:1634–1652.
- Attems J, Thal DR, Jellinger KA (2012) The relationship between subcortical tau pathology and Alzheimer’s disease. *Biochem Soc Trans* 40:711–715.
- Bai S, Mao M, Tian L, Yu Y, Zeng J, Ouyang K, Yu L, Li L, Wang D, Deng X, Wei C, Luo Y (2015) Calcium sensing receptor mediated the excessive generation of  $\beta$ -amyloid peptide induced by hypoxia in vivo and in vitro.
- Baimbridge KG, Celio MR, Rogers JH (1992) Calcium-binding proteins in the nervous system. *Trends Neurosci* 15:303–308.
- Bartus RT, Dean RL, Beer B, Lippa AS (1982) The cholinergic hypothesis of geriatric memory dysfunction. *Science* 217:408–414.
- Bateman RJ (2012) Clinical and Biomarker Changes in Dominantly Inherited Alzheimer’s Disease. *N Engl J Med* 367:795–804.
- Beninger RJ, Jhamandas K, Boegman RJ, El-Defrawy SR (1986) Kynurenic acid-induced protection of neurochemical and behavioural deficits produced by quinolinic acid injections into the nucleus basalis of rats. *Neurosci Lett* 68:317–321.
- Billings LM, Oddo S, Green KN, McGaugh JL, LaFerla FM (2005) Intraneuronal A $\beta$  causes the onset of early Alzheimer’s disease-related cognitive deficits in transgenic mice. *Neuron* 45:675–688.
- Blanchard V, Moussaoui S, Czech C, Touchet N, Bonici B, Planche M, Canton T, Jedidi I, Gohin M, Wirths O, Bayer TA, Langui D, Duyckaerts C, Tremp G, Pradier L (2003) Time sequence of maturation of dystrophic neurites associated with A $\beta$  deposits in APP/PS1 transgenic mice. *Exp Neurol* 184:247–263.
- Borchelt DR, Ratovitski T, Van Lare J, Lee MK, Gonzales V, Jenkins NA, Copeland NG, Price DL, Sisodia SS (1997) Accelerated amyloid deposition in the brains of transgenic mice coexpressing mutant presenilin 1 and amyloid precursor proteins. *Neuron* 19:939–945.
- Braak H, Braak E (1991) Neuropathological staging of Alzheimer-related changes. *Acta Neuropathol* 82:239–259.
- Braak H, Del Tredici K (2013) Evolutional Aspects of Alzheimer’s Disease Pathogenesis. *J Alzheimers Dis* 33:155–161.
- Braak H, Thal DR, Ghebremedhin E, Del Tredici K (2011) Stages of the Pathologic Process in Alzheimer Disease: Age Categories From 1 to 100 Years. *J Neuropathol Exp Neurol* 70:960–969.
- Braak H, Zetterberg H, Del Tredici K, Blennow K (2013) Intraneuronal tau aggregation precedes diffuse plaque deposition, but amyloid- $\beta$  changes occur before increases of tau in cerebrospinal fluid. *Acta Neuropathol* 126:631–641.
- Brady DR, Mufson EJ (1997) Parvalbumin-immunoreactive neurons in the hippocampal formation of Alzheimer’s diseased brain. *Neuroscience* 80:1113–1125.
- Brion JP, Rézibois A (1994) A subset of calretinin-positive neurons are abnormal in Alzheimer’s disease. *Acta Neuropathol* 88:33–43.
- Brodmann K (1909) Vergleichende Lokalisationslehre der Großhirnrinde: in ihren Prinzipien dargestellt auf Grund des Zellenbaues. Leipzig: Johann Ambrosius Barth.
- Brown EM, MacLeod RJ (2001) Extracellular calcium sensing and extracellular calcium signaling. *Physiol Rev* 81:239–297.
- Cai H, Wang Y, Mccarthy D, Wen H, Borchelt DR, Price DL, Wong PC (2001) BACE1

- is the major  $\beta$ -secretase for generation of A $\beta$  peptides by neurons. :233–234.
- Casas C et al. (2004) Massive CA1/2 neuronal loss with intraneuronal and N-terminal truncated Abeta42 accumulation in a novel Alzheimer transgenic model. *Am J Pathol* 165:1289–1300.
- Castellano JM, Kim J, Stewart FR, Jiang H, Demattos RB, Patterson BW, Fagan AM, Morris JC, Kwasi G, Cruchaga C, Goate AM, Bales KR, Steven M, Bateman RJ, Holtzman DM (2012) Human apoE isoforms differentially regulate brain amyloid- $\beta$  peptide clearance. *Sci Transl Med* 3.
- Cavanaugh SE, Pippin JJ, Barnard ND (2014) Animal models of Alzheimer disease: Historical pitfalls and a path forward. *ALTEX* 31:279–302.
- Chang W, Tu C, Cheng Z, Rodriguez L, Chen TH, Gassmann M, Bettler B, Margeta M, Jan LY, Shoback D (2007) Complex formation with the type B gamma-aminobutyric acid receptor affects the expression and signal transduction of the extracellular calcium-sensing receptor: Studies with HEK-293 cells and neurons. *J Biol Chem* 282:25030–25040.
- Chattopadhyay N, Espinosa-Jeffrey A, Tfelt-Hansen J, Yano S, Bandyopadhyay S, Brown EM, De Vellis J (2008) Calcium receptor expression and function in oligodendrocyte commitment and lineage progression: Potential impact on reduced myelin basic protein in CaR-null mice. *J Neurosci Res* 86:2159–2167.
- Chattopadhyay N, Jeong K-H, Yano S, Huang S, Pang JL, Ren X, Terwilliger E, Kaiser UB, Vassilev PM, Pollak MR, Brown EM (2007) Calcium receptor stimulates chemotaxis and secretion of MCP-1 in GnRH neurons in vitro: potential impact on reduced GnRH neuron population in CaR-null mice. *Am J Physiol Endocrinol Metab* 292:E523–E532.
- Chattopadhyay N, Legradi G, Bai M, Kifor O, Ye C, Vassilev PM, Brown EM, Lechan RM (1997) Calcium-sensing receptor in the rat hippocampus: a developmental study. *Brain Res Dev Brain Res* 100:13–21.
- Chattopadhyay N, Ye C, Yamaguchi T, Nakai M, Kifor O, Vassilev PM, Nishimura RN, Brown EM (1999a) The extracellular calcium-sensing receptor is expressed in rat microglia and modulates an outward K<sup>+</sup> channel. *J Neurochem* 72:1915–1922.
- Chattopadhyay N, Ye CP, Yamaguchi T, Kifor O, Vassilev PM, Nishimura R, Brown EM (1998) Extracellular calcium-sensing receptor in rat oligodendrocytes: expression and potential role in regulation of cellular proliferation and an outward K<sup>+</sup> channel. *Glia* 24:449–458.
- Chattopadhyay N, Ye CP, Yamaguchi T, Vassilev PM, Brown EM (1999b) Evidence for extracellular calcium-sensing receptor mediated opening of an outward K<sup>+</sup> channel in a human astrocytoma cell line (U87). *Glia* 26:64–72.
- Chaves ML, Camozzato AL, Ferreira ED, Piazenski I, Kochhann R, Dall’Igna O, Mazzini GS, Souza DO, Portela L V (2010) Serum levels of S100B and NSE proteins in Alzheimer’s disease patients. *J Neuroinflammation* 7:6–12.
- Chen W, Bergsman JB, Wang X, Gilkey G, Pierpoint CR, Daniel EA, Awumey EM, Dauban P, Dodd RH, Ruat M, Smith SM (2010) Presynaptic external calcium signaling involves the calcium-sensing receptor in neocortical nerve terminals. *PLoS One* 5:1–12.
- Chiarini A, Armato U, Liu D, Dal Prà I (2016) Calcium-Sensing Receptors of Human Neural Cells Play Crucial Roles in Alzheimer’s Disease. *Front Physiol* 7:134.
- Chiarini A, Dal Pra I, Menapace L, Pacchiana R, Whitfield J, Armato U (2005) Soluble amyloid  $\beta$ -peptide and myelin basic protein strongly stimulate, alone and in synergism with combined proinflammatory cytokines, the expression of functional nitric oxide synthase-2 in normal adult human astrocytes. *Int J Mol Med*.
- Chiarini A, Whitfield J, Bonafini C, Chakravarthy B, Armato U, Dal Prà I (2010) Amyloid- $\beta$ (25-35), an amyloid- $\beta$ (1-42) surrogate, and proinflammatory cytokines stimulate VEGF-A secretion by cultured, early passage, normoxic adult human

- cerebral astrocytes. *J Alzheimers Dis* 21:915–926.
- Chishti MA et al. (2001) Early-onset Amyloid Deposition and Cognitive Deficits in Transgenic Mice Expressing a Double Mutant Form of Amyloid Precursor Protein 695. *J Biol Chem* 276:21562–21570.
- Christopherson KS, Ullian EM, Stokes CCA, Mallowney CE, Hell JW, Agah A, Lawler J, Mosher DF, Bornstein P, Barres BA (2005) Thrombospondins are astrocyte-secreted proteins that promote CNS synaptogenesis. *Cell* 120:421–433.
- Chvátal A, Anděrová M, Hock M, Prajerová I, Neprašová H, Chvátal V, Kirchhoff F, Syková E (2007) Three-Dimensional Confocal Morphometry Reveals Structural Changes in Astrocyte Morphology In Situ. *J Neurosci Res* 85:260–271.
- Citron M (2004)  $\beta$ -Secretase inhibition for the treatment of Alzheimer's disease - Promise and challenge. *Trends Pharmacol Sci* 25:92–97.
- Conley YP, Mukherjee A, Kammerer C, DeKosky ST, Kamboh MI, Finegold DN, Ferrell RE (2009) Evidence supporting a role for the Calcium-Sensing Receptor in Alzheimer Disease. *Am J Med Genet B Neuropsychiatr, Genet* 150B(5):703–709.
- Cordero MI, Rodríguez JJ, Davies HA, Peddie CJ, Sandi C, Stewart MG (2005) Chronic restraint stress down-regulates amygdaloid expression of polysialylated neural cell adhesion molecule. *Neuroscience* 133:903–910.
- Cummings JL (2016) Alzheimer Disease. 287:2335–2338.
- Dal Prà I, Chiarini A, Gui L, Chakravarthy B, Pacchiana R, Gardenal E, Whitfield JF, Armato U (2015) Do Astrocytes Collaborate with Neurons in Spreading the “Infectious” A and Tau Drivers of Alzheimer's Disease? *Neurosci* 21:9–29.
- Dal Pra I, Chiarini A, Nemeth EF, Armato U, Whitfield JF (2005) Roles of Ca<sup>2+</sup> and the Ca<sup>2+</sup>-sensing receptor (CASR) in the expression of inducible NOS (nitric oxide synthase)-2 and its BH 4 (tetrahydrobiopterin)-dependent activation in cytokine-stimulated adult human astrocytes. *J Cell Biochem* 96:428–438.
- Dal Prà I, Chiarini A, Pacchiana R, Gardenal E, Chakravarthy B, Whitfield JF, Armato U (2014) Calcium-Sensing Receptors of Human Astrocyte-Neuron Teams: Amyloid- $\beta$ -Driven Mediators and Therapeutic Targets of Alzheimer's Disease. *Curr Neuropharmacol* 12:353–364.
- Dal Prà I, Whitfield JF, Pacchiana R, Bonafini C, Talacchi A, Chakravarthy B, Armato U, Chiarini A (2011) The amyloid- $\beta_{42}$  proxy, amyloid- $\beta(25-35)$ , induces normal human cerebral astrocytes to produce amyloid- $\beta_{42}$ . *J Alzheimer's Dis* 24:335–347.
- Danbolt NC (2001) Glutamate uptake. *Prog Neurobiol* 65:1–105.
- Del Río MR, DeFelipe J (1997) Synaptic connections of calretinin-immunoreactive neurons in the human neocortex. *J Neurosci* 17:5143–54.
- Del Río MR, DeFelipe J (1996) Colocalization of calbindin D-28k, calretinin, and GABA immunoreactivities in neurons of the human temporal cortex. *J Comp Neurol* 369:472–482.
- Dewitt DA, Perry G, Cohen M, Doller C, Silver J (1998) Astrocytes Regulate Microglial Phagocytosis of Senile Plaque Cores of Alzheimer ' s Disease. *Exp Neurol* 340:329–340.
- Dubois B et al. (2010) Revising the definition of Alzheimer's disease: A new lexicon. *Lancet Neurol* 9:1118–1127.
- Dubois B, Feldman HH, Jacova C, DeKosky ST, Barberger-Gateau P, Cummings J, Delacourte A, Galasko D, Gauthier S, Jicha G, Meguro K, O'Brien J, Pasquier F, Robert P, Rossor M, Salloway S, Stern Y, Visser PJ, Scheltens P (2007) Research criteria for the diagnosis of Alzheimer's disease: revising the NINCDS-ADRDA criteria. *Lancet Neurol* 6:734–746.
- Emsley JG, Macklis JD (2006) Astroglial heterogeneity closely reflects the neuronal-defined anatomy of the adult murine CNS. *Neuron Glia Biol* 2:175–186.
- Eng LF, Ghirnikar RS, Lee YL (2000) Glial Fibrillary Acidic Protein : GFAP-Thirty-One Years (1969-2000). *Neurochem Res* 25:1439–1451.

- Eng LF, Vanderhaeghen JJ, Bignami A, Gerstl B (1971) An acidic protein isolated from fibrous astrocytes. *Brain Res* 28:351–354.
- Fazzari P, Paternain A V., Valiente M, Pla R, Luján R, Lloyd K, Lerma J, Marín O, Rico B (2010) Control of cortical GABA circuitry development by Nrg1 and ErbB4 signalling. *Nature* 464:1376–1380.
- Ferrer I, Soriano E, Tuñón T, Fonseca M, Guionnet N (1991) Parvalbumin immunoreactive neurons in normal human temporal neocortex and in patients with Alzheimer's disease. *J Neurol Sci* 106:135–141.
- Ferrer I, Zújar MJ, Rivera R, Soria M, Vidal A, Casas R (1993) Parvalbumin-immunoreactive dystrophic neurites and aberrant sprouts in the cerebral cortex of patients with Alzheimer's disease. *Neurosci Lett* 158:163–166.
- Ferry S, Traiffort E, Stinnakre J, Ruat M (2000) Developmental and adult expression of rat calcium-sensing receptor transcripts in neurons and oligodendrocytes. *Eur J Neurosci* 12:872–884.
- Filous AR, Silver J (2016) “Targeting astrocytes in CNS injury and disease: A translational research approach.” *Prog Neurobiol* 144:173–187.
- Folstein MF, Folstein SE, McHugh PR (1975) “Mini-mental state”: A practical method for grading the cognitive state of patients for the clinician. *J Psychiatr Res* 12:189–198.
- Fonseca M, Soriano E (1995) Calretinin-immunoreactive neurons in the normal human temporal cortex and in Alzheimer's disease. *Brain Res* 691:83–91.
- Fonseca M, Soriano E, Ferrer I, Martinez A, Tuñón T (1993) Chandelier cell axons identified by parvalbumin-immunoreactivity in the normal human temporal cortex and in Alzheimer's disease. *Neuroscience* 55:1107–1116.
- Freund TF, Buzsáki G (1996) Interneurons of the hippocampus. *Hippocampus* 6:347–470.
- Gama L, Wilt SG, Breitwieser GE (2001) Heterodimerization of Calcium Sensing Receptors with Metabotropic Glutamate Receptors in Neurons. *J Biol Chem* 276:39053–39059.
- Games D, Adams D, Alessandrini R, Barbour R, Berthelette P, Blackwell C, Carr T, Clemens J, Donaldson T, Gillespie F (1995) Alzheimer-type neuropathology in transgenic mice overexpressing V717F beta-amyloid precursor protein. *Nature* 373:523–527.
- Gardenal E, Chiarini A, Armato U, Dal Prà I, Verkhatsky A, Rodríguez JJ (2017) Increased Calcium-Sensing Receptor Immunoreactivity in the Hippocampus of a Triple Transgenic Mouse Model of Alzheimer's Disease. *Front Neurosci* 11:81.
- Golgi C (1903) *Opera Omnia*. Milano: Hoepli.
- Götz J, Chen F, Barmettler R, Nitsch RM (2001) Tau filament formation in transgenic mice expressing P301L tau. *J Biol Chem* 276:529–534.
- Götz J, Probst A, Spillantini MG, Schäfer T, Jakes R, Bürki K, Goedert M (1995) Somatodendritic localization and hyperphosphorylation of tau protein in transgenic mice expressing the longest human brain tau isoform. *EMBO J* 14:1304–1313.
- Gotz J, Streffer JR, David D, Schild A, Hoernndli F, Pennanen L, Kurosinski P, Chen F (2004) Transgenic animal models of Alzheimer's disease and related disorders: histopathology, behavior and therapy. *Mol Psychiatry* 9:664–683.
- Gouras GK, Tsai J, Naslund J, Vincent B, Edgar M, Checler F, Greenfield JP, Haroutunian V, Buxbaum JD, Xu H, Greengard P, Relkin NR (2000) Intraneuronal Aβ<sub>42</sub> accumulation in human brain. *Am J Pathol* 156:15–20.
- Griffin WS, Sheng JG, McKenzie JE, Royston MC, Gentleman SM, Brumback RA, Cork LC, Del Bigio MR, Roberts GW, Mrazek RE (1998) Life-long overexpression of S100β in Down's syndrome: implications for Alzheimer pathogenesis. *Neurobiol Aging* 19:401–405.
- Gulyás a I, Hájos N, Freund TF (1996) Interneurons containing calretinin are specialized

- to control other interneurons in the rat hippocampus. *J Neurosci* 16:3397–3411.
- Haass C, Kaether C, Thinakaran G, Sisodia S (2012a) Trafficking and Proteolytic Processing of APP. *Cold Spring Harb Perspect Med*:1–26.
- Haass C, Kaether C, Thinakaran G, Sisodia S (2012b) Trafficking and proteolytic processing of APP. *Cold Spring Harb Perspect Med* 2.
- Han Z-S, Buhl EH, Lörinczi Z, Somogyi P (1993) A High Degree of Spatial Selectivity in the Axonal and Dendritic Domains of Physiologically Identified Local-circuit Neurons in the Dentate Gyrus of the Rat Hippocampus. *Eur J Neurosci* 5:395–410.
- Haughey and Mattson (2003) Alzheimer's Amyloid  $\beta$ -Peptide Enhances ATP/Gap Junction-Mediated Calcium-Wave Propagation in Astrocytes. *Neuromolecular Med* 3:173–180.
- Heneka MT, Rodríguez JJ, Verkhratsky A (2010) Neuroglia in neurodegeneration. *Brain Res Rev* 63:189–211.
- Henriques AG, Domingues SC, Fardilha M, da Cruz e Silva EF, da Cruz e Silva OA (2005) Sodium azide and 2-deoxy-D-glucose-induced cellular stress affects phosphorylation-dependent AbetaPP processing. *J Alzheimers Dis* 7:201–262.
- Hof PR et al. (1995) Age-Related Distribution of Neuropathologic Changes in the Cerebral Cortex of Patients With Down's Syndrome. *Arch Neurol* 52:379.
- Hof PR, Cox K, Young WG, Celio MR, Rogers J, Morrison JH (1991) Parvalbumin-immunoreactive neurons in the neocortex are resistant to degeneration in Alzheimer's disease. *JNeuropatholExpNeurol* 50:451–462.
- Hof PR, Morrison JH (1991) Neocortical neuronal subpopulations labeled by a monoclonal antibody to calbindin exhibit differential vulnerability in Alzheimer's disease. *Exp Neurol* 111:293–301.
- Hof PR, Nimchinsky EA, Celio MR, Bouras C, Morrison JH (1993) Calretinin-immunoreactive neocortical interneurons are unaffected in Alzheimer's disease. *Neurosci Lett* 152:145–148.
- Holcomb LA, Gordon MN, Jantzen P, Hsiao K, Duff K, Morgan D (1999) Behavioral changes in transgenic mice expressing both amyloid precursor protein and presenilin-1 mutations: Lack of association with amyloid deposits. *Behav Genet* 29:177–185.
- Holcomb L, Gordon MN, McGowan E, Yu X, Benkovic S, Jantzen P, Wright K, Saad I, Mueller R, Morgan D, Sanders S, Zehr C, O'Campo K, Hardy J, Prada CM, Eckman C, Younkin S, Hsiao K, Duff K (1998) Accelerated Alzheimer-type phenotype in transgenic mice carrying both mutant amyloid precursor protein and presenilin 1 transgenes. *Nat Med* 4:97–100.
- Hsiao K, Chapman P, Nilsen S, Eckman C, Harigaya Y, Younkin S, Yang F, Cole G (1996) Correlative memory deficits, A $\beta$  elevation, and amyloid plaques in transgenic mice. *Science* (80- ) 274:99–102.
- Inaguma Y, Shinohara H, Inagaki T, Kato K (1992) Immunoreactive parvalbumin concentrations in parahippocampal gyrus decrease in patients with Alzheimer's disease. *J Neurol Sci* 110:57–61.
- Jabs R, Matthias K, Grote A, Grauer M, Seifert G, Steinhäuser C (2007) Lack of P2X receptor mediated currents in astrocytes and GluR type glial cells of the hippocampal CA1 region. *Glia* 55:1648–1655.
- Jahn H (2013) Memory loss in alzheimer's disease. *Dialogues Clin Neurosci* 15:445–454.
- Jesse S, Steinacker P, Cepek L, von Arnim CAF, Tumani H, Lehnert S, Kretzschmar HA, Baier M, Otto M (2009) Glial fibrillary acidic protein and protein S-100B: different concentration pattern of glial proteins in cerebrospinal fluid of patients with Alzheimer's disease and Creutzfeldt-Jakob disease. *J Alzheimers Dis* 17:541–551.
- Jinno S, Kosaka T (2002) Patterns of Expression of Calcium Binding Proteins and Neuronal Nitric Oxide Synthase in Different Populations of Hippocampal GABAergic Neurons in Mice. 25:1–25.

- Jinno S, Kosaka T (2006) Cellular architecture of the mouse hippocampus: A quantitative aspect of chemically defined GABAergic neurons with stereology. *56:229–245*.
- Jones L et al. (2010) Genetic evidence implicates the immune system and cholesterol metabolism in the aetiology of Alzheimer's disease. *PLoS One 5*.
- Jonsson T et al. (2012) A mutation in APP protects against Alzheimer's disease and age-related cognitive decline. *Nature 488:96–99*.
- Kang J, Lemaire H-G, Unterbeck A, Salbaum JM, Masters CL, Grzeschik K-H, Multhaup G, Beyreuther K, Müller-Hill B (1987) The precursor of Alzheimer's disease amyloid A4 protein resembles a cell-surface receptor. *Nature 325:733–736*.
- Katz B, Miledi R (1967) a Study of Synaptic Transmission in the Absence of Nerve Impulses. *J Physiol 192:407–436*.
- Kempf M, Clement A, Faissner A, Lee G, Brandt R (1996) Tau binds to the distal axon early in development of polarity in a microtubule- and microfilament-dependent manner. *J Neurosci 16:5583–5592*.
- Kettenmann H, Ransom BR (2013) Neuroglia.
- Kim JY, Ho H, Kim N, Liu J, Tu C-L, Yenari M a, Chang W (2014) Calcium-sensing receptor (CaSR) as a novel target for ischemic neuroprotection. *Ann Clin Transl Neurol 1:851–866*.
- Koladiya RU, Jaggi AS, Singh N, Sharma BK (2009) Beneficial Effects of Donepezil on Vascular Endothelial Dysfunction-Associated Dementia Induced by L-Methionine in Rats. *J Heal Sci 55:215–225*.
- Kosaka T, Katsumaru H, Hama K, Wu JY, Heizmann CW (1987) GABAergic neurons containing the Ca<sup>2+</sup>-binding protein parvalbumin in the rat hippocampus and dentate gyrus. *Brain Res 419:119–130*.
- Kraepelin E (1910) *Psychiatrie. Ein Lehrbuch für Studierende und Ärzte. II. Band, Klinische Psychiatrie. [Psychiatry. A textbook for students and doctors. II. Volume, Clinical Psychiatry]. Leipzig: Verlag Johann Ambrosius Barth.*
- Kuchibhotla K V., Lattarulo CR, Hyman BT, Bacsikai BJ (2009) Synchronous Hyperactivity and Intercellular Calcium Waves in Astrocytes in Alzheimer Mice. *Science (80- ) 323:1211–1215*.
- Kulijewicz-Nawrot M, Syková E, Chvátal A, Verkhratsky A, Rodríguez JJ (2013) Astrocytes and glutamate homeostasis in Alzheimer's disease: a decrease in glutamine synthetase, but not in glutamate transporter-1, in the prefrontal cortex. *ASN Neuro 5:273–282*.
- Kulijewicz-Nawrot M, Verkhratsky A, Chvátal A, Syková E, Rodríguez JJ (2012) Astrocytic cytoskeletal atrophy in the medial prefrontal cortex of a triple transgenic mouse model of Alzheimer's disease. *J Anat 221:252–262*.
- Kumar A, Seghal N, Naidu PS, Padi SS V, Goyal R (2007) Colchicines-induced neurotoxicity as an animal model of sporadic dementia of Alzheimer's type. *Pharmacol Reports 59:274–283*.
- LaFerla FM, Green KN, Oddo S (2007) Intracellular amyloid- $\beta$  in Alzheimer's disease. *Nat Rev Neurosci 8:499–509*.
- Lalo U, Pankratov Y, Kirchhoff F, North RA, Verkhratsky A (2006) NMDA Receptors Mediate Neuron-to-Glia Signaling in Mouse Cortical Astrocytes. *26:2673–2683*.
- Lalo U, Pankratov Y, Wichert SP, Rossner MJ, North RA, Kirchhoff F, Verkhratsky A (2008) P2X 1 and P2X 5 Subunits Form the Functional P2X Receptor in Mouse Cortical Astrocytes. *28:5473–5480*.
- Lemmens MAM, Sierksma ASR, Rutten BPF, Dennissen F, Steinbusch HWM, Lucassen PJ, Schmitz C (2011) Age-related changes of neuron numbers in the frontal cortex of a transgenic mouse model of Alzheimer's disease. *Brain Struct Funct 216:227–237*.
- Leuba G, Kraftsik R, Saini K (1998) Quantitative Distribution of Parvalbumin,



- Calretinin, and Calbindin D-28k Immunoreactive Neurons in the Visual Cortex of Normal and Alzheimer Cases. 291:278–291.
- Lewis J, Dickson DW, Lin WL, Chisholm L, Corral A, Jones G, Yen SH, Sahara N, Skipper L, Yager D, Eckman C, Hardy J, Hutton M, McGowan E (2001) Enhanced Neurofibrillary Degeneration in Transgenic Mice Expressing Mutant Tau and APP. *Science* (80- ) 293:1487–1491.
- Lewis J, McGowan E, Rockwood J, Melrose H, Nacharaju P, Van Slegtenhorst M, Gwinn-Hardy K, Murphy PM, Baker M, Yu X, Duff K, Hardy J, Corral A, Lin W, Yen S, Dickson D, Davies P, Hutton M (2000) Neurofibrillary tangles, amyotrophy and progressive motor disturbance in mice expressing mutant (P301L) tau protein. *Nat Genet* 25:402–405.
- Liu AKL, Chang RCC, Pearce RKB, Gentleman SM (2015) Nucleus basalis of Meynert revisited: anatomy, history and differential involvement in Alzheimer’s and Parkinson’s disease. *Acta Neuropathol* 129:527–540.
- Luques L, Shoham S, Weinstock M (2007) Chronic brain cytochrome oxidase inhibition selectively alters hippocampal cholinergic innervation and impairs memory: Prevention by ladostigil. *Exp Neurol* 206:209–219.
- Maccaferri G, Lacaille J, Einstein A (2003) Interneuron Diversity series : Hippocampal interneuron classifications – making things as simple as possible , not simpler. 26:564–571.
- Magistretti PJ (2006) Neuron – glia metabolic coupling and plasticity. :2304–2311.
- Mandelkow EM, Mandelkow E (2011) Biochemistry and cell biology of Tau protein in neurofibrillary degeneration. *Cold Spring Harb Perspect Biol* 3:1–25.
- Martinez-Hernandez A, Bell KP, Norenberg MD (1977) Glutamine synthetase: glial localization in brain. *Science* 195:1356–1358.
- Masters CL, Selkoe DJ (2012) Biochemistry of amyloid  $\beta$ -protein and amyloid deposits in Alzheimer disease. *Cold Spring Harb Perspect Med* 2:a006262.
- Mastrangelo M a, Bowers WJ (2008) Detailed immunohistochemical characterization of temporal and spatial progression of Alzheimer’s disease-related pathologies in male triple-transgenic mice. *BMC Neurosci* 9:81.
- Matos M, Augusto E, Oliveira CR, Agostinho P (2008) Amyloid-beta peptide decreases glutamate uptake in cultured astrocytes: Involvement of oxidative stress and mitogen-activated protein kinase cascades. *Neuroscience* 156:898–910.
- Matyash V, Kettenmann H (2010) Heterogeneity in astrocyte morphology and physiology. *Brain Res Rev* 63:2–10.
- McGowan E, Sanders S, Iwatsubo T, Takeuchi a, Saido T, Zehr C, Yu X, Uljon S, Wang R, Mann D, Dickson D, Duff K (1999) Amyloid phenotype characterization of transgenic mice overexpressing both mutant amyloid precursor protein and mutant presenilin 1 transgenes. *Neurobiol Dis* 6:231–244.
- McKhann G, Drachman D, Folstein M, Katzman R (1984) Clinical diagnosis of Alzheimer’s disease: Report of the NINCDS-ADRDA Work Group under the auspices of Department of Health and Human Services Task Force on Alzheimer’s Disease. *Neurology* 34:939.
- McKhann G, Knopman DS, Chertkow H, Hyman B, Jack CR, Kawas C, Klunk W, Koroshetz W, Manly J, Mayeux R, Mohs R, Morris J, Rossor M, Scheltens P, Carrillo M, Weintraub S, Phelps C (2011) The diagnosis of dementia due to Alzheimer’s disease: Recommendations from the National Institute on Aging-Alzheimer’s Association workgroups on diagnostic guidelines for Alzheimer’s disease. *Alzheimers Dement* 7:263–269.
- Mesulam M, Shaw P, Mash D, Weintraub S (2004) Cholinergic nucleus basalis tauopathy emerges early in the aging-MCI-AD continuum. *Ann Neurol* 55:815–828.
- Mesulam MM, Geula C (1988) Nucleus basalis (Ch4) and cortical cholinergic innervation in the human brain: observations based on the distribution of acetylcholinesterase

- and choline acetyltransferase. *J Comp Neurol* 275:216–240.
- Mesulam MM, Mufson EJ, Levey AI, Wainer BH (1983) Cholinergic innervation of cortex by the basal forebrain: cytochemistry and cortical connections of the septal area, diagonal band nuclei, nucleus basalis (substantia innominata), and hypothalamus in the rhesus monkey. *J Comp Neurol* 214:170–197.
- Mikkonen M, Alafuzoff I, Tapiola T, Soininen H, Miettinen R (1999) Subfield- and layer-specific changes in parvalbumin, calretinin and calbindin-D28K immunoreactivity in the entorhinal cortex in Alzheimer's disease. *Neuroscience* 92:515–532.
- Mohajeri MH, Saini KD, Nitsch RM (2004) Transgenic BACE expression in mouse neurons accelerates amyloid plaque pathology. *J Neural Transm* 111:413–425.
- Mohs RC, Knopman D, Petersen RC, Ferris SH, Ernesto C, Grundman M, Sano M, Bieliauskas L, Geldmacher D, Clark C, Thal LJ (1997) Development of Cognitive Instruments for Use in Clinical Trials of Antidementia Drugs: Additions to the Alzheimer's Disease Assessment Scale That Broaden Its Scope. *Alzheimer Dis Assoc Disord* 11:S13–S21.
- Mori T, Koyama N, Arendash GW, Horikoshi-Sakuraba Y, Tan J, Town T (2010) Overexpression of human S100B exacerbates cerebral amyloidosis and gliosis in the Tg2576 mouse model of Alzheimer's disease. *Glia* 58:300–314.
- Morris JC (1997) Clinical dementia rating: a reliable and valid diagnostic and staging measure for dementia of the Alzheimer type. *Int psychogeriatrics* 9 Suppl 1:173–176–178.
- Morris M, Maeda S, Vossel K, Mucke L (2011) The Many Faces of Tau. *Neuron* 70:410–426.
- Msaouel P, Nixon AM, Bramos AP, Baiba E, Kentarchos NE, Physiology E (2004) Extracellular Calcium Sensing Receptor: An Overview of Physiology, Pathophysiology and Clinical Perspectives. 754:739–753.
- Naber PA, Witter MP, Lopes da Silva FH (2001) Evidence for a direct projection from the postrhinal cortex to the subiculum in the rat. *Hippocampus* 11:105–117.
- Nagele RG, D'Andrea MR, Lee H, Venkataraman V, Wang H (2003) Astrocytes accumulate A beta 42 and give rise to astrocytic amyloid plaques in Alzheimer disease brains. *Brain Res* 971:197–209.
- Nakano Y, Kondoh G, Kudo T, Imaizumi K, Kato M, Miyazaki J, Tohyama M, Takeda J, Takeda M (1999) SHORT COMMUNICATION Accumulation of murine amyloid $\beta$ 42 in a gene-dosage-dependent manner in PS1 “knock-in” mice. *Neuroscience* 11.
- Neha, Sodhi RK, Jaggi AS, Singh N (2014) Animal models of dementia and cognitive dysfunction. *Life Sci* 109:73–86.
- Noristani HN, Olabarria M, Verkhatsky A, Rodríguez JJ (2010) Serotonin fibre sprouting and increase in serotonin transporter immunoreactivity in the CA1 area of hippocampus in a triple transgenic mouse model of Alzheimer's disease. *Eur J Neurosci* 32:71–79.
- Noristani HN, Verkhatsky A, Rodríguez JJ (2012) High tryptophan diet reduces CA1 intraneuronal  $\beta$ -amyloid in the triple transgenic mouse model of Alzheimer's disease. *Aging Cell* 11:810–822.
- O'Brien RJ, Wong PC (2010) Amyloid Precursor Protein Processing and Alzheimer's Disease. *Annu Rev Neurosci* 34:183–202.
- Oakley H, Cole SL, Logan S, Maus E, Shao P, Craft J, Guillozet-Bongaarts A, Ohno M, Disterhoft J, Van Eldik L, Berry R, Vassar R (2006) Intraneuronal  $\beta$ -Amyloid Aggregates, Neurodegeneration, and Neuron Loss in Transgenic Mice with Five Familial Alzheimer's Disease Mutations: Potential Factors in Amyloid Plaque Formation. *J Neurosci* 26:10129–10140.
- Oberheim NA, Goldman SA, Nedergaard M (2012) Heterogeneity of Astrocytic form and

- Function. *Methods Mol Biol* 814:23–45.
- Oddo S, Caccamo A, Kitazawa M, Tseng BP, LaFerla FM (2003a) Amyloid deposition precedes tangle formation in a triple transgenic model of Alzheimer's disease. *Neurobiol Aging* 24:1063–1070.
- Oddo S, Caccamo A, Shepherd JD, Murphy MP, Golde TE, Kaye R, Metherate R, Mattson MP, Akbari Y, LaFerla FM (2003b) Triple-transgenic model of Alzheimer's Disease with plaques and tangles: Intracellular Abeta and synaptic dysfunction. *Neuron* 39:409–421.
- Ogata K, Kosaka T (2002) Structural and quantitative analysis of astrocytes in the mouse hippocampus. *Neuroscience* 113:221–233.
- Olabarria M, Noristani HN, Verkhratsky A, Rodríguez JJ (2010) Concomitant astroglial atrophy and astrogliosis in a triple transgenic animal model of Alzheimer's disease. *Glia* 58:831–838.
- Olabarria M, Noristani HN, Verkhratsky A, Rodríguez JJ (2011) Age-dependent decrease in glutamine synthetase expression in the hippocampal astroglia of the triple transgenic Alzheimer's disease mouse model: mechanism for deficient glutamatergic transmission? *Mol Neurodegener* 6:55.
- Park D, Joo SS, Kim TK, Lee SH, Kang H, Lee HJ, Lim I, Matsuo A, Tooyama I, Kim Y-B, Kim SU (2012) Human Neural Stem Cells Overexpressing Choline Acetyltransferase Restore Cognitive Function of Kainic Acid-Induced Learning and Memory Deficit Animals. *Cell Transplant* 21:365–371.
- Paxinos G, Franklin KBJ (2001) *Mouse Brain in Stereotaxic Coordinates*.
- Petersen RC, Knopman DS, Boeve BF, Yonas E, Ivnik RJ, Smith GE, Roberts RO, Jr CRJ (2011) Mild cognitive impairment: Ten years later. *Arch Neurol* 66:1447–1455.
- Planel E, Tatebayashi Y, Miyasaka T, Liu L, Wang L, Herman M, Yu WH, Luchsinger JA, Wadzinski B, Duff KE, Takashima A (2007) Insulin Dysfunction Induces In Vivo Tau Hyperphosphorylation through Distinct Mechanisms. *J Neurosci* 27:13635–13648.
- Popovi M, Caballero-Bleda M, Kadish I, van Groen T (2008) Subfield and Layer-Specific Depletion in Calbindin- D28K, Calretinin and Parvalbumin Immunoreactivity in the Dentate Gyrus of App/Ps1 Transgenic Mice. *Neuroscience* 155:182–191.
- Postina R, Schroeder A, Dewachter I, Bohl J, Schmitt U, Kojro E, Prinzen C, Endres K, Hiemke C, Blessing M, Flamez P, Dequenne A, Godaux E, van Leuven F, Fahrenholz F (2004) A disintegrin-metalloproteinase prevents amyloid plaque formation and hippocampal defects in an Alzheimer disease mouse model. *J Clin Invest* 113:1456–1464.
- Prince M, Wimo A, Guerchet M, Gemma-Claire A, Wu Y-T, Prina M (2015) World Alzheimer Report 2015: The Global Impact of Dementia - An analysis of prevalence, incidence, cost and trends. *Alzheimer's Dis Int*:84.
- Ramsden M, Kotilinek L, Forster C, Paulson J, McGowan E, SantaCruz K, Guimaraes A, Yue M, Lewis J, Carlson G, Hutton M, Ashe KH (2005) Age-dependent neurofibrillary tangle formation, neuron loss, and memory impairment in a mouse model of human tauopathy (P301L). *J Neurosci* 25:10637–10647.
- Rebeck GW, Reiter JS, Strickland DK, Hyman BT (1993) Apolipoprotein E in sporadic Alzheimer's disease: Allelic variation and receptor interactions. *Neuron* 11:575–580.
- Ribé EM, Pérez M, Puig B, Gich I, Lim F, Cuadrado M, Sesma T, Catena S, Sánchez B, Nieto M, Gómez-Ramos P, Morán MA, Cabodevilla F, Samaranch L, Ortiz L, Pérez A, Ferrer I, Avila J, Gómez-Isla T (2005) Accelerated amyloid deposition, neurofibrillary degeneration and neuronal loss in double mutant APP/tau transgenic mice. *Neurobiol Dis* 20:814–822.

- Rickmann M, Wolff JR (1995) S100 protein expression in subpopulations of neurons of rat brain. *Neuroscience* 67:977–991.
- Riedel G, Kang SH, Choi DY, Platt B (2009) Scopolamine-induced deficits in social memory in mice: Reversal by donepezil. *Behav Brain Res* 204:217–225.
- Rodríguez-Arellano JJ, Parpura V, Zorec R, Verkhratsky A (2015) Astrocytes in physiological aging and Alzheimer's disease. *Neuroscience*.
- Rodríguez J, Olabarria M, Rodríguez JJ, Olabarria M, Chvatal A, Verkhratsky A (2009a) Astroglia in dementia and Alzheimer's disease. *Cell Death Dis* 16:378–385.
- Rodríguez JJ, Jones VC, Tabuchi M, Allan SM, Knight EM, LaFerla FM, Oddo S, Verkhratsky A (2008) Impaired adult neurogenesis in the dentate gyrus of a triple transgenic mouse model of Alzheimer's Disease. *PLoS One* 3.
- Rodríguez JJ, Jones VC, Verkhratsky A (2009b) Impaired cell proliferation in the subventricular zone in an Alzheimer's disease model. *Neuroreport* 20:907–912.
- Rodríguez JJ, Noristani HN, Hilditch T, Olabarria M, Yeh CY, Witton J, Verkhratsky A (2013) Increased densities of resting and activated microglia in the dentate gyrus follow senile plaque formation in the CA1 subfield of the hippocampus in the triple transgenic model of Alzheimer's disease. *Neurosci Lett* 552:129–134.
- Rodríguez JJ, Witton J, Olabarria M, Noristani HN, Verkhratsky A (2010) Increase in the density of resting microglia precedes neuritic plaque formation and microglial activation in a transgenic model of Alzheimer's disease. *Cell Death Dis* 1:e1.
- Rodríguez JJ, Yeh CY, Terzieva S, Olabarria M, Kulijewicz-Nawrot M, Verkhratsky A (2014) Complex and region-specific changes in astroglial markers in the aging brain. *Neurobiol Aging* 35:15–23.
- Rose CF, Verkhratsky A, Parpura V (2013) Astrocyte glutamine synthetase: pivotal in health and disease. *Biochem Soc Trans* 41:1518–1524.
- Rovelet-Lecrux A, Hannequin D, Raux G, Le Meur N, Laquerrière A, Vital A, Dumanchin C, Feuillette S, Brice A, Vercelletto M, Dubas F, Frebourg T, Campion D (2006) APP locus duplication causes autosomal dominant early-onset Alzheimer disease with cerebral amyloid angiopathy. *Nat Genet* 38:24–26.
- Ruat M, Molliver ME, Snowman A M, Snyder SH (1995) Calcium sensing receptor: molecular cloning in rat and localization to nerve terminals. *Proc Natl Acad Sci U S A* 92:3161–3165.
- Ruat M, Traiffort E (2013) Roles of the calcium sensing receptor in the central nervous system. *Best Pract Res Clin Endocrinol Metab* 27:429–442.
- Saiz-Sanchez D, De la Rosa-Prieto C, Ubeda-Bañon I, Martínez-Marcos A (2014) Interneurons, tau and amyloid- $\beta$  in the piriform cortex in Alzheimer's disease. *Brain Struct Funct* 220:2011–2025.
- Saiz-Sanchez D, De La Rosa-Prieto C, Ubeda-Bañon I, Martínez-Marcos A (2013) Interneurons and beta-amyloid in the olfactory bulb, anterior olfactory nucleus and olfactory tubercle in appxps1 transgenic mice model of Alzheimer's disease. *Anat Rec* 296:1413–1423.
- Saiz-Sanchez D, Ubeda-Bañon I, De La Rosa-Prieto C, Martínez-Marcos A (2012) Differential expression of interneuron populations and correlation with amyloid- $\beta$  deposition in the olfactory cortex of an a $\beta$ PP/PS1 transgenic mouse model of Alzheimer's disease. *J Alzheimer's Dis* 31:113–129.
- Sampson VL, Morrison JH, Vickers JC (1997) The Cellular Basis for the Relative Resistance of Parvalbumin and Calretinin Immunoreactive Neocortical Neurons to the Pathology of Alzheimer's Disease. 302:295–302.
- Sassin I, Schultz C, Thal DR, Rüb U, Arai K, Braak E, Braak H (2000) Evolution of Alzheimer's disease-related cytoskeletal changes in the basal nucleus of Meynert. *Acta Neuropathol* 100:259–269.
- Satoh J, Tabira T, Sano M, Nakayama H, Tateishi J (1991) Parvalbumin-immunoreactive neurons in the human central nervous system are decreased in Alzheimer's disease.

- Acta Neuropathol 81:388–395.
- Savchenko VL, McKanna JA, Nikonenko IR, Skibo GG (2000) Microglia and astrocytes in the adult rat brain: Comparative immunocytochemical analysis demonstrates the efficacy of lipocortin 1 immunoreactivity. *Neuroscience* 96:195–203.
- Savonenko A, Xu GM, Melnikova T, Morton JL, Gonzales V, Wong MPF, Price DL, Tang F, Markowska AL, Borchelt DR (2005) Episodic-like memory deficits in the APP<sup>swe</sup>/PS1<sup>dE9</sup> mouse model of Alzheimer's disease: Relationships to  $\beta$ -amyloid deposition and neurotransmitter abnormalities. *Neurobiol Dis* 18:602–617.
- Schenk D, Basi GS, Pangalos MN (2012) Treatment strategies targeting amyloid  $\beta$ -protein. *Cold Spring Harb Perspect Med* 2:a006387–a006387.
- Scheuner D et al. (1996) Secreted amyloid beta-protein similar to that in the senile plaques of Alzheimer's disease is increased in vivo by the presenilin 1 and 2 and APP mutations linked to familial Alzheimer's disease. *Nat Med* 2:864–870.
- Scoville WB, Milner B (1957) Loss of recent memory after bilateral hippocampal lesions. *J Neuropsychiatry Clin Neurosci* 20:11–21.
- Selkoe DJ (2001) Alzheimer's Disease: Genes, Proteins, and Therapy. 81:741–766.
- Selkoe DJ, Hardy J (2016) The amyloid hypothesis of Alzheimer's disease at 25 years. *EMBO Mol Med* 8:1–14.
- Serrano-Pozo A, Frosch MP, Masliah E, Hyman BT (2011) Neuropathological alterations in Alzheimer disease. *Cold Spring Harb Perspect Med* 1:1–23.
- Shankar GM, Li S, Mehta TH, Garcia-Munoz A, Shepardson NE, Smith I, Brett FM, Farrell MA, Rowan MJ, Lemere CA, Regan CM, Walsh DM, Sabatini BL, Selkoe DJ (2008) Amyloid-beta protein dimers isolated directly from Alzheimer's brains impair synaptic plasticity and memory. *Nat Med* 14:837–842.
- Shaw LM, Vanderstichele H, Knapik-czajka M, Clark CM, Aisen PS, Petersen RC, Blennow K, Soares H, Simon A, Lewczuk P, Dean R, Siemers E, Potter W, Lee VM, Q J (2009) Cerebrospinal Fluid Biomarker Signature in Alzheimer's Disease Neuroimaging Initiative Subjects. *Ann Neurol* 65:403–413.
- Sherman KA, Friedman E (1990) Pre- and post-synaptic cholinergic dysfunction in aged rodent brain regions: new findings and an interpretative review. *Int J Dev Neurosci* 8:689–708.
- Söderberg O, Gullberg M, Jarvius M, Ridderstråle K, Leuchowius K-J, Jarvius J, Wester K, Hydbring P, Bahram F, Larsson L-G, Landegren U (2006) Direct observation of individual endogenous protein complexes in situ by proximity ligation. *Nat Methods* 3:995–1000.
- Sohal VS, Zhang F, Yizhar O, Deisseroth K (2009) Parvalbumin neurons and gamma rhythms enhance cortical circuit performance. *Nature* 459:698–702.
- Solodkin A, Veldhuizen SD, Hoesenl GW Van (1996) Contingent Vulnerability Neurons in Alzheimer's of Entorhinal Disease Parvalbumin-Containing. 76:3311–3321.
- Soriano E, Frotscher M (1989) A GABAergic axo-axonic cell in the fascia dentata controls the main excitatory hippocampal pathway. *Brain Res* 503:170–174.
- Steiner H, Fluhrer R, Haass C (2008) Intramembrane proteolysis by  $\gamma$ -secretase. *J Biol Chem* 283:29627–29631.
- Steinerman JR, Irizarry M, Scarmeas N, Raju S, Brandt J, Albert M, Blacker D, Hyman B, Stern Y (2008) Distinct Pools of A $\beta$  in Alzheimer's Disease Brain: A Clinical-Pathological Study. *Arch Neurol* 65:906–912.
- Stelzmann RA, Schnitzlein HN, Murtagh FR (1995) An english translation of alzheimer's 1907 paper, "Über eine eigenartige erkankung der hirnrinde." *Clin Anat* 8:429–431.
- Stix B, Reiser G (1998) Beta-amyloid peptide 25-35 regulates basal and hormone-stimulated Ca<sup>2+</sup> levels in cultured rat astrocytes. *Neurosci Lett* 243:121–124.
- Strange B a, Witter MP, Lein ES, Moser EI (2014) Functional organization of the hippocampal longitudinal axis. *Nat Rev Neurosci* 15:655–669.
- Sturchler-Pierrat C, Abramowski D, Duke M, Wiederhold KH, Mistl C, Rothacher S,

- Ledermann B, Bürki K, Frey P, Paganetti PA, Waridel C, Calhoun ME, Jucker M, Probst A, Staufenbiel M, Sommer B (1997) Two amyloid precursor protein transgenic mouse models with Alzheimer disease-like pathology. *Proc Natl Acad Sci U S A* 94:13287–13292.
- Sturchler-Pierrat C, Staufenbiel M (2000) Pathogenic mechanisms of Alzheimer's disease analyzed in the APP23 transgenic mouse model. *Ann N Y Acad Sci* 920:134–139.
- Suzuki WA, Amaral DG (1990) Cortical inputs to the CA1 field of the monkey hippocampus originate from the perirhinal and parahippocampal cortex but not from area TE. *Neurosci Lett* 115:43–48.
- Suzuki WA, Amaral DG (2004) Functional Neuroanatomy of the Medial Temporal Lobe Memory System. *Cortex* 40:220–222.
- Suzuki WA, Eichenbaum H (2000) The neurophysiology of memory. *Ann N Y Acad Sci* 911:175–191.
- Takahashi H, Brasnjevic I, Rutten BPF, Van Der Kolk N, Perl DP, Bouras C, Steinbusch HWM, Schmitz C, Hof PR, Dickstein DL (2010) Hippocampal interneuron loss in an APP/PS1 double mutant mouse and in Alzheimer's disease. *Brain Struct Funct* 214:145–160.
- Takano T, Han X, Deane R, Zlokovic B, Nedergaard M (2007) Two-photon imaging of astrocytic Ca<sup>2+</sup> signaling and the microvasculature in experimental mice models of Alzheimer's disease. In: *Annals of the New York Academy of Sciences*, pp 40–50.
- Tarawneh R, Holtzman DM (2012) The clinical problem of symptomatic Alzheimer disease and mild cognitive impairment. *Cold Spring Harb Perspect Med* 2:1–16.
- Tashiro K, Hasegawa M, Ihara Y, Iwatsubo T (1997) Somatodendritic localization of phosphorylated tau in neonatal and adult rat cerebral cortex. *Neuroreport* 8:2797–2801.
- Toledano A, Alvarez MI (2004) Lesions and dysfunctions of the nucleus basalis as Alzheimer's disease models: general and critical overview and analysis of the long-term changes in several excitotoxic models. *Curr Alzheimer Res* 1:189–214.
- Toledano A, Bentura ML (1994) Pyritinol facilitates the recovery of cortical cholinergic deficits caused by nucleus basalis lesions. *J Neural Transm - Park Dis Dement Sect* 7:195–209.
- Toodayan N (2016) Professor Alois Alzheimer (1864-1915): Lest we forget. *J Clin Neurosci* 31:47–55.
- van Groen T, Miettinen P, Kadish I (2003) The entorhinal cortex of the mouse: Organization of the projection to the hippocampal formation. *Hippocampus* 13:133–149.
- Verdaguer E, Brox S, Petrov D, Olloquequi J, Romero R, de Lemos ML, Camins A, Auladell C (2015) Vulnerability of calbindin, calretinin and parvalbumin in a transgenic/knock-in APP<sup>swe</sup>/PS1<sup>dE9</sup> mouse model of Alzheimer disease together with disruption of hippocampal neurogenesis. *Exp Gerontol* 69:176–188.
- Verkhatsky A, Butt AM (2013) *Glial physiology and pathophysiology: a handbook*. John Wiley & Sons.
- Verkhatsky A, Kirchhoff F (2007) NMDA Receptors in glia. *Neuroscientist* 13:28–37.
- Verkhatsky A, Olabarria M, Noristani HN, Yeh CY, Rodriguez JJ (2010) Astrocytes in Alzheimer's Disease. *Neurotherapeutics* 7:399–412.
- Verkhatsky A, Rodríguez JJ, Parpura V (2013) Astroglia in neurological diseases. *Future Neurol* 8:149–158.
- Verma M, Howard RJ (2012) Semantic memory and language dysfunction in early Alzheimer's disease: a review. *Int J Geriatr Psychiatry* 27:1209–1217.
- Verret L, Mann EO, Hang GB, Barth AMI, Cobos I, Ho K, Devidze N, Masliah E, Kreitzer AC, Mody I, Mucke L, Palop JJ (2012) Inhibitory Interneuron Deficit Links Altered Network Activity and Cognitive Dysfunction in Alzheimer Model. *Cell* 149:708–721.

- Vickers JC, Chin D, Edwards AM, Sampson V, Harper C, Morrison J (1996) Dystrophic neurite formation associated with age-related beta amyloid deposition in the neocortex: clues to the genesis of neurofibrillary pathology. *Exp Neurol* 141:1–11.
- Vickers JC, Riederer BM, Marugg RA, Buée-Scherrer V, Buée L, Delacourte A, Morrison JH (1994) Alterations in neurofilament protein immunoreactivity in human hippocampal neurons related to normal aging and Alzheimer's disease. *Neuroscience* 62:1–1.
- Vincent AJ, Gasperini R, Foa L, Small DH (2010) Astrocytes in Alzheimer's disease: Emerging roles in calcium dysregulation and synaptic plasticity. *J Alzheimer's Dis* 22:699–714.
- Vizard TN, O'Keefe GW, Gutierrez H, Kos CH, Riccardi D, Davies AM (2008) Regulation of axonal and dendritic growth by the extracellular calcium-sensing receptor. *Nat Neurosci* 11:285–291.
- Vyleta NP, Smith SM (2011) Spontaneous glutamate release is independent of calcium influx and tonically activated by the calcium-sensing receptor. *J Neurosci* 31:4593–4606.
- Walsh DM, Selkoe DJ (2007) A $\beta$  oligomers - A decade of discovery. *J Neurochem* 101:1172–1184.
- Wang S, Bolós M, Clark R, Cullen C, Southam KA, Foa L, Dickson T, Young KM (2016) Amyloid  $\beta$  precursor protein regulates neuron survival and maturation in the adult mouse brain. *Mol Cell Neurosci* 77:21–33.
- Ward BK, Magno AL, Davis EA, Hanyaloglu AC, Stuckey BGA, Burrows M, Eidne KA, Charles AK, Ratajczak T (2004) Functional deletion of the calcium-sensing receptor in a case of neonatal severe hyperparathyroidism. *J Clin Endocrinol Metab* 89:3721–3730.
- Weingarten MD, Lockwood AH, Hwo SY, Kirschner MW (1975) A protein factor essential for microtubule assembly. *Proc Natl Acad Sci U S A* 72:1858–1862.
- Whitaker-Azmitia PM, Wingate M, Borella A, Gerlai R, Roder J, Azmitia EC (1997) Transgenic mice overexpressing the neurotrophic factor S-100 $\beta$  show neuronal cytoskeletal and behavioral signs of altered aging processes: Implications for Alzheimer's disease and Down's syndrome. *Brain Res* 776:51–60.
- Wirhns O, Breyhan H, Cynis H, Schilling S, Demuth H-U, Bayer TA (2009) Intraneuronal pyroglutamate-A $\beta$  3-42 triggers neurodegeneration and lethal neurological deficits in a transgenic mouse model. *Acta Neuropathol* 118:487–496.
- Witter MP (2007) The perforant path: projections from the entorhinal cortex to the dentate gyrus. *Prog Brain Res* 163:43–61.
- Witter MP, Amaral DG (1991) Entorhinal cortex of the monkey: V. Projections to the dentate gyrus, hippocampus, and subicular complex. *J Comp Neurol* 307:437–459.
- Witter MP, Amaral DG (2004) Hippocampal formation. In: *The rat nervous system*, Third Edic., pp 635–704. Burlington: Academic Press.
- Witter MP, Moser EI (2006) Spatial representation and the architecture of the entorhinal cortex. *Trends Neurosci* 29:671–678.
- Witter MP, Wouterlood FG, Naber PA, Van Haeften T (2000) Anatomical organization of the parahippocampal-hippocampal network. *Ann N Y Acad Sci* 911:1–24.
- Wyss-Coray T, Loike JD, Brionne TC, Lu E, Anankov R, Yan F, Silverstein SC, Husemann J (2003) Adult mouse astrocytes degrade amyloid-beta in vitro and in situ. *Nat Med* 9:453–457.
- Yamada K, Nabeshima T (2000) Animal models of Alzheimer's disease and evaluation of anti-dementia drugs. *Pharmacol Ther* 88:93–113.
- Yamada K, Nabeshima T, Kameyama T (1991) Impairment of active avoidance response in rats with continuous infusion of quinolinic acid into the lateral ventricle. *J Pharmacobiodyn* 14:351–355.
- Yano S, Brown EM, Chattopadhyay N (2004) Calcium-sensing receptor in the brain. *Cell*

- Calcium 35:257–264.
- Yardan T, Erenler AK, Baydin A, Aydin K, Cokluk C (2011) Usefulness of S100B protein in neurological disorders. *J Pak Med Assoc* 61:276–281.
- Ye C, Ho-pao CL, Kanazirska M, Quinn S, Rogers K, Seidman CE, Seidman JG, Brown EM, Vassilev PM (1997) Rapid Communication Amyloid- $\beta$  Proteins Activate Ca<sup>2+</sup> Permeable Channels Through Calcium-Sensing Receptors. *J Neurosci* 19:5547–5554.
- Ye C, Kanazirska M, Quinn S, Brown EM, Vassilev PM (1996) Modulation by Polycationic Ca<sup>2+</sup>-Sensing Receptor Agonists of Nonselective Cation Channels in Rat Hippocampal Neurons. *Biochem Biophys Res Commun* 224:271–280.
- Yeh C, Vadhvana B, Verkhatsky A, Rodríguez JJ (2011) Early astrocytic atrophy in the entorhinal cortex of a triple transgenic animal model of Alzheimer's disease. *ASN Neuro* 3:271–279.
- Yeh CY, Verkhatsky A, Terzieva S, Rodríguez JJ (2013) Glutamine synthetase in astrocytes from entorhinal cortex of the triple transgenic animal model of Alzheimer's disease is not affected by pathological progression. *Biogerontology* 14:777–787.
- Young-Pearse TL, Bai J, Chang R, Zheng JB, LoTurco JJ, Selkoe DJ (2007) A Critical Function for  $\beta$ -Amyloid Precursor Protein in Neuronal Migration Revealed by In Utero RNA Interference. *J Neurosci* 27:14459–14469.
- Yu Y, Run X, Liang Z, Li Y, Liu F, Liu Y, Iqbal K, Grundke-Iqbal I, Gong CX (2009) Developmental regulation of tau phosphorylation, tau kinases, and tau phosphatases. *J Neurochem* 108:1480–1494.
- Zhang J, Li P, Wang Y, Liu J, Zhang Z, Cheng W, Wang Y (2013) Ameliorative Effects of a Combination of Baicalin, Jasminoidin and Cholic Acid on Ibotenic Acid-Induced Dementia Model in Rats. *PLoS One* 8:e56658.
- Zhang X, Li Y, Xu H, Zhang Y (2014) The  $\gamma$ -secretase complex: from structure to function. *Cell* 157:8–10.
- Zhao Z et al. (2016) Central role for PICALM in amyloid- $\beta$  blood-brain barrier transcytosis and clearance. *Nat Neurosci* 18:978–987.
- Zonta M, Angulo MC, Gobbo S, Rosengarten B, Hossmann K, Pozzan T, Carmignoto G (2002) Neuron-to-astrocyte signaling is central to the dynamic control of brain microcirculation. *Nat Neurosci* 5:43–50.



# Appendix



# Increased Calcium-Sensing Receptor Immunoreactivity in the Hippocampus of a Triple Transgenic Mouse Model of Alzheimer's Disease

Emanuela Gardenal<sup>1,2,3</sup>, Anna Chiarini<sup>1</sup>, Ubaldo Armato<sup>1</sup>, Ilaria Dal Prà<sup>1</sup>, Alexei Verkhratsky<sup>2,3,4</sup> and José J. Rodríguez<sup>2,3\*</sup>

<sup>1</sup> Human Histology and Embryology Unit, Medical School, University of Verona, Verona, Italy, <sup>2</sup> Basque Foundation for Science, Achúcarro Basque Center for Neuroscience, IKERBASQUE, Bilbao, Spain, <sup>3</sup> Department of Neuroscience, University of the Basque Country (UPV/EHU), Leioa, Spain, <sup>4</sup> Faculty of Biology, Medicine and Health, The University of Manchester, Manchester, UK

## OPEN ACCESS

### Edited by:

Wendy Noble,  
King's College London, UK

### Reviewed by:

Flavia Eugenia Saravia,  
IBYME CONICET and Faculty of  
Natural and Exact Sciences, Buenos  
Aires University, Argentina  
Ricardo Martínez-Murillo,  
Consejo Superior de Investigaciones  
Científicas, Spain  
Daniela Rossi,  
Istituti Clinici Scientifici Maugeri Spa  
SB, Italy

### \*Correspondence:

José J. Rodríguez  
j.rodriguez-arellano@ikerbasque.org

### Specialty section:

This article was submitted to  
Neurodegeneration,  
a section of the journal  
Frontiers in Neuroscience

Received: 15 December 2016

Accepted: 03 February 2017

Published: 16 February 2017

### Citation:

Gardenal E, Chiarini A, Armato U, Dal Prà I, Verkhratsky A and Rodríguez JJ (2017) Increased Calcium-Sensing Receptor Immunoreactivity in the Hippocampus of a Triple Transgenic Mouse Model of Alzheimer's Disease. *Front. Neurosci.* 11:81. doi: 10.3389/fnins.2017.00081

The Calcium-Sensing Receptor (CaSR) is a G-protein coupled, 7-transmembrane domain receptor ubiquitously expressed throughout the body, brain including. The role of CaSR in the CNS is not well understood; its expression is increasing during development, which has been implicated in memory formation and consolidation, and CaSR localization in nerve terminals has been related to synaptic plasticity and neurotransmission. There is an emerging evidence of CaSR involvement in neurodegenerative disorders and Alzheimer's disease (AD) in particular, where the over-production of  $\beta$ -amyloid peptides was reported to activate CaSR. In the present study, we performed CaSR immunohistochemical and densitometry analysis in the triple transgenic mouse model of AD (3xTg-AD). We found an increase in the expression of CaSR in hippocampal CA1 area and in dentate gyrus in the 3xTg-AD mice when compared to non-transgenic control animals. This increase was significant at 9 months of age and further increased at 12 and 18 months of age. This increase paralleled the accumulation of  $\beta$ -amyloid plaques with age. Increased expression of CaSR favors  $\beta$ -amyloidogenic pathway following direct interactions between  $\beta$ -amyloid and CaSR and hence may contribute to the pathological evolution of the AD. In the framework of this paradigm CaSR may represent a novel therapeutic target.

**Keywords:** Alzheimer's disease,  $\beta$ -amyloid, tau, calcium sensing receptor (CaSR), hippocampus

## INTRODUCTION

The calcium sensing receptor (CaSR) belongs to the extended family of plasmalemmal G protein-coupled heptahelical receptors (GPCRs); it shares the C subfamily of GPCRs with metabotropic glutamate receptors (mGluR) and  $\gamma$ -aminobutyric acid GABA<sub>B</sub> receptors (Brown and MacLeod, 2001). CaSRs are widely distributed throughout the brain, with highest expression in the

**Abbreviations:** AD, Alzheimer's disease; ANOVA, One-way Analysis of Variance; CaSR, Calcium-Sensing Receptor; DG, Dentate Gyrus; GCL, Granular Cell Layer; IOD, Inverted Optical Density; mGluR, metabotropic Glutamate Receptors; ML, Molecular Layer; OD, Optical Density; PB, Phosphate Buffer; PCL, Pyramidal Cell Layer; S.Mol, Stratum Lacunosum-Moleculare; SO, Stratum Oriens; S.Rad, Stratum Radiatum; TS, Trizma-base Saline; VEGF, Vascular Endothelial Growth Factor; 3xTg-AD, triple Transgenic mouse model of AD.

subfornical organ, hippocampus, striatum, cingulate cortex, cerebellum, ependymal zones of the cerebral ventricles and perivascular nerves around cerebral arteries, some CaSR expressing cells were found also in rat dorsal root ganglia (Ruat et al., 1995; Yano et al., 2004). The CaSR has been found abundantly expressed *in vivo* in neurons and in oligodendrocytes; *in vitro* studies demonstrated its expression in human primary astrocytes and in rat microglia (Ruat et al., 1995; Chattopadhyay et al., 1998, 1999a; Ferry et al., 2000; Dal Prà et al., 2005).

Numerous functions have been assigned to CaSR in the CNS from regulation of neuronal growth and migration, to the role in neurotransmission and synaptic plasticity (Ruat and Traiffort, 2013); CaSR can also contribute to astroglial functions, microglial reactivity and oligodendroglial development (Ruat and Traiffort, 2013). The level of extracellular ionized Ca<sup>2+</sup> ([Ca<sup>2+</sup>]<sub>o</sub>) is usually considered to be stable in the brain, which is not really the case, since [Ca<sup>2+</sup>]<sub>o</sub> undergoes rapid fluctuations in normal physiological processes such as development, synaptic transmission and aging as well as in pathological processes including neurodegeneration and Alzheimer's disease (AD; Small, 2009; Ruat and Traiffort, 2013).

Expression of CaSR markedly increases during development, specifically in perinatal and early post-natal periods just before and after birth (Chattopadhyay et al., 1997; Vizard et al., 2008). In the hippocampus CaSR was reported to regulate neuronal growth, as well as extension and branching of neurites (Vizard et al., 2008). In addition, CaSR has been identified in neocortical nerve terminals where it senses the [Ca<sup>2+</sup>]<sub>o</sub> and activates voltage dependent non-selective cation channels (NSCCs) (Chen et al., 2010). It has been proposed that the decrease in [Ca<sup>2+</sup>]<sub>o</sub> in the synaptic cleft may act as feedback to presynaptic CaSR and the associated increased activity of NSCCs may prolong action potentials; in this way CaSR may influence synaptic transmission through a homeostatic pathway to prevent synaptic failure when [Ca<sup>2+</sup>]<sub>o</sub> falls (Ye et al., 1996). Studies *in vitro* conducted in the human astrocytoma cell line U87, and in primary cultures of rat microglia and oligodendroglia showed that CaSR stimulates Ca<sup>2+</sup>-activated K<sup>+</sup> channels, thus contributing to local ionic homeostasis following the lowering of [Ca<sup>2+</sup>]<sub>o</sub> due to increased neuronal activity; there are also indications that CaSR could also play a role in microglia activation (Chattopadhyay et al., 1998, 1999a,b). CaSR can form heterodimers with others GPCRs, like GABA<sub>B</sub> receptors and mGluRs, which might be important for their trafficking to the membrane, their ligand binding sensitivity and thus the regulation of signaling responses (Gama et al., 2001; Chang et al., 2007). Activation of CaSR was also demonstrated to induce a distinct form of glutamate release independent on Ca<sup>2+</sup> influx (Vyleta and Smith, 2011).

In the context of AD, CaSR has been reported to be directly activated by  $\beta$ -amyloid as well as by apoE (isoforms 3 and 4) (Conley et al., 2009). In rat hippocampal neurons exposure to  $\beta$ -amyloid stimulated openings of NSCCs linked to CaSR activation (Ye et al., 1997). How  $\beta$ -amyloid interacts with CaSR remains unclear, although it is possible that either  $\beta$ -amyloid fibrils or variously sized oligomers, having regular positive charges, mimic CaSR agonists, or hydrophobic interactions between  $\beta$ -amyloid and CaSR may take place (Ye et al., 1997). Thus, extracellular

accumulation of  $\beta$ -amyloid can activate CaSR which, in turn, may contribute to Ca<sup>2+</sup> dyshomeostasis observed in AD (Lim et al., 2014, 2015).

Previous studies on human cultured primary adult astrocytes showed that their exposure to exogenous  $\beta$ -amyloid<sub>25–35</sub>, a surrogate of  $\beta$ -amyloid<sub>42</sub>, triggers CaSR-dependent signaling cascade that stimulates the expression of nitric oxide synthase-2 (NOS-2) followed by an excessive release of nitric oxide (Chiarini et al., 2005), and increased expression of vascular endothelial growth factor (VEGF)-A (Chiarini et al., 2010). Most importantly, cultured human cortical astrocytes and neurons exposed to  $\beta$ -amyloid<sub>25–35</sub>, which binds and activates CaSR (Dal Prà et al., 2014), begin to excessively produce and secrete  $\beta$ -amyloid<sub>42</sub> oligomers, contributing in this way to the  $\beta$ -amyloid load (Dal Prà et al., 2011; Armato et al., 2013).

In the present study, for the first time we aimed to determine *in vivo* CaSR expression in the 3xTg-AD mouse model and correlate its changes with  $\beta$ -amyloid load.

## MATERIALS AND METHODS

All animal procedures were carried out in accordance with the United Kingdom Animals (Scientific Procedures) Act of 1986 under the license from the Home Office. All efforts were made to reduce the number of animals by following the 3R's (reduction, refinement and replacement).

### Mice

Experiments were performed on male 3xTg-AD mice generated on 129/C57BL6 background (the wild type of which was employed as a non-Tg control). The 3xTg-AD mice harbor the mutant genes for amyloid precursor protein (APP<sup>Swe</sup>), presenilin 1 PS1M146V and tauP301L (Oddo et al., 2003a,b; Rodríguez et al., 2008). All 3xTg-AD and non-Tg control mice were obtained by crossing homozygous breeders. Animals were housed in groups of the same genotype and in the same cage according to their age, kept in 12 h light-dark cycles with *ad libitum* access to food and water.

The experimental groups chosen were of 9, 12, and 18 months of age, since it is at these ages that the amyloid and tau pathologies emerge resembling the human Alzheimer's disease progression. Indeed, the 3xTg-AD mice exhibit the highest intracellular  $\beta$ -amyloid deposition at 9 months of age, they start showing extracellular  $\beta$ -amyloid plaques followed by intracellular tau deposition at 12 months of age and they present massive A $\beta$  plaques and neurofibrillary tangles at 18 months of age (Rodríguez et al., 2008; Olabarria et al., 2010).

### Fixation and Tissue Processing

As described previously (Olabarria et al., 2010; Kulijewicz-Nawrot et al., 2012) 3xTg-AD and non-Tg control mice at 9, 12, 18 months of age (Ns for non-Tg = 5, 5, 4; ns for 3xTg-AD = 4, 5, 3, respectively) were intraperitoneally anesthetized with sodium pentobarbital (50 mg/kg). Mice were trans-cardially perfused with 4% paraformaldehyde (PFA, Sigma, UK) and 0.1 M phosphate buffer (PB) at pH 7.4. Brains were removed and post-fixed in 4% paraformaldehyde overnight, then cut

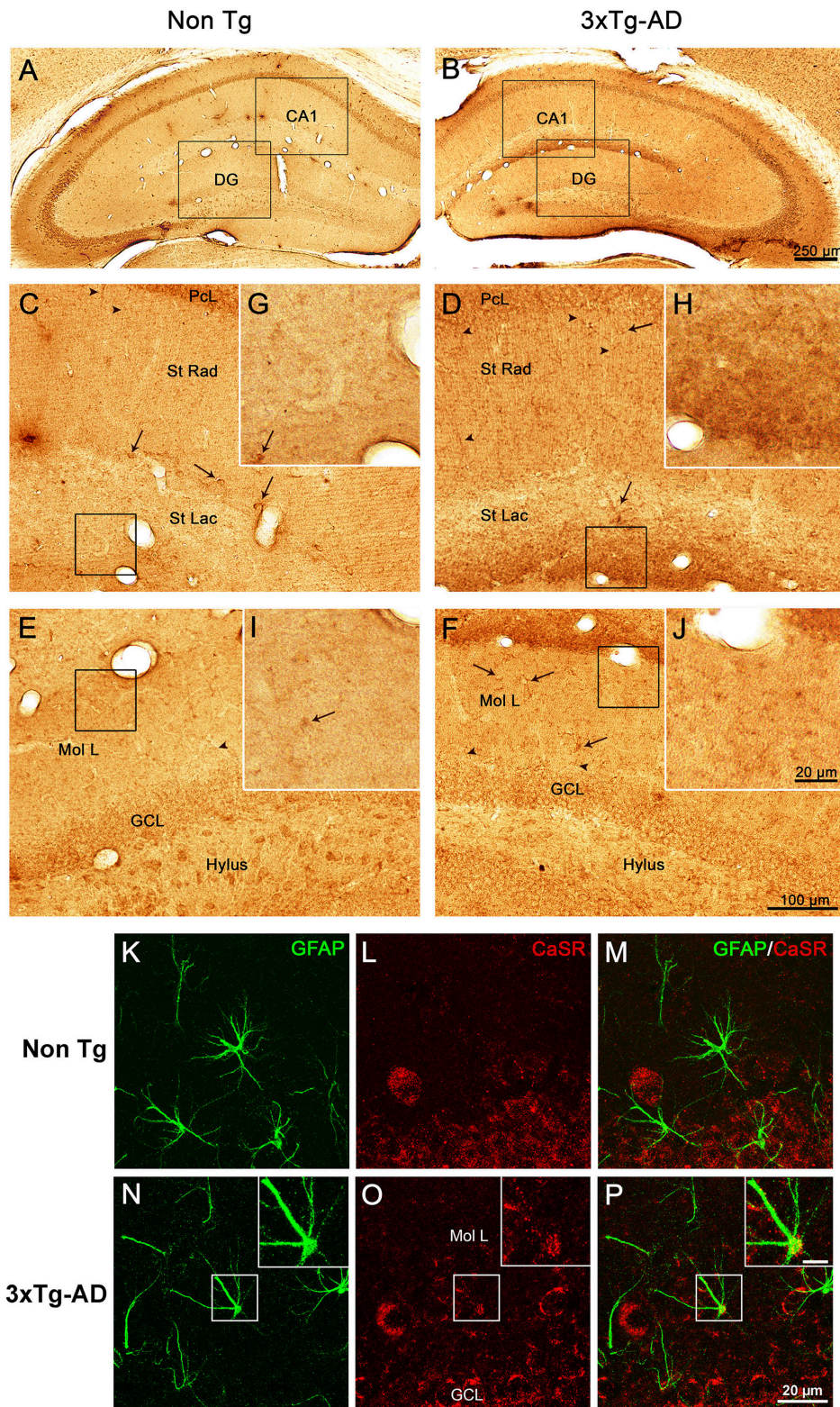


**FIGURE 1 | CaSR expression and localization in hippocampus.** Brightfield micrographs showing the distribution of CaSR-IR within the dorsal hippocampus of 18 months old non-Tg controls (**A,C,E,G,I**) and 3xTg-AD mice (**B,D,F,H,J**); arrowheads show neuropil elements, whilst full arrows indicate interneurons). Confocal micrographs showing the immunoreactivity for CaSR (red) and for GFAP (green), in Non-Tg (**K–M**) and 3xTg-AD mice (**N–P**). Inserts in (**N–P**) show an astrocyte bearing CaSR at higher magnification (scale bar 20  $\mu$ m). CA1, Cornu Ammonis 1; DG, Dentate Gyrus; St Rad, Stratum Radiatum; St Lac, Stratum Lacunosum-Moleculare; Mol L, Molecular Layer; GCL, Granular Cell Layer.

into 4–5 mm coronal slabs of tissue containing the entire rostrocaudal extent of the hippocampus, as previously described (Olabarria et al., 2011). The tissue was further sectioned in 40–50  $\mu\text{m}$ -thick slices with a vibrating microtome (VT1000S, Leica, Milton Keynes, UK). Free floating sections were collected in 0.1 M PB and stored in a cryoprotectant solution containing 25% sucrose and 3.5% glycerol in 0.05 M PB at pH 7.4. Three coronal sections at levels  $-1.58$  mm/ $-2.46$  mm (dorsal hippocampus) posterior to Bregma, were selected from each animal for immunohistochemistry according to the mouse brain atlas of Paxinos and Franklin (2012).

## Antibodies

A mouse monoclonal anti-Calcium Sensing Receptor antibody (anti-CaSR; Sigma-Aldrich, UK; C0493) was used for the determination of CaSR expression throughout the dorsal hippocampus. For the identification of intracellular  $\beta$ -amyloid deposits and plaques a monoclonal mouse antibody that reacts with abnormally processed isoforms, as well as precursor forms of A $\beta$ , recognizing an epitope within amino acids 3–8 (EFRHDS; anti-A $\beta$  6E10 [SIG-39320] Signet Laboratories, Dedham, MA) was used, for hyperphosphorylated Tau we employed the mouse monoclonal antibody anti-PHF Tau AT8 (Innogenetics, Gent, Belgium). For double immunostaining of CaSR with GFAP and A $\beta$ , a rabbit anti-GFAP (Sigma-Aldrich, UK; G9269) and a mouse anti-A $\beta$  Alexa 488 6E10 conjugated antibody (Covance, USA) were used. To assess for non-specific background labeling or cross reactivity between antibodies derived from different host species, a series of control experiments were performed, including the omission of primary (Supplementary Figure 1C) and/or secondary antibodies from the incubation solutions; resulting all of them in a total absence of target labeling.

## Immunohistochemistry

All the sections were processed at the same time using the same experimental conditions to minimize methodological variability (Noristani et al., 2010; Olabarria et al., 2011; Kulijewicz-Nawrot et al., 2012). Then sections were incubated for 30 min in 30% methanol in 0.1 M PB and 30% hydrogen peroxide ( $\text{H}_2\text{O}_2$ ; Sigma, UK). Sections were then rinsed with 0.1 M PB for 5 min and placed in 1% sodium borohydride (Sigma, UK) for 30 min. The sections were then washed with PB profusely before rinsing in 0.1 M Trizma base saline (TS) for 10 min. Brain sections were then incubated in 0.5% bovine serum albumin (Sigma, UK) in 0.1 M TS and 0.25% Triton X-100 (Sigma, UK) for 30 min. Sections were incubated for 72 h at room temperature in primary antibody (mouse anti-CaSR, 1:250, Sigma, UK). The sections were rinsed in 0.1 M TS for 30 min and incubated in 1:400 dilutions of biotinylated horse anti-mouse IgG (Vector Laboratories, Peterborough, UK) for 1 h at room temperature. Sections were rinsed with 0.1 M TS for 30 min followed by incubation for 30 min in avidin-biotin peroxidase complex (Vector Laboratories, Peterborough, UK). The peroxidase reaction product was visualized by incubation in a solution containing 0.022% of 3,3' diaminobenzidine (DAB, Aldrich, Gilligham, UK) and 0.003%  $\text{H}_2\text{O}_2$  for 7 min. The reaction was stopped by rinsing the sections in 0.1 M TS

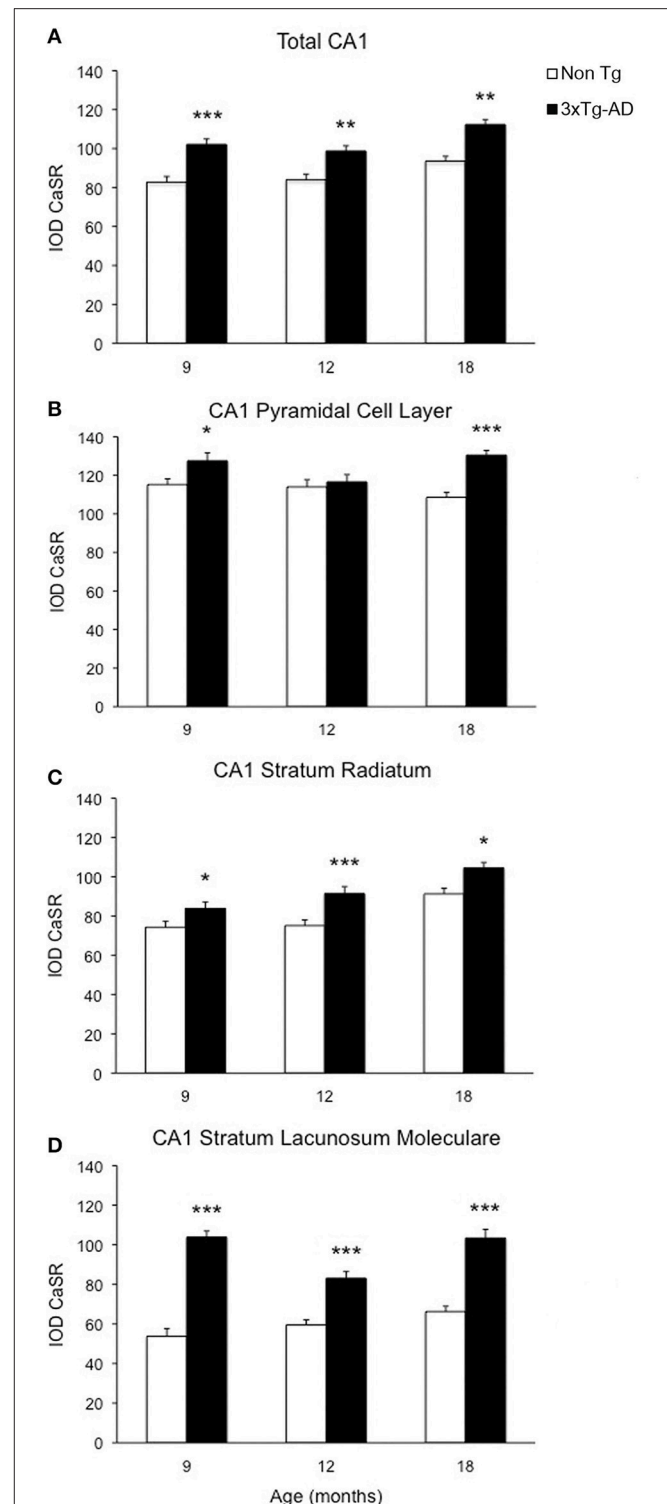


**FIGURE 2 | Changes of CaSR expression in hippocampal CA1.** Bar graphs illustrating CaSR-IR IOD within CA1 subfield of hippocampus between non-Tg controls and 3xTg-AD mice at 9, 12 and 18 months of age (Ns for non-Tg = 5, 5, 4; ns for 3xTg-AD = 4, 5, 3, respectively; 3 slices have been analyzed per each animal). (A) Total CA1, (B) CA1 Pyramidal Cell Layer, (C) CA1 Stratum Radiatum, (D) CA1 Stratum Lacunosum-Moleculare. Bars represent means  $\pm$  SEM (\* $p \leq 0.05$ , \*\* $p \leq 0.01$ , \*\*\* $p \leq 0.001$ ).

**TABLE 1 | Summary of CaSR IOD values in the hippocampal CA1 and DG subfields and their respective layers in both non-Tg and 3xTg-AD.**

CaSR IOD	9 months NTG	9 months 3xTg-AD	12 months NTG	12 months 3xTg-AD	18 months NTG	18 months 3xTg-AD
Total CA1	82.71 ± 2.98	102.1 ± 2.72***	83.92 ± 2.51	98.71 ± 2.56***	93.51 ± 3.39	112.30 ± 4.68**
PCL CA1	115.20 ± 3.78	127.50 ± 3.80*	114.00 ± 2.49	116.60 ± 2.39ns	108.60 ± 4.57	130.50 ± 3.40**
St Rad CA1	74.23 ± 2.91	83.83 ± 3.60*	75.08 ± 2.85	91.38 ± 2.75***	91.23 ± 3.31	104.5 ± 5.99*
St Lac CA1	53.78 ± 2.60	103.9 ± 3.33***	59.53 ± 2.71	83.09 ± 4.41***	66.25 ± 5.31	103.4 ± 6.25***
Total DG	82.68 ± 3.11	97.41 ± 3.56**	81.35 ± 3.33	93.34 ± 2.80**	89.78 ± 4.75	108.40 ± 4.96*
ML	73.06 ± 3.16	84.68 ± 4.88*	80.58 ± 4.18	90.51 ± 3.01*	90.00 ± 4.11	108.8 ± 6.91*
GCL	98.30 ± 3.55	117.30 ± 4.27**	87.76 ± 3.15	97.13 ± 2.78*	82.18 ± 6.16	112.90 ± 3.54***

Values are expressed as means ± SEM (\* $p \leq 0.05$ , \*\* $p \leq 0.01$ , \*\*\* $p \leq 0.001$ ).

for 5 min followed by 0.1 M PB for 15 min. Brain sections were permanently mounted onto gelatinized slides and allowed to dry overnight. Sections were then dehydrated in ascending concentration of ethanol (50, 70, 80, 90, 95, and 100%) and, finally, xylene. Sections were then permanently mounted and coverslipped using Entellan (Merck KGaA, Darmstadt, Germany) and slides were left to dry overnight.

For the dual immunofluorescence labeling with CaSR and GFAP the sections were simultaneously incubated with both antibodies (mouse anti-CaSR, 1:250; rabbit anti-GFAP, 1:20,000) for 48 h at room temperature. Then CaSR and GFAP were detected in a sequential manner on the same sections by incubation of 2 h with Alexa Fluor 594-conjugated goat anti-mouse and Alexa Fluor 488-conjugated goat anti-rabbit (1:400, Invitrogen, Paisley, UK), respectively.

For the dual immunofluorescence labeling with CaSR and A $\beta$  the sections were first incubated for 48 h at room temperature in CaSR antibody solution then in the Alexa 594 conjugated goat anti-mouse for 2 h, finally for 24 h in Alexa 488-conjugated mouse anti-A $\beta$  antibody (1:1,000, Covance, USA).

Sections were rinsed with 0.1 M TS for 30 min and permanently mounted in an aqueous medium (Vectashield; Vector laboratories, Peterborough, UK).

## Optical Density (OD) Measurement

Using computer-assisted imaging analysis (ImageJ 2.0.0-rc-39/1.50b; NIH, USA) we analyzed the expression of CaSR by measuring its OD, as described previously (Cordero et al., 2005; Noristani et al., 2010, 2012). Briefly, to exclude any experimental errors and/or bias, all images were taken at constant light intensity with a Nikon Eclipse 80i microscope coupled with an 8001 MicroFIRE camera. Optical filters were used to ensure the specificity of the signal recorded by the camera. The OD was calculated from a relative scale of intensity ranking from 0 to 250, with a measurement of 250 corresponding to the area with very low CaSR expression and 0 corresponding to the area with highest labeling. The calibration density was kept constant for measuring all sections to avoid experimental variances. Non-specific OD in sections was measured from the corpus callosum (CC). CaSR density of the complete CA subfields of the hippocampus and their different layers (stratum pyramidale, PCL; stratum oriens, SO; stratum radiatum, S.Rad and stratum lacunosum-moleculare, S.Mol), except CA3 where

we also studied stratum lucidum, were measured independently. Similarly, CaSR density of the dentate gyrus (DG) and its different layers (granular cell layer, GCL, molecular layer, ML and hilus) were measured individually. The OD of the region of interest is determined by outlining each layer and obtaining the mean value of the intensities in the selected area (**Supplementary Figures 1A,B**). The changes in CaSR density were analyzed against a constant control region (CC): 250 was divided by control region and the obtained factor was multiplied by the region of interest in every given section. Inverse OD (IOD) was obtained by subtracting the OD (after the control region normalization) from 250. Values of IOD were taken and averaged in both the left and right hemisphere of each slice. The results are shown as inverse optical CaSR density (IOD/pixel).

## Counting of A $\beta$ -Positive Cells

$\beta$ -amyloid containing neurons were counted in the entire extent of the CA1 region of the hippocampus, since this field shows the earliest and strongest accumulation of A $\beta$  intracellular deposits. This quantification was carried out on six non-consecutive sections from dorsal hippocampus of three non-Tg and 3xTg-AD animals of 9 months of age immunolabeled with anti-A $\beta$  6E10 antibody.

## Statistical Analysis

One-way analysis of variance (ANOVA) was used to determine changes in CaSR density between 3xTg-AD animals and their non-transgenic controls at different ages, followed by unpaired  $t$ -test comparisons at the different time points. Significance was accepted at  $P \leq 0.05$ . The data were analyzed using GraphPad Prism software (La Jolla, CA, USA). Results are expressed as mean ± SEM.

## RESULTS

Immunohistochemical labeling demonstrated that CaSR is present in the hippocampus of both 3xTg-AD and non-Tg control animals at all ages (9, 12, and 18 months) with a rather homogeneous distribution throughout all hippocampal areas (**Figures 1A,B**). Punctate CaSR labeling is mainly present in pyramidal neurons of the different CA subfields and in granule cells of the DG as well as in the pleomorphic cells of the hilus, being more evident in the soma, nucleus excluded, although it

is also detectable in the neuropil, including both dendrites and axons (Figures 1C–F). Astroglial occurrence of CaSR was rather rare and when detected was of very low intensity as compared to neurons; appearing as puncta mainly restricted to the astrocytic soma (Figures 1K–P).

### Increase of CaSR Expression in 3xTg-AD Animals

Optical density analysis of CaSR staining in the hippocampus of the 3xTg-AD mouse showed a significant increase in its expression in CA1 and DG subfields [ $F_{(7, 166)} = 11.32, p < 0.0001$  and  $F_{(7, 166)} = 7.994, p < 0.0001$ , respectively] at all ages (9, 12, and 18 months; Figures 1, 2). An increase in CaSR optical density of 23.44, 17.62, and 20.09% at 9, 12, and 18 months of age respectively when compared to control non-Tg animals was detected in CA1 area (Figures 1C,D, 2A; Table 1). Similar increase in CaSR optical density was observed in DG: 17.82, 14.74, and 20.74%, at 9, 12, and 18 months respectively in 3xTg-AD animals compared to non-Tg (Figures 1E,F, 3A; Table 1). No significant alterations in the optical density of CaSR were identified in the CA2 and in CA3 sub-fields.

### CaSR Expression Increase in CA1 and DG Is Layer-Specific

In CA1 we found that the increase in CaSR expression in 3xTg-AD animals mainly occurred in the pyramidal cell layer (PCL, 10.68% at 9 months, 2.28% at 12 months, 20.17% at 18 months; Figure 2B), in the stratum radiatum (SR, 12.93% at 9 months, 27.71% at 12 months, 14.55% at 18 months; Figure 2C) and in the stratum lacunosum moleculare (SLM, 93.19% at 9 months, 39.58% at 12 months, 56.08% at 18 months; Figures 1G,H, 2D; Table 1).

In the DG an increase in CaSR expression was most prominent in the molecular layer (ML) of 3xTg-AD animals respect to their controls (15.90% at 9 months, 12.32% at 12 months, 20.98% at 18 months; Figure 3B) and in the granular cell layer (GCL, 19.33% at 9 months, 10.68% at 12 months, 37.38% at 18 months; Figures 1I,J, 3C; Table 1). The increase in the molecular layer was similar in all subdivisions; the inner, middle and outer ML (data not shown).

Increased level of CaSR labeling in the projections layers described above doesn't appear to derive from neuronal somata, despite its presence in some interneurons cell bodies, but mainly from the neuropil comprising both dendrites and axons (Figures 1D,F).

### CaSR Increase in Hippocampus Occurs in the Areas Affected by $\beta$ -Amyloid Accumulation

In 3xTg-AD mice intracellular  $\beta$ -amyloid in hippocampal neurons appears between 4 and 6 months of age and reaches its maximum at 9 months of age (Figures 4G,H); extracellular  $\beta$ -amyloid depositions start to mount from 9 to 12 months, being maximal at 18 months. At 18 months the  $\beta$ -amyloid plaques are big and expanded through the hippocampus mainly concentrating in the CA1 subfield (Figures 4E,F,I,J); with later

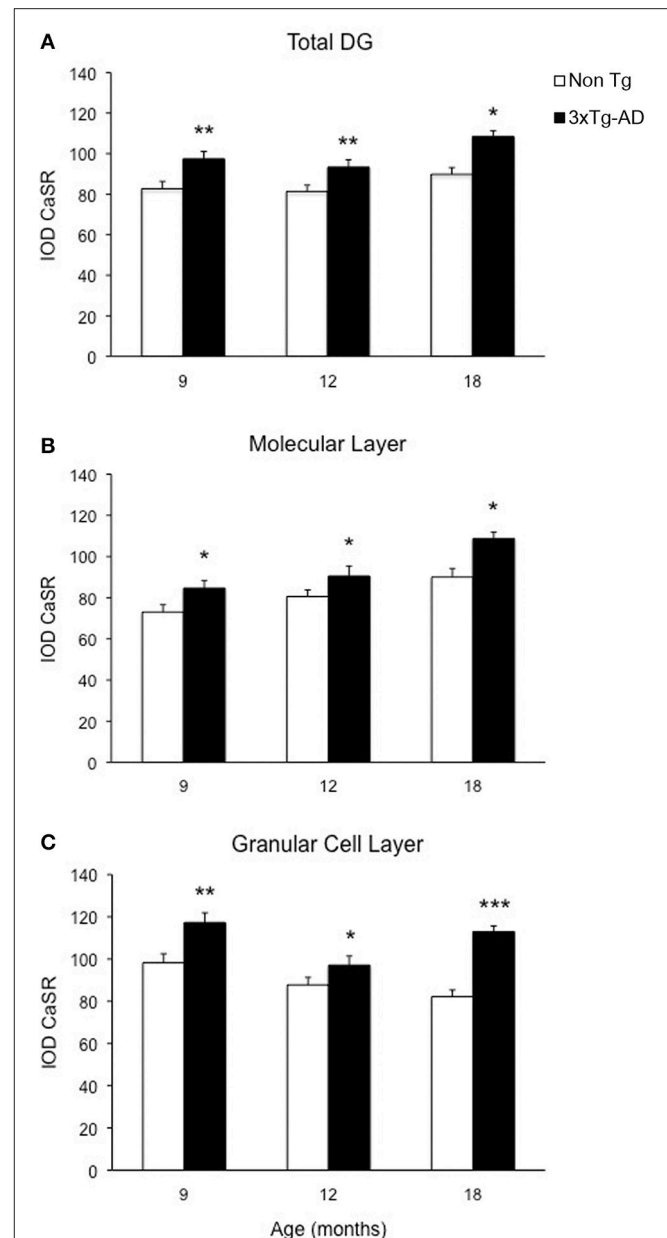
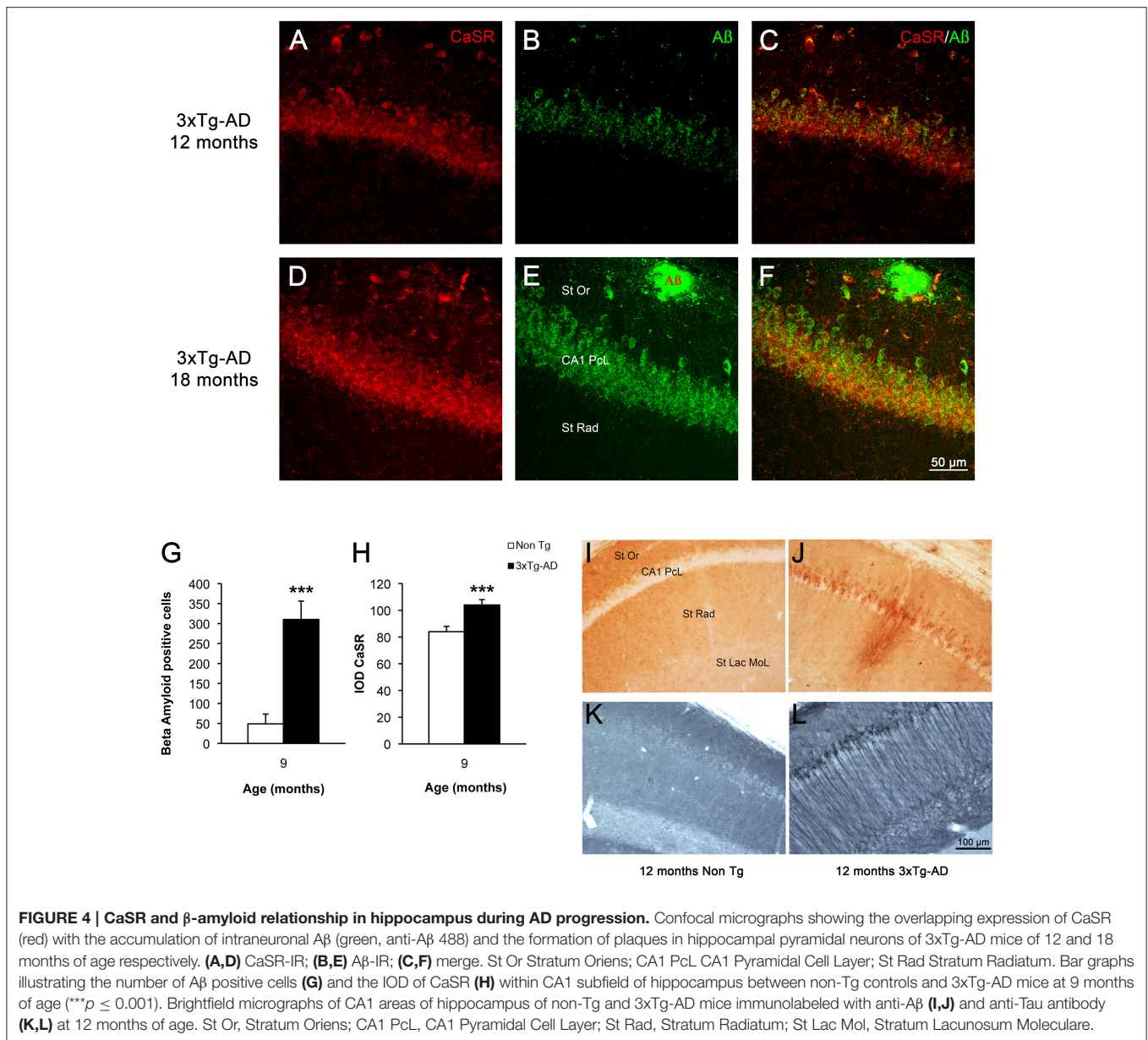


**FIGURE 3 | Modification of CaSR expression in hippocampal DG.** Bar graphs illustrating CaSR-IR IOD within DG subfield between non-Tg controls and 3xTg-AD mice at 9, 12, and 18 months of age (Ns for non-Tg = 5, 5, 4; ns for 3xTg-AD = 4, 5, 3, respectively; 3 slices have been analyzed per each animal). (A) Total DG; (B) Molecular Layer; (C) Granular Cell Layer. Bars represent means  $\pm$  SEM (\* $p \leq 0.05$ , \*\* $p \leq 0.01$ , \*\*\* $p \leq 0.001$ ).

appearance in the DG (Noristani et al., 2012; Rodríguez et al., 2013). In a similar way hyper-phosphorylated Tau protein begins to be detectable in 3xTg-AD mice at 12 months causing the formation of tangles by 18 months, and it is also concentrated in CA1 region affecting all the layers (Figures 4K,L). The increase of CaSR intensity in the CA1 region follows the same spatio-temporal pattern as that of  $\beta$ -amyloid deposition (Figures 4A–F),



while in the DG it appears even before the accumulation of  $A\beta$  becomes evident.

## DISCUSSION

*In vitro* exposure of human cortical astrocytes and neurons to a truncated form of  $\beta$ -amyloid, the  $A\beta_{25-35}$  peptide, which binds and activates the CaSR (Dal Prà et al., 2014), stimulated the intracellular production and secretion of  $\beta$ -amyloid by both cell types with the subsequent death of a fraction of neurons (Armato et al., 2013). While neurons were vulnerable to  $\beta$ -amyloid toxicity, cultured astrocytes survived and they showed a transient increase of CaSR expression. The cytotoxic effects on neurons were fully inhibited following addition of CaSR antagonist NPS 2143 to the incubation media. Indeed, the NPS prevented the

death of neurons and it deeply and steadily downregulated the receptor in the  $A\beta$ -treated astrocytes, and completely blocked the  $A\beta$  self-induction mechanism (Armato et al., 2013).

This *in vitro* study conceptually complements results we obtained in the 3xTg-AD mice model described in the present paper; these results further corroborate links existing between increases in CaSR expression and  $\beta$ -amyloid accumulation. In the 3xTg-AD mice, intraneuronal  $\beta$ -amyloid starts to accumulate in the CA1 pyramidal neurons at 4–6 months of age reaching maximum at 9 months of age, while extracellular  $\beta$ -amyloid deposits emerge from 12 months of age. Appearance of senile plaques is associated with specific astrogliosis around the plaques despite the generalized hippocampal astrocytic atrophy and with an increase in the density of activated microglia and recruitment of new ramified microglial cells (Rodríguez et al., 2009, 2010,



2013; Olabarria et al., 2010). Accumulation of Tau that occurs later follows similar pattern with maximum presence from 18 months. The 3xTg-AD mouse model not only develops the typical histopathological hallmarks of Alzheimer's disease, but also manifests synaptic dysfunction with impaired long-term-potential (LTP) (Oddo et al., 2003b; Rodríguez et al., 2008).

Analysis of an acute hypoxia/ischemia in rats revealed that A $\beta$  overproduction due to hypoxic injury is mediated by CaSR hyperexpression (Bai et al., 2015). Experiments on rat hippocampal neurons demonstrated that hypoxia induces an up-regulation of CaSR which in turn promotes the elevation of cytosolic [Ca<sup>2+</sup>] thereby producing an increase of BACE1 expression that results in the rise of A $\beta$ <sub>40</sub> and A $\beta$ <sub>42</sub> generation. In addition, specific inhibition of CaSR with Calhex 231, an allosteric antagonist of CaSR, induced a decrease of BACE1 and A $\beta$  both *in vitro* and *in vivo* in hypoxic conditions (Bai et al., 2015). The prominent effect of the increased expression and activity of CaSR in hippocampus is confirmed also by analysing a mouse model of acute ischemic injury where a transient global cerebral ischemia (TGI) was induced. In this model CaSR was overexpressed in parallel with GABA<sub>B</sub> receptor 1 downregulation and was followed by neuronal death. The administration of the calcilytic compound NPS89636 through intracerebroventricular injections after the TGI specifically blocked the activity of CaSR, restored GABA<sub>B</sub>R1 expression and protected hippocampal neurons from cell death. Furthermore, the treatment of TGI mice with calcilytics significantly improved learning and memory (Kim et al., 2014).

Altogether these findings reveal the importance and the impact which altered expression of CaSR has on maintaining the normal brain function, supporting the idea that its changes could contribute to the development and progression of pathologies such as Alzheimer's disease and stroke. Our present data in an AD mouse model show that expression of CaSR is increasing while neuropathology progresses. Previous works demonstrated that the administration of A $\beta$ <sub>42</sub> oligomers to neuronal and astrocytic human cell cultures increases the endogenous A $\beta$ <sub>42</sub> production and secretion resulting in a progressive death of neurons. This mechanism of A $\beta$  self-induction, which contribute to the advance of AD, was demonstrated to be completely suppressed by adding a specific calcilytic like NPS 2143 to the cell culture (Armato et al., 2013; Dal Prà et al., 2015; Chiarini et al., 2016). It needs to be emphasized that the CaSR could

be a promising target of investigation for not only further understanding AD pathology onset and spread but also for evaluating new therapeutic solutions.

## AUTHOR CONTRIBUTIONS

EG: Experimental work, data analysis, result preparation and writing of the manuscript. JR: Conception of the study, experimental design, data analysis, result preparation interpretation, discussion and writing of the manuscript. AV: Results interpretation and discussion and writing of the manuscript. AC, UA, and ID: Results interpretation and discussion.

## ACKNOWLEDGMENTS

We thank Dr Fátima Zallo Díaz, for her help and assistance with the figures. Authors research was supported by Alzheimer's Research Trust (UK) Programme Grant [grant number ART/PG2004A/1 (to AV and JR)]; by the Grant Agency of the Czech Republic [grant number GACR 309/09/1696 (to JR); GACR 305/08/1381 and GACR 305/08/1384 (to AV)] as well as by the Spanish Government Plan Nacional de I+D+I 2008-2011, and ISCIII Subdirección General de Evaluación y Fomento de la investigación co-financed by FEDER [grant number PI10/02738 (to JR and AV)]. The Government of the Basque Country [grant number AE-2010-1-28; AEGV10/16, GV2011111020 (to JR)]; as well as by the Spanish Ministerio de Economía y Competitividad, RETOS Colaboración [grant number RTC-2015-3542-1 co-financed by FEDER (to JR)] and by the Ministry of Italian University and Research (MIUR) to EG, AC, UA, and ID.

## SUPPLEMENTARY MATERIAL

The Supplementary Material for this article can be found online at: <http://journal.frontiersin.org/article/10.3389/fnins.2017.00081/full#supplementary-material>

**Supplementary Figure 1 | Brightfield micrographs showing the anatomy of the dorsal hippocampus in a section stained with toluidine blue (A)** and the delimited areas that were chosen in each single analyzed section as region of interest for the OD analysis in a representative section of a 3xTg-AD animal labeled for CaSR **(B)** as detailed in the Materials and Methods. **(C)** Micrograph showing the lack of staining in the negative control, after omission CaSR antibody.

## REFERENCES

- Armato, U., Chiarini, A., Chakravarthy, B., Chioffi, F., Pacchiana, R., Colarusso, E., et al. (2013). Calcium-sensing receptor antagonist (calcilytic) NPS 2143 specifically blocks the increased secretion of endogenous A $\beta$ <sub>42</sub> prompted by exogenous fibrillary or soluble A $\beta$ <sub>25-35</sub> in human cortical astrocytes and neurons—Therapeutic relevance to Alzheimer's disease. *Biochim. Biophys. Acta* 1832, 1634–1652. doi: 10.1016/j.bbdis.2013.04.020
- Bai, S., Mao, M., Tian, L., Yu, Y., Zeng, J., Ouyang, K., et al. (2015). Calcium sensing receptor mediated the excessive generation of  $\beta$ -amyloid peptide induced by hypoxia *in vivo* and *in vitro*. *Biochem. Biophys. Res. Commun.* 459, 568–573. doi: 10.1016/j.bbrc.2015.02.141
- Brown, E. M., and MacLeod, R. J. (2001). Extracellular calcium sensing and extracellular calcium signaling. *Physiol. Rev.* 81, 239–297. Available online at: <http://physrev.physiology.org/content/81/1/239.long>
- Chang, W., Tu, C., Cheng, Z., Rodriguez, L., Chen, T. H., Gassmann, M., et al. (2007). Complex formation with the type B  $\gamma$ -aminobutyric acid receptor affects the expression and signal transduction of the extracellular calcium-sensing receptor: studies with HEK-293 cells and neurons. *J. Biol. Chem.* 282, 25030–25040. doi: 10.1074/jbc.M700924200
- Chattopadhyay, N., Legradi, G., Bai, M., Kifor, O., Ye, C., Vassilev, P. M., et al. (1997). Calcium-sensing receptor in the rat hippocampus: a developmental study. *Brain Res. Dev. Brain Res.* 100, 13–21. doi: 10.1016/S0165-3806(97)00009-6

- Chattopadhyay, N., Ye, C. P., Yamaguchi, T., Kifor, O., Vassilev, P. M., Nishimura, R., et al. (1998). Extracellular calcium-sensing receptor in rat oligodendrocytes: expression and potential role in regulation of cellular proliferation and an outward K<sup>+</sup> channel. *Glia* 24, 449–458. doi: 10.1002/(SICI)1098-1136(199812)24:4<449::AID-GLIA10>3.0.CO;2-9
- Chattopadhyay, N., Ye, C. P., Yamaguchi, T., Vassilev, P. M., and Brown, E. M. (1999b). Evidence for extracellular calcium-sensing receptor mediated opening of an outward K<sup>+</sup> channel in a human astrocytoma cell line (U87). *Glia* 26 64–72. doi: 10.1002/(SICI)1098-1136(199903)26:1<64::AID-GLIA7>3.0.CO;2-X
- Chattopadhyay, N., Ye, C., Yamaguchi, T., Nakai, M., Kifor, O., Vassilev, P. M., et al. (1999a). The extracellular calcium-sensing receptor is expressed in rat microglia and modulates an outward K<sup>+</sup> channel. *J. Neurochem.* 72, 1915–1922. doi: 10.1046/j.1471-4159.1999.0721915.x
- Chen, W., Bergsman, J. B., Wang, X., Gilkey, G., Pierpoint, C. R., Daniel, E. A., et al. (2010). Presynaptic external calcium signaling involves the calcium-sensing receptor in neocortical nerve terminals. *PLoS ONE* 5:e8563. doi: 10.1371/journal.pone.0008563
- Chiarini, A., Armato, U., Liu, D., and Dal Prà, I. (2016). Calcium-sensing receptors of human neural cells play crucial roles in Alzheimer's disease. *Front. Physiol.* 7:134. doi: 10.3389/fphys.2016.00134
- Chiarini, A., Dal Prà, I., Menapace, L., Pacchiana, R., Whitfield, J., and Armato, U. (2005). Soluble amyloid  $\beta$ -peptide and myelin basic protein strongly stimulate, alone and in synergism with combined proinflammatory cytokines, the expression of functional nitric oxide synthase-2 in normal adult human astrocytes. *Int. J. Mol. Med.* 16, 801–807. doi: 10.3892/ijmm.16.5.801
- Chiarini, A., Whitfield, J., Bonafini, C., Chakravarthy, B., Armato, U., and Dal Prà, I. (2010). Amyloid- $\beta$ (25–35), an amyloid- $\beta$ (1–42) surrogate, and proinflammatory cytokines stimulate VEGF-A secretion by cultured, early passage, normoxic adult human cerebral astrocytes. *J. Alzheimers. Dis.* 21, 915–926. doi: 10.3233/JAD-2010-100471
- Conley, Y. P., Mukherjee, A., Kammerer, C., DeKosky, S. T., Kamboh, M. I., Finegold, D. N., et al. (2009). Evidence supporting a role for the calcium-sensing receptor in Alzheimer disease. *Am. J. Med. Genet. B Neuropsychiatr. Genet.* 150B, 703–709. doi: 10.1002/ajmg.b.30896
- Cordero, M. I., Rodríguez, J. J., Davies, H. A., Peddie, C. J., Sandi, C., and Stewart, M. G. (2005). Chronic restraint stress down-regulates amygdaloid expression of polysialylated neural cell adhesion molecule. *Neuroscience* 133, 903–910. doi: 10.1016/j.neuroscience.2005.03.046
- Dal Prà, I., Chiarini, A., Gui, L., Chakravarthy, B., Pacchiana, R., Gardenal, E., et al. (2015). Do astrocytes collaborate with neurons in spreading the "Infectious"  $\alpha$  and tau drivers of Alzheimer's disease? *Neuroscientist* 21, 9–29. doi: 10.1177/1073858414529828
- Dal Prà, I., Chiarini, A., Nemeth, E. F., Armato, U., and Whitfield, J. F. (2005). Roles of Ca<sup>2+</sup> and the Ca<sup>2+</sup>-sensing receptor (CASR) in the expression of inducible NOS (nitric oxide synthase)-2 and its BH 4 (tetrahydrobiopterin)-dependent activation in cytokine-stimulated adult human astrocytes. *J. Cell. Biochem.* 96, 428–438. doi: 10.1002/jcb.20511
- Dal Prà, I., Chiarini, A., Pacchiana, R., Gardenal, E., Chakravarthy, B., Whitfield, J. F., et al. (2014). Calcium-sensing receptors of human astrocyte-neuron teams: amyloid- $\beta$ -driven mediators and therapeutic targets of Alzheimer's disease. *Curr. Neuropharmacol.* 12, 353–364. doi: 10.2174/1570159X12666140828214701
- Dal Prà, I., Whitfield, J. F., Pacchiana, R., Bonafini, C., Talacchi, A., Chakravarthy, B., et al. (2011). The amyloid- $\beta$ 42 proxy, amyloid- $\beta$ (25–35), induces normal human cerebral astrocytes to produce amyloid- $\beta$ 42. *J. Alzheimers Dis.* 24, 335–347. doi: 10.3233/JAD-2011-101626
- Ferry, S., Traiffort, E., Stinnakre, J., and Ruat, M. (2000). Developmental and adult expression of rat calcium-sensing receptor transcripts in neurons and oligodendrocytes. *Eur. J. Neurosci.* 12, 872–884. doi: 10.1046/j.1460-9568.2000.00980.x
- Gama, L., Wilt, S. G., and Breitwieser, G. E. (2001). Heterodimerization of calcium sensing receptors with metabotropic glutamate receptors in neurons. *J. Biol. Chem.* 276, 39053–39059. doi: 10.1074/jbc.M105662200
- Kim, J. Y., Ho, H., Kim, N., Liu, J., Tu, C., Yenari, M. A., et al. (2014). Calcium-sensing receptor (CaSR) as a novel target for ischemic neuroprotection. *Ann. Clin. Transl. Neurol.* 1, 851–866. doi: 10.1002/acn3.118
- Kulijewicz-Nawrot, M., Verkhratsky, A., Chvátal, A., Syková, E., and Rodríguez, J. J. (2012). Astrocytic cytoskeletal atrophy in the medial prefrontal cortex of a triple transgenic mouse model of Alzheimer's disease. *J. Anat.* 221, 252–262. doi: 10.1111/j.1469-7580.2012.01536.x
- Lim, D., Rodríguez-Arellano, J. J., Párpura, V., Zorec, R., Zeidán-Chuliá, F., Genazzani, A. A., et al. (2015). Calcium signalling toolkits in astrocytes and spatio-temporal progression of Alzheimer's disease. *Curr. Alzheimer Res.* 13, 359–369. doi: 10.2174/1567205013666151116130104
- Lim, D., Ronco, V., Grolla, A. A., Verkhratsky, A., and Genazzani, A. A. (2014). Glial calcium signalling in Alzheimer's disease. *Rev. Physiol. Biochem. Pharmacol.* 167, 45–65. doi: 10.1007/112\_2014\_19
- Noristani, H. N., Olabarria, M., Verkhratsky, A., and Rodríguez, J. J. (2010). Serotonin fibre sprouting and increase in serotonin transporter immunoreactivity in the CA1 area of hippocampus in a triple transgenic mouse model of Alzheimer's disease. *Eur. J. Neurosci.* 32, 71–79. doi: 10.1111/j.1460-9568.2010.07274.x
- Noristani, H. N., Verkhratsky, A., and Rodríguez, J. J. (2012). High tryptophan diet reduces CA1 intraneuronal  $\beta$ -amyloid in the triple transgenic mouse model of Alzheimer's disease. *Aging Cell* 11, 810–822. doi: 10.1111/j.1474-9726.2012.00845.x
- Oddo, S., Caccamo, A., Kitazawa, M., Tseng, B. P., and LaFerla, F. M. (2003a). Amyloid deposition precedes tangle formation in a triple transgenic mouse model of Alzheimer's disease. *Neurobiol. Aging* 24, 1063–1070. doi: 10.1016/j.neurobiolaging.2003.08.012
- Oddo, S., Caccamo, A., Shepherd, J. D., Murphy, M. P., Golde, T. E., Kaye, R., et al. (2003b). Triple-transgenic model of Alzheimer's Disease with plaques and tangles: intracellular A $\beta$  and synaptic dysfunction. *Neuron* 39, 409–421. doi: 10.1016/S0896-6273(03)00434-3
- Olabarria, M., Noristani, H. N., Verkhratsky, A., and Rodríguez, J. J. (2010). Concomitant astroglial atrophy and astrogliosis in a triple transgenic animal model of Alzheimer's disease. *Glia* 58, 831–838. doi: 10.1002/glia.20967
- Olabarria, M., Noristani, H. N., Verkhratsky, A., and Rodríguez, J. J. (2011). Age-dependent decrease in glutamine synthetase expression in the hippocampal astroglia of the triple transgenic Alzheimer's disease mouse model: mechanism for deficient glutamatergic transmission? *Mol. Neurodegener.* 6:55. doi: 10.1186/1750-1326-6-55
- Paxinos, G., and Franklin, K. (2012). *The Mouse Brain in Stereotaxic Coordinates, 4th Edn.* Academic Press, 360.
- Rodríguez, J. J., Jones, V. C., Tabuchi, M., Allan, S. M., Knight, E. M., LaFerla, F. M., et al. (2008). Impaired adult neurogenesis in the dentate gyrus of a triple transgenic mouse model of Alzheimer's disease. *PLoS ONE* 3:e2935. doi: 10.1371/journal.pone.0002935
- Rodríguez, J. J., Noristani, H. N., Hilditch, T., Olabarria, M., Yeh, C. Y., Witton, J., et al. (2013). Increased densities of resting and activated microglia in the dentate gyrus follow senile plaque formation in the CA1 subfield of the hippocampus in the triple transgenic model of Alzheimer's disease. *Neurosci. Lett.* 552, 129–134. doi: 10.1016/j.neulet.2013.06.036
- Rodríguez, J. J., Witton, J., Olabarria, M., Noristani, H. N., and Verkhratsky, A. (2010). Increase in the density of resting microglia precedes neuritic plaque formation and microglial activation in a transgenic model of Alzheimer's disease. *Cell Death Dis.* 1:e1. doi: 10.1038/cddis.2009.2
- Rodríguez, J., Olabarria, M., Rodríguez, J. J., Olabarria, M., Chvátal, A., and Verkhratsky, A. (2009). Astroglia in dementia and Alzheimer's disease. *Cell Death Differ.* 16, 378–385. doi: 10.1038/cdd.2008.172
- Ruat, M., Molliver, M. E., Snowman, A. M., and Snyder, S. H. (1995). Calcium sensing receptor: molecular cloning in rat and localization to nerve terminals. *Proc. Natl. Acad. Sci. U.S.A.* 92, 3161–3165. doi: 10.1073/pnas.92.8.3161
- Ruat, M., and Traiffort, E. (2013). Roles of the calcium sensing receptor in the central nervous system. *Best Pract. Res. Clin. Endocrinol. Metab.* 27, 429–442. doi: 10.1016/j.beem.2013.03.001
- Small, D. H. (2009). Dysregulation of calcium homeostasis in Alzheimer's disease. *Neurochem. Res.* 34, 1824–1829. doi: 10.1007/s11064-009-9960-5
- Vizard, T. N., O'Keefe, G. W., Gutierrez, H., Kos, C. H., Riccardi, D., and Davies, A. M. (2008). Regulation of axonal and dendritic growth by the extracellular

- calcium-sensing receptor. *Nat. Neurosci.* 11, 285–291. doi: 10.1038/nn2044
- Vyleta, N. P., and Smith, S. M. (2011). Spontaneous glutamate release is independent of calcium influx and tonically activated by the calcium-sensing receptor. *J. Neurosci.* 31, 4593–4606. doi: 10.1523/JNEUROSCI.6398-10.2011
- Yano, S., Brown, E. M., and Chattopadhyay, N. (2004). Calcium-sensing receptor in the brain. *Cell Calcium* 35, 257–264. doi: 10.1016/j.ceca.2003.10.008
- Ye, C., Ho-pao, C. L., Kanazirska, M., Quinn, S., Rogers, K., Seidman, C. E., et al. (1997). Amyloid- $\beta$  proteins activate Ca<sup>(2+)</sup>/ $\gamma$ ( $\beta$ )-permeable channels through calcium-sensing receptors. *J. Neurosci. Res.* 47, 547–554. doi: 10.1002/(SICI)1097-4547(19970301)47:5<547::AID-JNR10>3.0.CO;2-V
- Ye, C., Kanazirska, M., Quinn, S., Brown, E. M., and Vassilev, P. M. (1996). Modulation by polycationic Ca<sup>2+</sup>-sensing receptor agonists of nonselective cation channels in rat hippocampal neurons. *Biochem. Biophys. Res. Commun.* 224, 271–280. doi: 10.1006/bbrc.1996.1019
- Conflict of Interest Statement:** The authors declare that the research was conducted in the absence of any commercial or financial relationships that could be construed as a potential conflict of interest.

Copyright © 2017 Gardenal, Chiarini, Armato, Dal Prà, Verkhatsky and Rodríguez. This is an open-access article distributed under the terms of the Creative Commons Attribution License (CC BY). The use, distribution or reproduction in other forums is permitted, provided the original author(s) or licensor are credited and that the original publication in this journal is cited, in accordance with accepted academic practice. No use, distribution or reproduction is permitted which does not comply with these terms.